MINISTRY OF EDUCATION, RESEARCH, YOUTH AND SPORT

THE ANNALS OF "DUNAREA DE JOS" UNIVERSITY OF GALATI

Fascicle IX
METALLURGY AND MATERIALS SCIENCE

YEAR XXVIII (XXXIII),
September 2010, no. 3

ISSN 1453-083X

2010
GALATI UNIVERSITY PRESS

EDITING MANAGEMENT

RESPONSIBLE EDITOR: **Prof.Dr.Eng. Viorel MINZU**

ASSISTANT EDITORS: **Prof.Dr.Fiz. Mirela PRAISLER**
Prof.Dr.Eng. Teodor MUNTEANU
Prof.Dr. Ing. Iulian BÎRSAN
Prof.Dr.Ec. Daniela ŞARPE
Prof.Dr. Elena MEREUŢĂ
SECRETARY: **Assoc.Prof.Dr.Eng. Ion ALEXANDRU**

EDITING BOARD

Fascicle IX

METALLURGY AND MATERIALS SCIENCE

PRESIDENT OF HONOUR: **Prof.Dr.Chim. Olga MITOŞERIU**
EDITOR IN CHIEF: **Prof.Dr.Eng. Nicolae CĂNĂNĂU**
EDITORIAL SECRETARY: **Prof.Dr.Eng. Marian BORDEI**

MEMBERS:

Acad.Prof.Dr.Hab. **Valeriu CANTSER**–Coordinator of the Technical and Scientific Section of the Academy of Moldova Republic
Acad.Prof.Dr.Hab. **Ion BOSTAN**–Rector of Technical University of Moldova, member of the Academy of Moldova Republic
Prof.Dr.**Rodrigo MARTINS**–President of the Department of Materials Science, Faculty of Science and Technology,NOVA University of Lisbon,Portugal
Prof.Dr.Hab. **Vasile MARINA**–Head of the Materials Resistance Department, State Technical University of Moldova, Kishinau, Moldova Republic
Prof.Dr. **Antonio de SAJA**–Head of Department of Physics of Condensed Material, Faculty of Sciences, University of Valladolid, Spain
Prof.Dr. **Strul MOISA**–Chief Engineer Department of Materials Engineering, Ben Gurion University of the Negev, Israel
Prof.Dr. **Alexander SAVAIDIS**–Aristotle University of Thessaloniki, Dept. of Mechanical Engineering, Greece
Prof.Dr.Hab. **Valeriu DULGHERU**–Head of Department, Faculty of Engineering and Management in Machine Building, Technical University of Moldova
Prof.Dr. **Ion SANDU** –ARHEOINVEST Platform, Laboratory of Scientific Investigation and Cultural Heritage Conservation, „Al.I.Cuza” University of Iasi

Prof.Dr.Eng. **Elena DRUGESCU**
Prof.Dr.Eng. **Anişoara CIOCAN**
Prof.Dr.Eng. **Maria VLAD**
Prof.Dr.Eng. **Petre Stelian NIŢĂ**
Prof.Dr.Eng. **Alexandru IVĂNESCU**
Prof.Dr.Chim. **Viorica MUŞAT**
Prof.Dr.Eng. **Florentina POTECAŞU**
Assoc.Prof.Dr.Eng. **Sanda LEVCOVICI**

Table of Content

1.Petre Stelian Nita - Solutocapillary Effects of Sulphur in CaO-Al_2O_3 Slags, in Marangoni Instability and Convection Onset, Related to the Desulphurization of low Carbon, Aluminium Killed Steels.. 5

2.Aurel Crişan, Diana Ţuţuianu, Tibor Bedő, Ioan Ciobanu- Influence of Inclinations Applied to Ribs on the Solidification of Cast Parts.................................. 15

3.Anisoara Ciocan, Florentina Potecasu - Scrap Quality and Metallurgical Effects Associated with Copper and Tin as Tramp Elements in the Casting Steels…............. 22

4.Tibor Bedő, Viorel Ene, Ioan Cioban – Some Considerations on Environmental Sand Cores with Inorganic Binder.. 28

5.Ioan Ciobanu, Diana Ţuţuianu, Tibor Bedő, Aurel Crişan - Influence of Rib Length on the Solidification of Cast Parts.. 33

6.G. Florea, C. Oancea, C. Gheorghies L. Gheorghies - New Achievements in Manufacturing of Church Bells…………………………………………………. 42

7.Gheorghe Croitoru, Ion Rusu - History of Faberge Eggs..................................... 47

8. Nicolae Cananau, Alexandru Chiriac, Vasile Bratu - Quality Assurance of Cylindrical Casted Parts with Small Thickness... 54

9.Jordan Georgiev, Stefan Stefanov, Dimitar Teodosiev, Lubomir Anestiev - A Setup for Preparation of Glass-Carbon Coatings on TiO_2-Nb_2O_5 Intended for Hip Joint Prostheses.. 58

10. Tamara Radu, Lucica Balint, Viorel Dragan - Research on the Effect of Temperature and Duration of Immersion on the Layer Thickness of Zinc Coating Obtained in Microalloyed Zinc Melts…...…... 62

11.Alexandru Chiriac, Gheorghe Florea, Marian Neacsu, Ioan Saracin, Olimpia Panda - Structural Aspects of Antifriction Properties Brass........................ 66

12.Lidia Benea, Alina Ciubotariu, Bernard Tribollet, Wolfgang Sand - Influence of SiC/Ni Nanocomposite Coatings on SrB Attachment and Biofilm Formation……….. 71

13.Dumitru Popa, Aurel Ciurea, Marian Bordei - Air Pollution Control.………... 78

14.Daniela Zhelezarova, Silviu Macuta, Ivan Balashev - Automated Apparatus-Program System for Evaluating the Strength of a Reducer Shaft................................ 82

THE ANNALS OF "DUNAREA DE JOS" UNIVERSITY OF GALATI.
FASCICLE IX. METALLURGY AND MATERIALS SCIENCE
N^0. 3 – 2010, ISSN 1453 – 083X

SOLUTOCAPILLARY EFFECTS OF SULPHUR IN CAO-AL$_2$O$_3$ SLAGS, IN MARANGONI INSTABILITY AND CONVECTION ONSET, RELATED TO THE DESULPHURIZATION OF LOW CARBON, ALUMINIUM KILLED STEELS

Petre Stelian NITA
"Dunarea de Jos" University of Galati
email: pnita @ugal.ro

ABSTRACT

Based on the "one layer model" applied to desulphurization slag layer with boundary conditions, imposed due to the sulphur transfer through the interface steel-slag during desulphurization process, the threshold conditions of instability for Marangoni convection in the desulphurization slag at 1873K are evaluated in the CaO-Al$_2$O$_3$ system at ratios CaO/Al$_2$O$_3$=1.5 and 1.0, for sulphur concentration lower than the solubility limit and in conditions of fully liquid slag. Threshold critical values $\Delta\sigma_c=(51-79.62)10^{-6}$ N/m, for the surface tension in slag and interfacial tension slag-steel, closed to the value $\Delta\sigma_{crit}=30.748\cdot10^{-6}$ N/m obtained in steel and $\Delta(S)_{crit}=(20-44.73)10^{-4}$ mass%, for the local fluctuations of sulphur concentration , were found for onset instability and Marangoni convection in slag, at the minimal value of the critical dimensionless solutal number $Ma_s^c=80$. There are small differences between numerical values of the quantities for threshold conditions obtained on the base of the surface tension of the slag and on the base of the interfacial tension steel-slag. The instability with onset of the turbulent convection is predicted to take place starting from values $\Delta\sigma>(312.36-501.61)\cdot10^{-6}$ N/m, corresponding of $\Delta(S)=(126-228.82)\cdot10^{-4}$mass%. An enhancement coefficient of the mass transfer of sulphur at interface on the slag side is established in the conditions of the onset Marangoni flow and convection. The solutal parameter $\Delta(S)$ is the most sensitive in contributing to instability conditions and in producing mixing effects in slag in a thickness layer δ_{eff} at interface, by energy dissipation of Marangoni flow and helps to make important differences between conditions in slags C/A=1.5 and C/A=1.

KEYWORDS: solutocapillary, desulphurization process, Marangoni effect

1. Introduction

During steel refining under slags, surface active elements such as oxygen and sulfur, induce additional interfacial convection flow, which is able to promote an enhancement of the mass transfer in certain conditions. The sulphur removal from a low carbon, aluminium killed steel, in a CaO-Al$_2$O$_3$ base slag is described by the reaction:

$$[S]+(CaO)_s+2/3[Al]\Leftrightarrow(CaS)+1/3(Al_2O_3)$$
$$\Delta G_T^0<0 \qquad \text{(I)}$$

The usual desulphurization slags belong to the system CaO-MgO-Al$_2$O$_3$-SiO$_2$ in the range of mass% contents corresponding to ratios CaO/ Al$_2$O$_3$≈1-1.5 and low contents of SiO$_2$ and MgO (less than 5-10mass%).

Treatments under such slags are applied also to obtain clean steel, by the advanced removal of the non-metallic inclusions, especially of alumina. In the present paper, the contributions of the sulphur presence in slag during such treatments, to some aspects of the interfacial dynamics the process, are evaluated. Experimental data regarding the surface tension in slags and the interfacial tension in systems steel-slag reflect the influence of the chemical composition of the CaO-Al$_2$O$_3$ slags, in the presence of sulphur$^{1)}$ or in absence of it$^{2)}$.The analysis of the influence exerted by the chemical composition variations of the slag will be evaluated from the point of view of producing flow and convection, based on the Marangoni dimensionless number, in the form proposed in ref.$^{3)}$, adapted for solutocapillary effect, produced by the sulphur content, under the form of the rel.(1):

$Ma_s = |\partial\sigma/\partial(S)|\cdot\Delta(S)\cdot L/\rho\cdot\nu\cdot D = |\partial\sigma/\partial(S)|\cdot\Delta(S)\cdot L/\eta\cdot D$ (1)

Where:

$|\partial\sigma/\partial(S)|$ - absolute value of the concentration coefficient of the surface tension or of the interfacial tension, related to the sulphur as surface active component, in $N\cdot m^{-1}\cdot(mass\%)^{-1}$ or in $N\cdot m^{-1}\cdot$(mole fraction)$^{-1}$; $\Delta(S)$-is a characteristic concentration difference across the liquid layer of slag or along its surface, expressed in terms of sulphur content, in mass % or mole fraction, or a characteristic concentration of the sulphur in slag $(S)_0$; L- is a characteristic length, in m; ρ- density of the slag, in kg/m^3; ν-kinematic viscosity of slag, m^2/s; D-diffusion coefficient of sulphur, m^2/s;$\eta=\rho\cdot\nu$-dynamic viscosity of the slag, Pa·s.

Further, any reference to the content of any component will be taken as mass %. In the rel. (1) the absolute value for $\partial\sigma/\partial(S)$ is an alternative method to the use of the (-) sign, to make positive the concentration coefficient of the surface tension or of the interfacial tension, whose values are negative when sulphur content increases in CaO/ Al_2O_3 slags. The surface tension gradient upon the concentration of the sulphur acts as a share stress exerted by the interface on the adjoining bulk liquid (Marangoni stress) and will generate flow or it will alter an already existing one (Marangoni effect). In the solutal case, the variation of surface tension along an interface may be due to the appearance of a concentration gradient of a surface active solute, along the interface or perpendicular to it. In the first situation an instantaneous convection occurs, but in the second situation the flow occurs when an instability threshold is overcome.4) As it was mentioned,4) when a transfer of a superficial active solute between two immiscible fluid phases (liquid-liquid or liquid- gas), accompanied by a chemical reaction takes place, the interface becomes instable, even at low amplitudes of the local fluctuations of the solute concentration resulting long-waves length waves which represent a deformational monotonic mode. The diffusion of sulphur in slag is recognized, under certain conditions, as a limitating step of the global rate of sulphur transfer through the interface slag-steel. An additional mass transfer superimposed on the normal mass transfer, due to the confirmed interfacial convection was evaluated at 1873K, in the case of the sulphur transfer through the interface between liquid iron-slag (CaO-MgO-Al_2O_3-SiO_2).5) Also it was directly observed the inhibition of interfacial convection as consequence of the precipitation of calcium sulfide crystals in slag at the slag/metal interface.5) Although the increasing of sulphur content, in a similar slag, reduces the values of the surface and interfacial tension steel-slag, it was not reported an adverse effect on removal of CaS from the iron-melt in the presence in slag of 3-5% CaS, in the equilibrium conditions.1)An adequate knowledge of the dynamic processes at interfaces requires a deeper analysis of the specific possible contributions to the enhancement of mass transfer coefficient.6,7) The aim of the paper is to simulate the behaviour of the slag in the conditions of local instability and further, during the desulphurizing process, especially as occurrence of short-scale Marangoni convection. Also, it is intended to find the corresponding thresholds of sulphur concentration as inhomogeneity, the corresponding thresholds of the surface and interfacial tension and also to reveal aspects of dynamics of the slag. On this base, at least at a local scale, an evaluation of the Marangoni convection and the possible enhancement of the mass transfer coefficient will be made.

2. Relevant properties in the CaO-Al_2O_3-CaS system related to solutal Marangoni number

The existing experimental data are summarized in the **Table 1** where are presented also points derived from curves mentioned in references and statistical relations derived in the present paper. The abbreviations used in this paper are slag A, or (C/A=1,5), for slags containing 60%CaO-40% Al_2O_3 and slag B, or (C/A=1), for slags containing 50%CaO-50%Al_2O_3. There are only few data on the density values in CaO-Al_2O_3 slags at the two considered compositions (Tab.1) and they exhibit a relative dispersion.8-14) There are not any data regarding the influence of the sulphur content on the density and on the viscosity in slags based on the simple CaO-Al_2O_3 system. Some trends of influence could be evaluated only by similitude, based on data in the system CaO-CaS-SiO_2, at 1873K9,15) and in the system CaO-SiO_2-Al_2O_3-MgO-MnO-CaS) at 1773K15,16). On these bases, a negligible influence of the sulphur content on the viscosity in the system CaO-Al_2O_3-CaS at 1873K, is presumed for concentrations below the saturation limit. Values of the dynamic viscosity η for CaO-Al_2O_3 slags, at C/A=1,5 and C/A=1, are given in tab.1(a)-d)), mainly according to ref.15-18). The adopted diffusion coefficient of sulphur in the slag was $D_S=2{,}9\cdot10^{-10}m^2/s$ (**Table1**), recomputed from data at 1773K,9) compared with another value $D_S=2{,}48.10^{-10}m^2/s$ used in the ref.20). The largely accepted experimental data on the sulphur solubility in CaO-Al_2O_3 slags at 1873K are given in the ref.21). Based on them, statistical regression relations have been obtained in this paper and they are given in the **Table 1** and represented in the **Figure 1**.

***Table 1**. Relevant quantities and parameters for $CaO-Al_2O_3$ slags at 1873*

Quantity, symbol, units	Value, reference
Density, ρ, $kg \cdot m^{-3}$: 1)slagA, (C/A=1.5) 2)slagB, (C/A=1.0)	1) 2685[8,9] 2) 2710[10,11], 2750[12,13], 2870[14]
Dynamic viscosity, η, Pa·s: 1)slagA 2)slag B	1) [a]0.1184[17], [b]0.162[!8], [c]0.2735* 2) [d]0.197 [18], [e]0.23[17]. *Urbain model
Diffusion coefficient of sulphur D_S , $m^2 \cdot s^{-1}$	[g]$2.9 \cdot 10^{-10}$;[19] [h]$2.48 \cdot 10^{-10}$; [20]
Solubility of sulphur in $CaO-Al_2O_3$ slags as function of the ratio (C/A)	(%S)= 1,5492Ln(C/A)+1,4639 (%CaS)= 3,4717Ln(C/A)+3,2989
Surface tension(σ) dependence on sulphur content (S, mass%), in $10^{-3}N \cdot m^{-1}$	σ_A= 2.1217$(\%S)^2$-22.922(%S)+563 σ_B= 1.4781$(\%S)^2$-22.159(%S)+546
Interfacial tension (σ_i) dependence on sulphur content (mass%), in $10^{-3}N \cdot m^{-1}$	$\sigma_{i.A}$= 0.7353$(\%S)^2$-25.504(%S)+1284.8 $\sigma_{i.B}$ = 0.7928$(\%S)^2$-31.548(%S)+1316.5
Ratio R= σ_i/σ between the interfacial tension (σ_i) and the surface tension (σ).	R_A= -0.0076$(\%S)^2$+0.0489(%S)+2.282 R_B= -0.0051$(\%S)^2$+0.0425(%S)+2.412
Ratio M=$[\partial\sigma_i/\partial(S)]/[\partial\sigma/\partial(S)]$, between the sulphur concentration coefficient of the interfacial tension and of the surface tension.	M_A= 0.0613$(\%S)^2$+0.1056(%S)+1.1179 M_B= 0.0221$(\%S)^2$+0.1148(%S)+1.4247

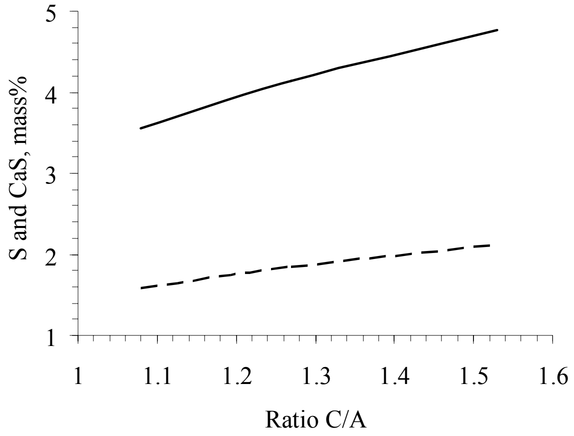

***Fig. 1.** Solubility limit of sulphur (——) and of CaS(— —) in slags CaO- Al_2O_3 at 1873K, as function of the ratio C/A,based on data from ref.[21].*

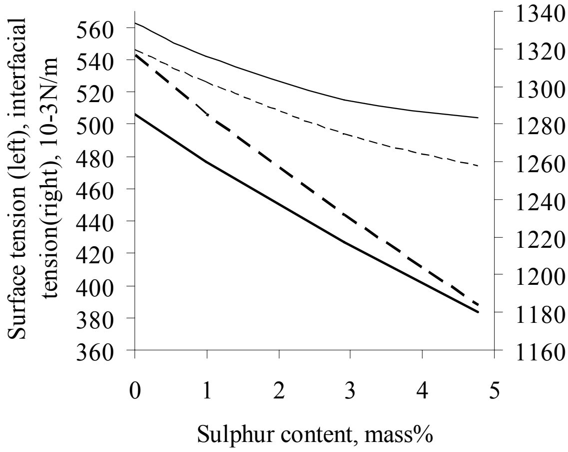

***Fig. 2.** Influence of the sulphur content in slag $CaO-Al_2O_3-CaS$ at 1873K, on the surface tension of the slag and on the interfacial tension slag-steel. Surface tension (−−−) C/A=1.5; (− − −) C/A=1. Interfacial tension (——) C/A=1.5; (— — —) C/A=1.*

The maximal solubilities at the temperature1873K, obtained from the regression relation are S=2,092% in slag C/A=1,5 and S=1,464% in slag C/A=1, identical with experimental values[21].

Data regarding the influence of the sulphur content in terms of mass content on the surface tension of slags in the system $CaO-Al_2O_3$ and on the interfacial tension steel-slag were found only in the ref.[1,2] at temperature 1873K, for slag A and B.

Based on them, using points derived from curves, statistical relations were derived (**Table 1**) for the dependence upon sulphur content, of the surface tension in slags and of the interfacial tension steel–slag (**Figure 2**).

In the **Figure 3** it is shown the variation of the concentration coefficients of the surface tension $|\partial\sigma/\partial(S)|$, and of the interfacial tension $|\partial\sigma_i/\partial(S)|$ upon the sulphur content in slag for slags C/A=1.5 and C/A=1. In the reported experiments[1,2] a low carbon steel (0.11%C; 0.44%Si; 1.32%Mn; 0.022%P; 0.035%S; 0.0045%O; 0.0115%N) and ARMCO® iron have been used. According to the **Figure 2**, there is a closed relation between the interfacial tension in the system steel-slag ($CaO-Al_2O_3-CaS$) and the surface tension in the slag $CaO-Al_2O_3-CaS$, at 1873K.

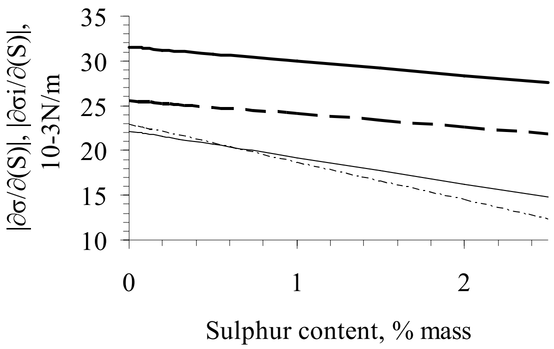

***Fig. 3**. Variation of the concentration coefficients of the surface tension|$\partial\sigma/\partial(S)$|, and of the interfacial tension |$\partial\sigma_i/\partial(S)$| upon the sulphur content in slag.*
|$\partial\sigma/\partial(S)$| ━━C/A=1.5 ; ━ ━ C/A=1;
|$\partial\sigma_i/\partial(S)$| —— C/A=1.5 ; — · — C/A=1;

This is expressed using a coefficient R, representing the ratio between the two quantities, computed for each value of the ratio C/A (**Figure 4**). Values of R_A and R_B show a similar evolution up to contents of 1.5-2.0%S, which are frequent at the end of desulphurization process at a plant scale, applied to low carbon steels under slags, based on CaO-Al_2O_3 system. Respecting the ratios R_A and R_B, it would be possible a treatment of some aspects regarding the interfacial tension slag-steel on the basis of the surface tension in the slag.

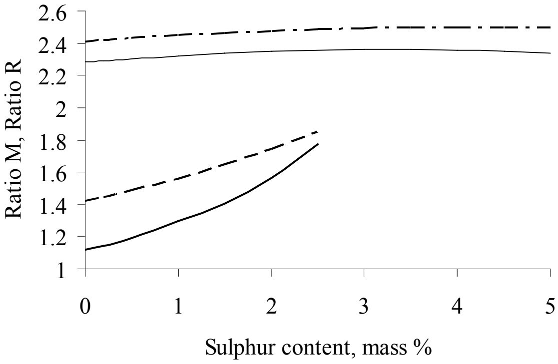

***Fig. 4.** Evolution of the ratio R=σ_i/σ and of the ratio M=$\partial\sigma_i/\partial(S)$ /$\partial\sigma/\partial(S)$ upon the sulphur content in slag CaO-Al_2O_3-CaS at 1873K; σ-surface tension in slag, σ_i-interfacial tension steel- slag, $\partial\sigma_i/\partial(S)$-concentration coefficient of the interfacial tension, $\partial\sigma/\partial(S)$- concentration coefficient of the surface tension.*
Ratio R (−−−) C/A=1.5;(− · − · −)C/A=1.
Ratio M (——) C/A=1.5; (− − −) C/A=1.

In general terms this would suggest that in order to study the solutal effects in the desulphurization slag, due to sulphur content, besides the classical treatment according to the two layers model (slag-steel) with an interface between them, the ”one layer” model would be applicable in the conditions of introducing factors representing the essential aspects of the connection with the real system. In this sense it is to be taken into account the variation of the concentration coefficients of the surface tension |$\partial\sigma/\partial(S)$|, and of the interfacial tension |$\partial\sigma_i/\partial(S)$| upon the sulphur content in slag, shown in **Figure 3** and the evolution of the ratio M = $\partial\sigma_i/\partial(S) \,/\, \partial\sigma/\partial(S)$, between the concentration coefficient of the interfacial tension and the concentration coefficient of surface tension. In **Figure 4**, both relations are shown, being derived in this paper from initial relations given in **Table 1** and represented in the **Figure 1**. The quantity viscosity is sensitive to the local precipitation of CaS and exerts an influence on the local dynamics induced by solutal effects of the sulphur content. Therefore, in this paper the slag will be considered at concentrations of sulphur in slag, far from saturation, being fully liquid.

3. Parameters for the onset of solutal Marangoni instability in slag due to sulphur

If the thermal equilibrium in the system steel-slag is considered and the electrical phenomena at interface are neglected, the instability/stability at the interface on the slag side is determinate by the competition between the actions of gravity, diffusion/viscosity and capillarity due to the solutal effects, further called as solutocapillar effects or solutocapillarity. In this paper the slag will be considered according to the concept of one layer model. The slag is taken as a separate fully liquid phase, connected to the desulphurization process by the effective transfer coefficient of sulphur (k_{eff}), also by the evolution of the surface tension and of the interfacial tension steel- slag. The Marangoni solutal effect acts at macroscale, by imposing gradients of concentration through external actions[22)], or at microscale when local gradients of concentration appear due to local inhomogeneities of different origins, along the interface or across it. The actions of gravity, diffusion/viscosity (called also viscous diffusion) and solutocapillarity are competing according to their time scales:

- the gravitational time scale, $t^2_{grav}= L/g$ (2)
- the diffusive-viscosity time scale,
$t^2_{diff}=t_{diff}\cdot t_{visc}=(L^2/D)(L^2/\nu)=L^4/\nu\cdot D$ (3)
- the solutocapillary time scale,
$t^2_{solutocap}=\rho\cdot L^3/|\partial\sigma/\partial(S)|\cdot\Delta S$ (4)

The solutocapillarity is a factor of instability while the viscosity/diffusion and gravity act as stabilizing factors by damping the effects of this instability. Viscous diffusion acts to dampen the concentration fluctuations and the associated fluid flow. The gravity acts physically to flatten the interface and thus to stabilize the deformational perturbations. All these actions are competing and the dominating action in this competition is the one having the shortest time scale. When solutocapillary effects are analysed in local dynamics, the conditions when solutocapillarity time scale is the shortest, among the others, must be evaluated. The overcoming of the neutral stability conditions, mainly of a threshold, leads to the hydrodynamic instability of the interface on short scale and on long-scale, caused by the surface tension gradients (the Marangoni effect). This instability presents different convective patterns as regular convective structures (rolls, hexagons), interfacial waves and chaotic convective motions in the vicinity of the interface, called also interfacial turbulence. In this paper only the short scale of solutal capillary effects are considered, in the form of local Marangoni flow and adjacent convection, because the most part of observed waves at steel-slag interface are short-wavelength waves[23)] and there are not satisfactory explanations for this. Taking into consideration values of the characteristic difference $\Delta(S)$, representing a moderate fraction from the limit of sulphur solubility, possible to appear by normal local fluctuation of factors, it remains to consider the value of the coefficient $|\partial\sigma/\partial(S)|$ of interfacial tension variation with concentration and the magnitude of the characteristic length (L).The characteristic length scale(L) is very important when the characteristic time scales of different actions, involved in the appearance of instability, are computed. The characteristic length can be scaled using the dimensionless number Galilei, used in fluid dynamics and defined by the following equivalent relations:

$$\text{Ga}=\text{gravity force}/\text{viscosity force}=\text{Bo}/\text{C} \qquad (5)$$

$$\text{Ga}=t^2_{\text{diff}}/t^2_{\text{grav}}=g\cdot L^3/\nu\cdot D \qquad (6)$$

The dimensionless number Bond (Bo) is the most common comparison of gravity and surface tension effects, usually used to find the characteristic length scale in complex scaling problems. The dimensionless Bo number allows a comparison of the effect of surface tension in making a spherical meniscus with the effect of gravity in keeping the surface flat over length scales of order L.A value Bo<1 indicates that surface tension dominates. The crispation dimensionless number (C) represents the relative effect of viscous/ diffusion forces versus surface tension acting across an interface between a liquid and a gas, or between two immiscible liquids, on a certain thickness. At values $C<10^{-5}$, flow is strongly dominated by surface tension forces. This is the case of the system steel- slag (CaO-Al_2O_3) which presents high value of the interfacial tension, also of the desulphurization slag slag CaO-Al_2O_3, containing sulphur in the limits of solubility. The characteristic length scale is frequently understood as depth, considered from the free surface or from an interfacial surface towards inside of a liquid. It can be equally considered also as an non-oriented distance from a point on interface along it, because of the radial aspect of the diffusion. The neutral stability boundary, for monotonic instability mode, giving values of the Ma(k)-Marangoni number is a function of the wave number k. The neutral curve has only one minimum Ma_s^c for critical values $k_c\neq0$, at around around $k_c=1.993$, for the dimensionless numbers Biot solutal $Bi_s=0$ and adsorption $N_a=0$ which correspond to the moments just before the onset of the convection due to solutal effect. By linear analysis, a minimal value for $Ma_s^c=79.6\approx80$[3)] was computed. For convenience a round value $Ga=3/2Ma_s^c=120$ is adopted, considering that it is large sufficiently, so that the response time of gravity is short enough that deformational perturbations are quickly stabilized, and the short scale convection, due to solutal perturbations, is the primary instability. Scaling the characteristic length (L) using the value of Ga=120 at $Ma_s^c=80$ and taking the normal gravity acceleration $g=9{,}81m^2/s$, the following relations are obtained for the treshold of stability/instability and for convection onset:

$$L=(Ga\cdot\nu\cdot D\cdot g^{-1})^{1/3}=(3/2Ma_s^c\cdot\nu\cdot D\cdot g^{-1})^{1/3}=$$
$$=2.30411(\nu\cdot D)^{1/3} \quad \text{, m} \qquad (7)$$

$$Ma_s^c=2/3Ga^c=2/3gL^3\cdot\nu\cdot D \qquad (8)$$

Based on the rel. (1)(7)(8), the resulting critical thresholds of concentration $\Delta(\%S)^c$ and of the surface tension $\Delta\sigma_c$ for the value of $Ma_s^c = 80$ are given by the folowing relations:

$$\Delta(S)^c=Ma_s^c\cdot\rho\cdot\nu\cdot D\cdot L^{-1}|\partial\sigma/\partial(S)|^{-1}=$$
$$=34.721\rho\cdot(\nu\cdot D)^{2/3}\cdot|\partial\sigma/\partial(S)|^{-1} \qquad (9)$$

$$\Delta\sigma_c=|\partial\sigma/\partial(S)|\cdot\Delta(S)^c=Ma_s^c\cdot\rho\cdot\nu\cdot D\cdot L^{-1}=$$
$$=34.721\rho\cdot(\nu\cdot D)^{2/3} \qquad (10)$$

The parameters of the onset solutal instability depend on the physical data ρ, ν, D and on the coefficient of surface/ interfacial tension variation with concentration of sulphur. The values of the characteristic length scale L and of the parameters $\Delta\sigma_c$, $\Delta\sigma_c$ are given in **Table 2** for available values of density ρ and dynamic viscosity η of CaO-Al_2O_3 slags at 1873K and the established dependences for $\partial\sigma/\partial(S)$ and $\partial\sigma_i/\partial(S)$, given in **Table 1**.

4. Parameters of solutal Marangoni effect acting in the local mass transfer enhancement

The Marangoni flow, at a velocity scaled by Marangoni velocity ($V_M=|\partial\sigma/\partial(S)|/\nu$) will affect the movement of the layers beneath the interface, on the side of the slag, up to a certain depth considered from the flat surface.

The characteristic thickness of the layer, within which the velocity changes significantly, due to the dissipation of the movement energy is given in the relation (11), according to the ref.$^{24)}$:

$$\delta_v \cong (\nu_0\tau)^{1/2}\text{ , m} \qquad (11)$$

where ν_0-kinematic viscosity; τ-time scale of the tangential motion, here this being the solutocapillary time scale taken only as the dominant action.

The significant velocity changes must be understood as a decrease with one order of magnitude. Inserting the time scale of Marangoni motion, given by the relation (3) the following relation is obtained:

$$\delta_v \cong \{\nu_0[\rho\cdot L^3/|\partial\sigma/\partial(S)|\cdot\Delta(S)]^{1/2}\}^{1/2}= =\nu_0^{1/2}[\rho\cdot L^3/|\partial\sigma/\partial(S)|\cdot\Delta(S)]^{1/4}\text{ , m} \qquad (12)$$

The characteristic thickness, corresponding to critical conditions is the following:

$$\delta_\upsilon^c \cong \nu^{1/2}(\rho\cdot L^3/\ Ma_s^c\cdot\ \rho\cdot\nu\cdot D\cdot L^{-1})^{1/4} = =0.53474(Ma_s^c)^{1/12}(\nu^7\cdot D)^{1/12}=0.7704\nu^{0,58(3)}\cdot D^{0,08(3)}\text{, m} \qquad (13)$$

***Table 2**. Values of relevant parameters in characterization of the influence of the sulphur content in instability threshold and onset of Marangoni convection in desulphurization slags CaO-Al$_2$O$_3$ at 1873K.*

Slags data / Characteristic Quantities, parameters	C/A=1.5;ρ=2685kg·m^{-3}		C/A=1.0; ρ=2710kg·m^{-3}	
	Surface tension	Interfacial tension	Surface tension	Interfacial tension
Characteristic length scale L, 10^{-6}m	$^{a)}$ 53.881; $^{b)}$ 59.882; $^{c)}$ 71.227		$^{d)}$63.651; $^{e)}$67.529	
$\Delta\sigma_{crit}$=[($\partial\sigma/\partial$(S))Δ(S)]$_{crit}$, 10^{-6} N·m^{-1}	$^{a)}$51.01 ; $^{b)}$62.83; $^{c)}$89.09		^{d})71.81; $^{e)}$79.62	
Characteristic thickness δ_v^c, 10^{-6} m	$^{a)}$355.76; $^{b)}$427.15; $^{c)}$579.77		$^{d)}$476.20; $^{e)}$521.23	
Concentration coefficients $\partial\sigma/\partial$(S), $\partial\sigma_i/\partial$(S), 10^{-3} N·m^{-1}·(mass% S)$^{-1}$	4.2434(S)- -22.922	1.4706(S)- -25.504	2.9562(S)- - 22.159	1.5856(S)- -31.548
Critical concentration of sulphur Δ(S)$_{crit.}$, 10^{-4} mass % C/A=1.5: 0-2.092(%S) C/A=1.0: 0- 1.464(%S)	$^{a)}$22.25-36.32 $^{b)}$27.41-44.73 $^{c)}$38.86-63.43	$^{a)}$20.0-22.74 $^{b)}$24.63-28.0 $^{c)}$34.93-39.72	$^{d)}$32.41-40.27 $^{e)}$35.93-42.41	$^{d)}$22.76-24.57 $^{e)}$25.24-27.24
Minimal concentration of sulphur Δ(S), (10^{-4} %) for onset instability with turbulent convection (ε=6.3)	$^{a)}$140.18-228.82 $^{b)}$172.68-281.8 $^{c)}$244.82-399.61	$^{a)}$126-143.26 $^{b)}$155.17-176.46 $^{c)}$220.06-250.24	$^{d)}$204.18-253.70 $^{e)}$226.36-267.18	$^{d)}$143.4-154.8 $^{e)}$159-171.6

Quantities and parameters in **Table 2**, noted $^{a),b),c), d),e)}$, followed by computed values corresponding to the same noted dynamic viscosities in **Table 1**.

According to rel. (12), the increasing of the value of $\Delta\sigma =|\partial\sigma/\partial(S)|\cdot\Delta(S)>\Delta\sigma_c$ will lead to a local and temporary decreasing of the value of δ_v. On Earth (g=9.81m/s^2), the critical values of the quantities involved in the threshold conditions for onset of instability at Ma_s^c=80, that means L, $\Delta\sigma_c$, δ_υ^c, at an established temperature, depend only upon the physico-chemical values of the slag, ν-kinematic viscosity of slag and D- mass diffusion coefficient of sulphur in slag. These values are presented in **Table 2**, together with other important parameters in the evaluation of the Marangoni convection, also in other conditions than those critical. The magnitude of δ_v is the same with the diffusion layer thickness and decreases when the time scale of the tangential motion(τ) decreases. The obtained values of δ_υ^c (**Table 2**) sustain that the Marangoni convection by natural gradients of surface/interface tension, including those solutal of different origins as interfacial reactions or the transport of a surface active solute through interface, acts at microscale, in interface layers of thickness below 10^{-3}m. A comparison with data obtained for a low carbon steel, aluminium killed, similar as composition to the steel in ref.$^{1,2)}$, at 1873K leads to interesting results. In this case taking the for the kinematic viscosity a value ν=5.425·10^{-7}m^2/s,$^{25)}$ ρ= 6970kg/m^3 and the sulphur coefficient in steel D=4.4·10^{-9} m^2/s,$^{26)}$ the similar critical values for an unperturbed flat steel layer of infinite depth are L=25.972·10^{-6}m, $\Delta\sigma_{crit}$=30.748·10^{-6} N.m^{-1} , δ_υ^c =32.911·10^{-6}m. It is obvious the nearness of the critical value for the instability threshold of the quantity $\Delta\sigma_{crit}$ for slag and steel, and the values of the characteristic length L in steel are half from the values in slag. The major differences are observed when the values of δ_υ^c are compared. In both phases, the interfacial instability of solutocapillary origin, could arise almost simultaneously and further, this could be a source of self-sustained capillary effects, including the appearance of the strong turbulent, up to violent aspects at interface, with favourable consequences for desulphurization of steels under adequate slags. A mass transfer coefficient of sulphur through the interface between slag and steel k_{eff}=5.52·10^{-5} m·s^{-1} is reported,$^{5)}$ at 1873K in systems containing lime saturated slag (CaO-MgO-Al$_2$O$_3$-SiO$_2$), under definite and very moderate flow conditions of liquid aluminium-deoxidized iron, induced by argon bubbling. This value could be obtained by the boundary-layer theory applied to the metal/slag interface. 5)Taking a thickness of the liquid film at interface in steel $\delta=(100-200)\cdot10^{-6}$m, in conditions of local interfacial turbulence and the mass diffusion coefficient of sulphur in liquid steel $D_{[S]}=4.4\cdot10^{-9}$m^2/s, it results a mass transfer coefficient in the liquid steel $k_{steel}=(2.2-4.4)\cdot10^{-5}$m^2/s, confirming by comparison with the value of k_{eff} that the limiting step of the sulphur transfer is the sulphur transport in slag, which opposes the main resistance to this transfer. According to the film layer theory, taking into account the diffusion of sulphur through the limit layer in slag as transport mechanism in quasi-static conditions, the mass transfer coefficient is $k_D = D/\delta$. A value $D_{(S)}=2.9\cdot10^{-10}$ m^{2}s^{-1} at 1873K is computed from data at 1718K 19) and a thickness of the liquid film in the slag $\delta=200\cdot10^{-6}$m is obtained in dynamic conditions.

It results a mass transfer coefficient, by the simple mass diffusion in slag for sulphur, $k_D=1.45\cdot10^{-6}$ ms^{-1}. in quasi-static conditions and an enhancement factor of the mass transfer $\varphi=k_{eff}/k_D \cong 38$. This leads to the necessity to consider also another type of mass transfer which assumes that mass transfer is a nonsteady-plate process, in this case due to the Marangoni flow and convection by solutocapillary effects. This could be the boundary diffusion layer theory but in a modified vision.

The main modification consists in considering the mass transfer in a boundary layer at interface on the slag side where the surface tangential stress due to sulphur solutal Marangoni effect, scaled by Marangoni speed, increases the mass transfer of sulphur. This takes place by energy dissipation of the slag flow, towards the bulk, in a boundary layer of thickness $\delta_{eff}= \delta_v$, this last being given by the rel. (12).

In **Figure 5 a** and **5b** are established the conditions of sulphur characteristic concentration, Δ(S) leading to the obtaining of values $\delta_{eff}=200\cdot10^{-6}$m and $\delta_{eff}=300\cdot10^{-6}$m.Values $\delta_{eff}=200\cdot10^{-6}$m are obtained in a restricted area of accessible conditions.

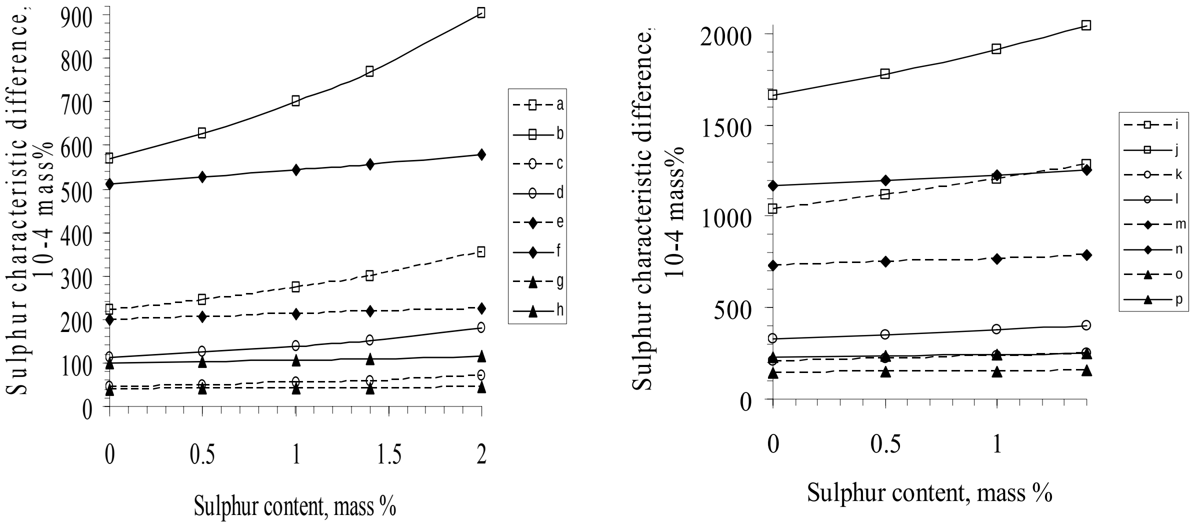

Fig. 5. a, b. *Computed values of the sulphur characteristic difference Δ(S) for obtaining imposed values of effective layer thickness (δ_{eff}), in CaO-Al$_2$O$_3$ slags at 1873, as function of sulphur concentration in slag, at C/A=1.5 (fig. 5a) and C/A=1.0 (fig. 5b), for quantities and parameters from tab.1 and tab.2. 1)$\delta_{eff}=200\cdot10^{-6}$m (a,b,e,f-fig. 5a) (i,j,m,n-fig. 5b); 2)$\delta_{eff}=300\cdot10^{-6}$m (c,d,g,h-fig. 5a) (k,l,o,p-fig. 5b); 3) considering the sulphur concentration coeficient of surface tension(a,b,c,d-fig. 5a)(i,j,k,l-fig. 5b); 4) considering the sulphur concentration coeficient of interfacial tension(e,f,g,h-fig5a) (m,n,o,p-fig. 5b); 5) η=0.1184Pa·s(a,c,e,g-fig5a); for η=0.162Pa·s(b,d,f,h-fig5a); η=0.197Pa·s (i,k,m,o-fig. 5b); η=0.23Pa·s (j,l,n,p-fig. 5b).*

Boundary layers δ, also the scales of phenomena and instabilities are different for different species and processes and co-exist many in the same time. Therefore it must be mentioned once again that in this paper only the influence of sulphur is analysed, as solute in the mentioned slag. In these conditions, the mass is transferred through the interface not only by molecular diffusion but also by turbulent diffusion, determining a kinetic characteristic under the form of an effective diffusion coefficient D_{eff}, taken into account as the sum of the molecular diffusion (D) and the turbulent diffusion (D_t):

$$D_{eff}=D+D_t=D(1+D_t/D) \qquad (14)$$

In fully turbulent conditions, considered at local scale, due to high values of Marangoni speed, the transfer by turbulent diffusion is dominant and at weak tangential surface stress, the main mass transfer mechanism is the molecular diffusion. In intermediary conditions both two mechanisms participate at the mass transfer, in a sensitive manner.

Dividing the rel (14) at the effective thickness δ_{eff} it is obtained:

$D_{eff}/\delta_{eff} = D/\delta_{eff} + D_t/\delta_{eff}$ (15)

Noting $k_{eff} = D_{eff}/\delta_{eff}$; $k_D = D/\delta_{eff}$; $k_t = D_t/\delta_{eff}$, (16)

the relation (15) becomes:

$k_{eff} = k_D + k_t = k_D(1+k_t/k_D)$ (17)

An adequate effective thickness of the boundary layer δ_{eff} will be convenient simultaneously for molecular and the turbulent diffusion and could be the thickness δ_v (rel 12.) for the dynamic case by Marangoni effect. In this paper the ratio $\Delta\sigma/\Delta\sigma_c$ is proposed as a measure for the ratio k_t/k_D. Besides the known significance of $\Delta\sigma_c$, $\Delta\sigma$ is variation of the surface tension of the slag at a value $\Delta(S)>\Delta(S)^c$ at the considered sulphur concentration of slag in bulk. A relation, giving the effective mass transfer coefficient k_{eff}, as a function of the mass transfer coefficient by diffusion k_D and of the variation of the interfacial tension $\Delta\sigma$, exceeding a certain critical value $\Delta\sigma_{crit}$, was proposed[28)], in the following form:

$k_{eff} = k_D[1+\alpha(\Delta\sigma-\Delta\sigma_{crit})]$ (18)

Taking into consideration the the proposal made in the present paper and identifying here $\Delta\sigma_{crit}$ from rel. (18), by $\Delta\sigma_c$ from the rel (10), the relation (18) can be written under other useful forms:

$k_{eff} = k_D[1+\alpha(\Delta\sigma-\Delta\sigma_c)] = k_D[1+ \alpha\Delta\sigma_c(\Delta\sigma/\Delta\sigma_c-1)] = k_D[1+ \alpha\Delta\sigma_c(Ma/Ma_c-1)]$ (19)

$k_{eff}/k_D = 1+k_t/k_D = 1+ \alpha\Delta\sigma_c (Ma/Ma_c-1)$ (20)

The proportionality constant α has the dimension [m/N] and in the present case it has very high values because of the very small values of $\Delta\sigma_c$ (Tab2). It was established that in the above mentioned condition, the distance from the threshold of the instability is given by a parameter ε:[29)]

$\varepsilon = (Ma_s - Ma_s^c)/Ma_s^c$ (21)

At values $2.1<\varepsilon<6.3$, convection consists in rolls and hexagonal cells.The turbulent convection is installed at values $\varepsilon>6.3$[29)] and consists in mixed rolling cells and hexagonal cells, becoming directly turbulent, even chaotic at higher values of Ma_s and respective of ε. The analysis of instability threshold and convection at high and very high Marangoni numbers needs a specific treatment. It results from rel. (18)–(21):

$k_{eff} = k_D(1+ \alpha\cdot\varepsilon\cdot\Delta\sigma_{crit}) = k_D(1+\beta\varepsilon)$ (22)

The rel.22 makes a reunion of the specific and critical conditions by the product between $\beta = \alpha\cdot\Delta\sigma_{crit}$ and the distance from the threshold of instability ε, in the local enhancement of the mass transfer coefficient. The rel.(22) contains factors which can be computed, including the proportionality constant α.For $\varepsilon=6.3$, $k_{eff}=5.52\cdot10^{-5}$ m·s^{-1},[5)] $\Delta\sigma_{crit}$ (**Table1**),

$D_{(S)} = 2{,}9\cdot10^{-10}$ m^2/s(tab1), $\delta_{eff} = 200\cdot10^{-6}$m, it results α=115349m/N and β=5.88 for slags C/A=1.5. The use of coefficient β is more convenient for magnitude and missing of dimension reasons.

The contribution of the surface and interfacial tension, by their individual sulphur concentration coefficients to the development of surface driven instability and convection, depends upon the magnitude of the sulphur characteristic concentration Δ(S). It is remarkable the great sensitivity of the parameter Δ(S) to the cumulated action of the involved factors giving its value. Separately, each of these factors does not differ too much from one set of conditions to another (**Table 1** and **Table 2**).

The effective influence of the solutal effect of sulphur, exerted by the threshold of the characteristic difference of concentration of sulphur in slag Δ(S) and of the influence exerted by the slag characteristics results more clarely, in from **Figure 5a** and **5b** which were built to obtain imposed values of effective layer thickness-δ_{eff} ($200\cdot10^{-6}$m and $300\cdot10^{-6}$m) in CaO-Al_2O_3 slags at 1873K, as function of sulphur concentration in slag, at C/A=1.5 and C/A=1.

The values of δ_{eff} were selected because of their large acceptance as limits of magnitude of the boundary layers thickness, included in diffusive problems, in many metallurgical liquid systems strongly stirred. The local dissipative flow, due to the short scale and short wave-length waves Marangoni convection, at the mentioned characteristic length scales L_c (**Table 2**) and δ_{eff} (including also other values than the two considered) represents an important stirring factor, intensifying the mass transfer.As it is shown in **Figure 5a, b** the range of the required values of Δ(S), for the same set of values of factors, varies within a maximal range up to 12-15 times considering the sulphur concentration coefficient of surface tension and the sulphur concentration coefficient of interfacial tension in the case of slag C/A=1.5. This parameter, involved in the threshold conditions of instability, represents in fact a threshold value of local fluctuation of the concentration of sulphur, taking into consideration its possible origins and the mechanisms which average these fluctuations. The magnitude of the local effective fluctuations, which cannot be however high, leading to an effective influence, could be considered statistically in the range up to about 3- 4% from the maximal solubility of sulphur in slag and these are taken into account as reference values in the present paper. At higher contents of sulphur in slag, closed to the maximal solubility in slag, a higher level of the sulphur fluctuation of concentration could overcome locally this solubility and the amount of sulphur exceeding its precipitates as CaS, thus modifying the local dynamic viscosity of slags. Such a situation must be evaluated separately as consequences in instability and mass transfer enhancement. An important reason for which only local and small amplitude of sulphur concentration fluctuations are taken into account in this paper is that, at higher values of these, local gradients of other quantities become of a significant magnitude for the instability conditions and deviate from the conditions of the present analysis. The computed data show an increased sensitivity of $\Delta(S)$ values upon the sulphur content in slags when sulphur concentration coefficient of surface tension is taken into account according to curves (a,b,c,d-**Figure 5a**) and (i,j,k,l-**Figure 5b**) and a less important sensitivity when the sulphur concentration coeficient of interfacial tension is considered, according to curves (e,f,g,h-**Figure 5a**) and (m,n,o,p-**Figure 5b**), mainly determined by the regression relations established statistically (**Table 1**).

The considered values of the dynamic viscosities of slags exert a major influence in the obtained values of $\Delta(S)$ at the same value of δ_{eff} for the considered slags. In slag C/A=1.5, considering the case $\delta_{eff} = 200 \cdot 10^{-6}$m and the sulphur concentration coefficient of surface tension, a value $\Delta(S)=215\text{-}320 \cdot 10^{-4}$ mass % is obtained for the dynamic viscosity $\eta=0.1184$Pa·s and a value $\Delta(S)=570\text{-}900 \cdot 10^{-4}$ mass % is obtained for the dynamic viscosity $\eta=0.162$Pa·s. Both values of $\Delta(S)$ seem to be acceptable according to the before mentioned aspects regarding the possible magnitude of the sulphur concentration fluctuations considered. In slags C/A=1, mainly because of the higher values of the dynamic viscosities, the required values of $\Delta(S)$ to produce mixing effects in the diffusion of boundary layers at interface are too high to be accepted when sulphur concentration coefficient of surface tension is taken into account (**Figure 5b**-i,j) also for considering the sulphur concentration coefficient of interfacial tension (**Figure 5b**-n,m). To all these aspects it must be added the lower value of the sulphur solubility limit S=1.464mass% (**Table 1**), which acts as a prohibitive factor in the range of higher values of sulphur contents in slag C/A=1.

5. Conclusions and commentaries

Using the one layer model of slag, it was simulated the local possible dynamic behaviour of the interface slag-steel on the slag side, when the sulphur content in slag increases during desulphurization of steel under slag. For the considered data, it was found that despite the major differences in magnitude between the surface tension of the slag $CaO\text{-}Al_2O_3$ and of the interfacial tension steel –slag the dependences upon the sulphur content at both two considered compositions, the two quantities present a quasi-parallel evolution up to 1.5-2mass% sulphur contents in slag, also their concentration coefficients for more than this, the sulphur concentration of the surface tension of the slag $CaO\text{-}Al_2O_3$ and the interfacial tension steel –slag are very closed as values. Therefore only them alone can not contribute to clarify major aspects of solutocapillarity effect and its possible contributions to local interfacial dynamics of slag and further to mass transfer aspects, especially of sulphur. In established conditions where the solutocapillary Marangoni effect has the smallest time of action, the instability threshold consisting in values for the critical differences $\Delta\sigma_c$ and $\Delta(S)^c$ were established for onset solutal Marangoni convection in slag, for critical value of the solutal Marangoni number $Ma_s^c=80$ and wave number $k_c=1.993$. Despite their differences, the threshold found values in slags C/A=1.5 and C/A=1; they are very closed and depends only on the physico-chemical data of the slag, density ρ, kinematic viscosity ν and mass diffusion coefficient of sulphur in slag D_S, at the considered temperature. Values of the local sulphur content differences taken as local possible fluctuations of sulphur content in the threshold of instability for onset the Marangoni flow and convection by in minimal conditions of monotonic neutral stability, are of order of tens of ppm sulphur, being below the usual contents of sulphur in slags and of the precision of usual analyse is methods. The threshold of sulphur concentration and of the variation of surface tension/interfacial tension for onset the turbulent flow and further for the chaotic flow are functions of a parameter ε describing the distance from the threshold of the instability. An enhancement coefficient of the mass transfer of sulphur at interface on the slag side is established in the conditions of the onset Marangoni flow and convection. A parameter β was introduced to makes a reunion of the specific and critical conditions in the local enhancement of the mass transfer coefficient, besides the existing parameter ε for the distance from the threshold of instability. The parameter $\Delta(S)$ was found to express better the instability conditions and the conditions of mixing effects in layers near the interface, by energy dissipation of Marangoni flow and seems to be able to take account of important differences between conditions in slags C/A=1.5 and C/A=1. Due to the cumulated actions of $CaO\text{-}Al_2O_3$ slag parameters, it was established that in the case of slag C/A=1.5 the magnitude of the parameter $\Delta(S)$ is sensible lower than in slag C/A=1 that means in the slag C/A=1.5.

Small fluctuations of sulphur concentrations, higher enough than the critical values $\Delta(S)^c$, up to values representing 3-4% from limit of sulphur solubility in $CaO\text{-}Al_2O_3$ slags can excite and sustain Marangoni instability at interface, determining the corresponding Marangoni flow of turbulent character and energy dissipation in an effective layer of thickness δ_{eff} of the same magnitude with thickness of the diffusion bondary layer. In slags C/A=1.5 compared to slag C/A=1 there are better conditions that desulphurization contributes to its self-sustaining of surface dynamics and sulphur mass transfer enhancement by solutal effect of sulphur. An important uncertainty of computed values is introduced by the differences between the reported values of slags parameters in different published papers, mainly of the kinematic viscosity, dynamic viscosity, also of the density, but in a lower measure and of the isothermal mass diffusion coefficient of sulphur, determined experimentally or established using models. The approach of the presented problem and the quantitative results obtained on the mentioned basis contributes to an improved vision on the efficiency of CaO-Al_2O_3 slag contribution, in the dynamic aspects of desulphurization of aluminium killed steels, under slag. The results plead for a self-sustained dynamics of desulphurization of steels under CaO-Al_2O_3 slag, in determine conditions.

The revealed dynamic aspects can contribute also to evaluating the role of CaO-Al_2O_3 slag in the assimilation of Al_2O_3 inclusions and possible of other inclusions in the slag, regarding of steel reoxidization and slag dispersion in steel. It is given a quantitative evaluation of the variation of the interfacial tension between CaO-Al_2O_3 slag and steel, during the mentioned desulphurization process, which can contribute quantitatively in more realistically establishing the conditions of occurring the interfacial instability Kelvin- Helmholtz and its specific wavelength.

References

[1]. van Muu, B. Frenzke, H-W - Freib. Forshungs.B Metall. Werkstofftech., B252(1985), 40.

[2]. van Muu, B. Frenzke, H-W.Neuhof, G. - Neue Hutte, 29(1984), 128.

[3]. J.Pearson - J.Fluid Mech., 4(1958), 489.

[4]. V.G.Levich, V.S. Krylov - Annu.Rev. Fluid Mech., 1(1969), 293.

[5]. J.Deng, F.Oeters - Steel Res., 61(1990), 438.

[6]. P.Colinet, J.C. Legros, M.G.Velarde - *Nonlinear Dynamics of Surface Tension Driven Instabilities*, Wiley-VCH, Berlin,(2001),95,128.

[7]. C.A. Miller, P. Neogi editors - *Interfacial Phenomena: equilibrium and dynamic effects,* second edition, CRC Press, Taylor&Francis Group,(2008), 317-369.

[8]. A.S. Panov, I.S.Kulikov, L.M. Selev - Isv.Akad.Nauk SSSR, otdel Teckn.nauk, Metallurgiya i toplivo, 3(1961), 25.

[9]. V.V Dymov, V.V. Baidov - Sb.Tr.Tsent. Nauch-Issled Inst. Chem.Met., 619(1968), 78.

[10]. G.I. Zhmoidin, L.N.Sokolov, G.V.Podgornov, G.S. Smirnov - Teoriya Metallurgicheskih Protsesov, 3(1975), 150.

[11]. S. Hara, K.Ogino - Can.Met.Quaterly, 20(1981), 113.

[12]. M. Zelinski, B. Sikora - Pr.Inst.Metall, Zelaza im St.Staszica, 29 (1977), 157.

[13]. T. El Gammal, R.-D. Müllenberg - Arch. Eisenhüttenw.51 (1980), 221.

[14]. B.Sikora, M. Zelinski - Hutnik 41(1974), 433.

[15].*** Slag Atlas, 2nd Edition, Verlag Stahleisen, D-Düsseldorf, (1995), fig.9.61.b., tab.9.15, tab9.22, 8.13, 8.14, 8.17.

[16]. P. Kozakevich - Rev. Metall , 51(1954), 571.

[17]. Elyutin, V. P., Kostikov, V.I.Mitin, B.S. Nagibin Yu.A. - Russian Journal of Physical Chemistry, 43(1969), 316.

[18]. I.I Bornatskii - Desulfuratsiya metalla, Metallurgiya, Moskva,(1970), citation Shalimov, A.G.: Ph.Dr.Thesis, Moskow, 1957

[19]. Y. Waseda, J. M. Toguri - Structure and Properties of Oxide Melts, World Scientific, Singapore, (1998), 140.

[20]. L. Jonsson, Du Sichen, P.Jonsson -ISIJ int., 38(1998), 260.

[21]. B. Özturk, E. T. Turkdogan - Met. Sci., 15(1984), 299.

[22]. G. R. Elton, T.J. Evans, L. Strezov - Phil. Trans.R. Soc.London A, 356(1998), 941.

[23]. Y. Chung, A. W. Cramb - Metall. Mater.Trans.B, 26(2000) 957.

[24]. L. D. Landau, E. M. Lifshitz - Fluid Mechanics, Pergamon Press, Oxford, (1984).

[25]. N. E. Bodakin, B. A. Baum, G. V. Tyagunov, M. N. Kushnir - Izv. A.N. SSSR Metalli, 2(1977), 59.

[26]. Y. Kaway, Y. Shiraishi - Handbook of Physico-Chemical properties at High Temperature Ed by ISIJ, Tokyo,(1982), 2.

[27]. H. L. Torr, J. M. Marchello - AIChEJ., 4(1958), 97.

[28) N. G. Maroudas, H. Sawistowski - Chem. Eng.Sci., 19(1964), 919.

[29]. J. Bragard, S. C. Slatvchev, G. Lebon - J. Colloid. Interf.Sci., 168(1994), 402.

THE ANNALS OF “DUNAREA DE JOS” UNIVERSITY OF GALATI.
FASCICLE IX. METALLURGY AND MATERIALS SCIENCE
N^0. 3 – 2010, ISSN 1453 – 083X

INFLUENCE OF INCLINATIONS APPLIED TO RIBS ON THE SOLIDIFICATION OF CAST PARTS

Aurel CRIŞAN, Diana ŢUŢUIANU,
Tibor BEDŐ, Ioan CIOBANU
„Transilvania” University of Braşov,
Faculty of Materials Science and Engineering
email: crisan.a@unitbv.ro

ABSTRACT

The inclinations and corner radii applied to ribs are designed for enhancing both stiffness and aesthetics. The presence of inclinations applied to ribs modifies the conditions of heat transmission and implicitly the solidification of the alloy in the joining area of the rib to the part wall. This is highlighted by changing the radius of circles inscribed in the wall - rib joining area. The diameter of the circles inscribed in this area is greater than of those in rest of the part wall. This leads to the assumption that the solidification of the alloy in the wall-rib joining area is slowed. The paper presents the results of a study concerning the influence of inclinations applied to ribs on the duration of cast part solidification and on the position of the hot spots. The study was conducted by computer simulation of solidification. The results have revealed that for certain limits this influence is negligible. Instead, in case of large inclinations, solidification time increases considerably. The limits for which the influence of inclinations applied to ribs becomes significant are determined.

KEYWORDS: rib inclination, cast part solidification, hot spots

1. Introduction

While representing the technological elements required by the designer or manufacturing engineer, ribs, casting slopes and corner radii of the cast parts also have an aesthetic function. Generally ribs have the role of stiffening the walls of the cast parts.

These technological elements (ribs, slopes, corner radii) influence the solidification of cast parts.

Ribs determine a local thickening of parts in the rib – part wall joining area, as highlighted by the local increase of the circle radii inscribed in the part perimeter, as shown in Figure 1.

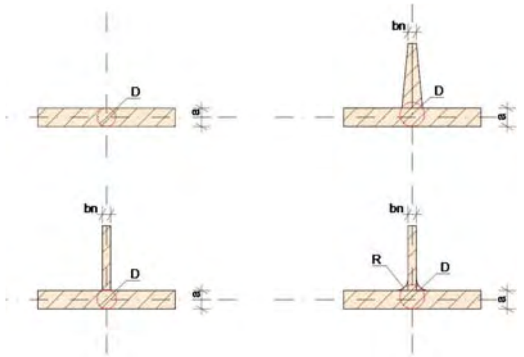

Fig. 1. *Influence of rib thickness, casting slopes and corner radii on the diameter of the circle inscribed in the contour of the cast parts.*

Consequently it is to be expected that these technological elements determine a local increase of solidification time and hence the generation of hot spots, causing on their turn solidification-specific defects (porosity, shrinkholes, cracks, etc.). The paper presents the results of a study on the influence of inclinations applied to ribs on the solidification of cast parts, and thus on the tendency of defect generation caused by solidification. The aim is to establish the magnitude of this influence and the opportunity of prevention measures. Research was conducted by computer aided simulation of the solidification process.

The dedicated „Sim-3D" software, developed at the Faculty of Materials Science and Engineering of the Transilvania University of Brasov was used.

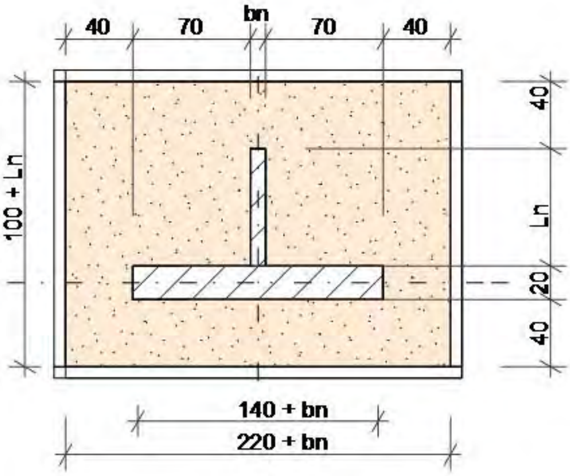

Fig. 2. *Geometry and dimensions of the part and mould.*

2. Influence of rib inclination on cast part solidification

It has been conducted a study on the influence of rib lateral face inclination on the solidification of cast parts. The study was conducted for a part of 20 mm thickness. Figure 2 shows the geometry and the dimensions of the cast parts and the mould involved in the study. Rib length was of L_n = 60 mm. The study was conducted for rib widths of b_n = 3 mm, 5 mm and 15 mm Rib inclination varied between tgα = 0 and tgα = 3/20. The rib lateral face inclination was applied by rib wall thickening. The part was cast from eutectic cast iron in a silica sand mould.

Computer simulation was used to study the influence of the rib lateral wall inclination on the position of the hot spots, solidification time, and temperature variation of the solidified fraction in the hot spots.

Table 1 features the thermo-physical characteristics of the alloy and the mould used for simulation.

Table 1. *Values of the quantities used for simulation of solidification*

No.	Parameter	Physical symbol	Measure unit	Value
1	Mesh width of mould dividing	Δ	m	0.001
2	Time interval	τ	s	0.02
3	Environment temperature for the exterior of the mould	T_{ex}	^{0}C	20
4	Thermal exchange coefficient of mould-exterior environment	α_{ex}	$W\cdot m^{-2}\cdot K^{-1}$	10.0
5	Solidus temperature of the cast alloy	T_{sme}	^{0}C	1150
6	Thermal conductibility coefficient of the mould	λ_{sfo}	$W\cdot m^{-1}\cdot K^{-1}$	0.85
7	Thermal conductibility coefficient of the solidified alloy	λ_{sme}	$W\cdot m^{-1}\cdot K^{-1}$	40
8	Thermal conductibility coefficient of the liquid alloy	λ_{lme}	$W\cdot m^{-1}\cdot K^{-1}$	30
9	Specific heat of the mould	C_{sfo}	$J\cdot kg^{-1}\cdot K^{-1}$	1170
10	Specific heat of the liquid cast iron	C_{lme}	$J\cdot kg^{-1}\cdot K^{-1}$	850
11	Specific heat of the solid cast iron	C_{sme}	$J\cdot kg^{-1}\cdot K^{-1}$	750
12	Mould density	ρ_{fo}	$kg\cdot m^{-3}$	1550
13	Alloy density	ρ_{me}	$kg\cdot m^{-3}$	6700
14	Specific latent heat of the cast alloy	L_{me}	$J\cdot kg^{-1}$	250000
15	Initial temperature of the mould	T_{0fo}	^{0}C	20
16	Initial temperature of the cast alloy	T_{0me}	^{0}C	1350

Figures 3 ÷ 14 show the distribution of isotherms in the cast part and in the mould at the solidification time of the hot spots in a number of the studied cases. Tables 2 ÷ 4 feature the coordinates of the hot spots and their corresponding solidification times. The coordinates of the hot spots are given in relation to a frame of reference corresponding to the symmetry axis of the cast part and of the rib, as shown in Figure 15.

Figure 16 presents the influence of rib wall inclination of the solidification time of the hot spots. Figures 17 ÷ 20 feature the variation curves of temperature and the solid fraction in the hot spots for several of the studied cases.

Table 2. *Coordinates of the hot spots and solidification time versus rib wall inclination (ribs of thickness b_n = 3 mm and length L_n = 60 mm).*

No.	**Rib inclination**	**No. of hot spots**	**Coordinates of hot spots**	**Solidification time**
Symbol	tg α	N_n	(x,y)	t_{sol}
u.m.	-	-	(mm,mm)	s
1	0	2	(-20.0; -0.5) and (+20.0; -0.5)	233.08
2	1/60	2	(-20.0; -0.5) and (+20.0; -0.5)	264.94
3	2/60	2	(-19.0; +0.5) and (+19.0; +0.5)	270.16
4	3/60	2	(-18.0; +0.5) and (+18.0; +0.5)	277.12
5	4/60	2	(-16.0; +0.5) and (+16.0; +0.5)	284.98
6	5/60	2	(-15.0; +0.5) and (+15.0; +0.5)	293.92
7	9/60	1	(0; -0.5)	340.36

Table 3. *Coordinates of the hot spots and solidification time versus rib wall inclination (ribs of thickness b_n = 5 mm and length L_n = 60 mm).*

No.	**Rib inclination**	**No. of hot spots**	**Coordinates of hot spots**	**Solidification time**
Symbol	tg α	N_n	(x,y)	t_{sol}
u.m.	-	-	(mm,mm)	s
1	0	2	(-19.0; +0.5) and (+19.0; +0.5)	271.58
2	1/60	2	(-18.0; +0.5) and (+18.0; +0.5)	277.42
3	2/60	2	(-17.0; +0.5) and (+17.0; +0.5)	284.88
4	3/60	2	(-15.0; +0.5) and (+15.0; +0.5)	193.44
5	4/60	2	(-13.0; +0.5) and (+13.0; +0.5)	302.62
6	5/60	2	(-12.0; +0.5) and (+12.0; +0.5)	312.64
7	9/60	1	(0; +1.5)	366.12

Table 4. *Coordinates of the hot spots and solidification time versus rib wall inclination (ribs of thickness b_n = 15 mm and length L_n = 60 mm).*

No.	**Rib inclination**	**No. of hot spots**	**Coordinates of hot spots**	**Solidification time**
Symbol	tg α	N_n	(x,y)	t_{sol}
u.m.	-	-	(mm,mm)	s
1	0	1	(0; +1.5)	365.30
2	1/60	1	(0; +2.5)	379.58
3	2/60	1	(0; +2.5)	393.66
4	3/60	1	(0; +3.5)	407.58
5	4/60	1	(0; +4.5)	421.42
6	5/60	1	(0; +5.5)	435.22
7	9/60	1	(0; +9.5)	490.94

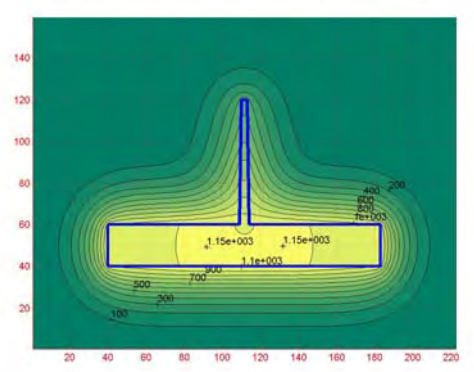

Fig. 3. *Distribution of isotherms at the end of solidification for a rib of inclination Tg α = 1/60 and thickness b_n = 3 mm (at the moment of solidification t_{sol}=264.94s).*

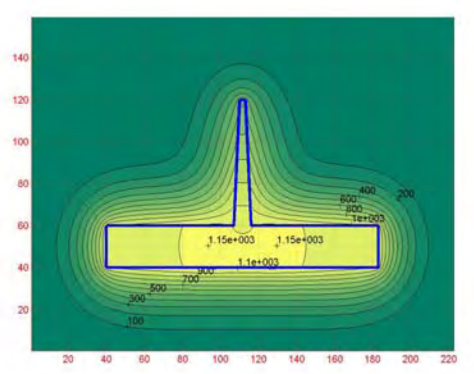

Fig. 4. *Distribution of isotherms at the end of solidification for a rib of inclination tg α = 3/60 and thickness b_n = 3 mm (at the moment of solidification t_{sol}=277.12s).*

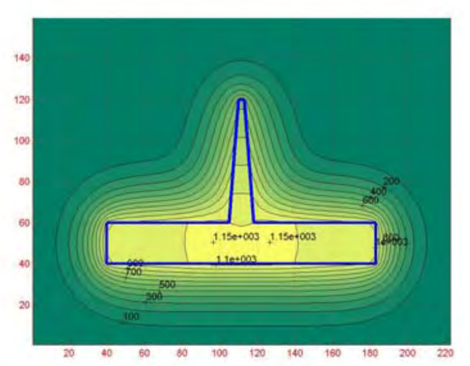

Fig. 5. *Distribution of isotherms at the end of solidification for a rib of inclination tg α = 5/60 and thickness b_n = 3 mm (at the moment of solidification t_{sol}=293.92s).*

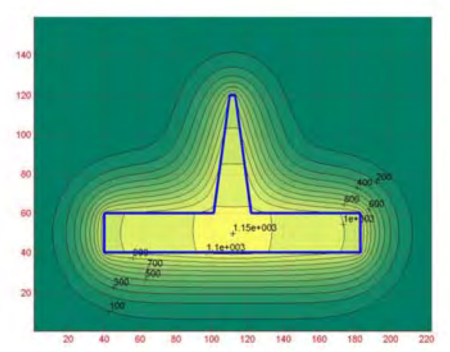

Fig. 6. *Distribution of isotherms at the end of solidification for a rib of inclination tg α = 9/60 and thickness b_n = 3 mm (at the moment of solidification t_{sol}=340.36s).*

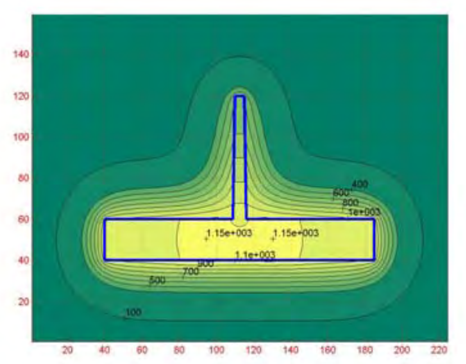

Fig. 7. *Distribution of isotherms at the end of solidification for a rib of inclination tg α = 1/60 and thickness b_n = 5 mm (at the moment of solidification t_{sol}=277.42s).*

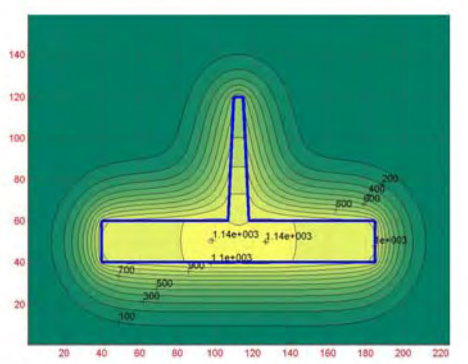

Fig. 8. *Distribution of isotherms at the end of solidification for a rib of inclination tg α = 3/60 and thickness b_n = 5 mm (at the moment of solidification t_{sol}=193.44s).*

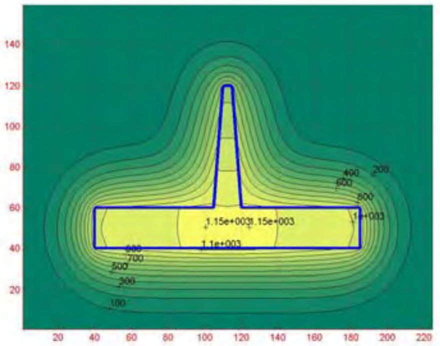

Fig. 9. *Distribution of isotherms at the end of solidification for a rib of inclination tg α = 5/60 and thickness b_n = 5 mm (at the moment of solidification t_{sol}=312.64s).*

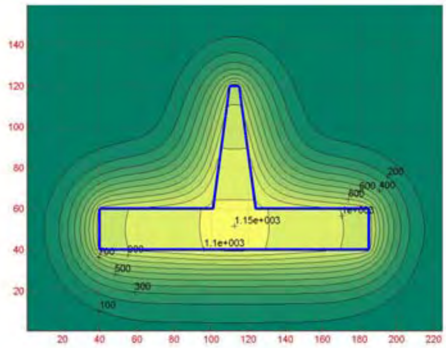

Fig. 10. *Distribution of isotherms at the end of solidification for a rib of inclination tg α = 9/60 and thickness b_n = 5 mm (at the moment of solidification t_{sol}=366.12s).*

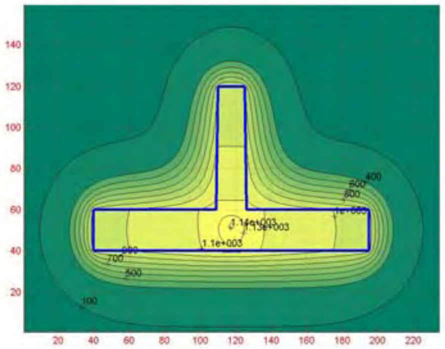

Fig. 11. *Distribution of isotherms at the end of solidification for a rib of inclination tg α = 1/60 and thickness b_n = 15 mm (at the moment of solidification t_{sol}=379.58s).*

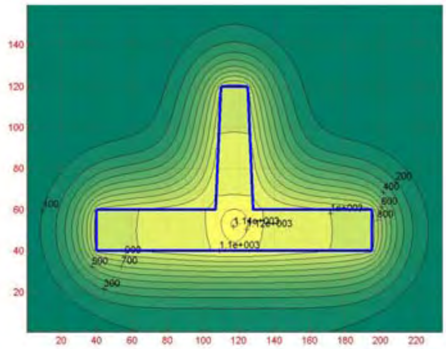

Fig. 12. *Distribution of isotherms at the end of solidification for a rib of inclination tg α = 3/60 and thickness b_n = 15 mm (at the moment of solidification t_{sol}=407.58s).*

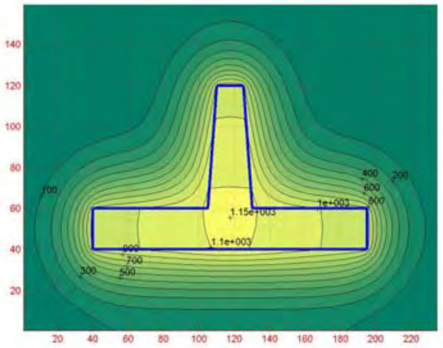

Fig. 13. *Distribution of isotherms at the end of solidification for a rib of inclination tg α = 5/60 and thickness b_n = 15 mm (at the moment of solidification t_{sol}=435.22s).*

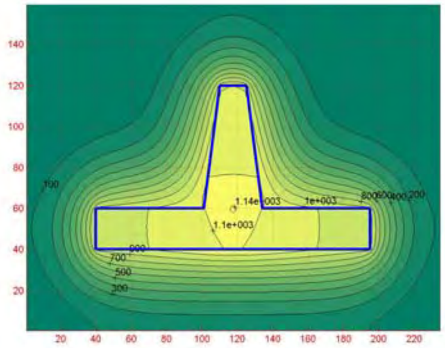

Fig. 14. *Distribution of isotherms at the end of solidification for a rib of inclination tg α = 9/60 and thickness b_n = 15 mm (at the moment of solidification t_{sol}=490.94s).*

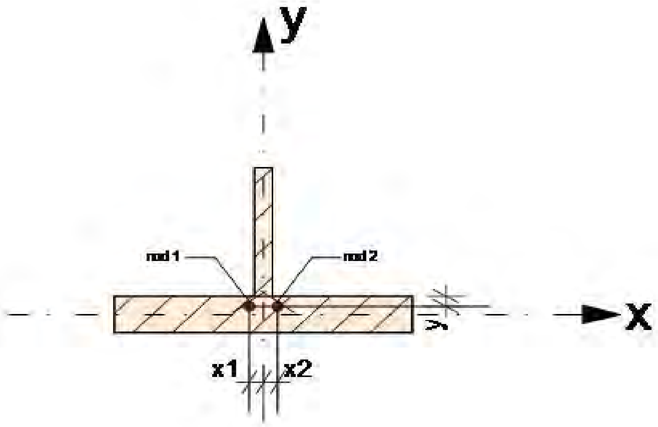

Fig. 15. *Coordinates of the hot spots.*

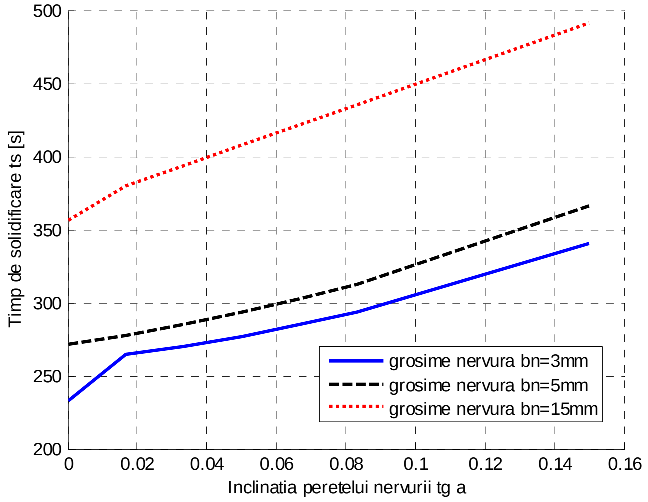

Fig. 16. *The influence of rib inclination (tg α) on solidification time (part thickness a = 20mm, inclinations by increasing rib wall thickness) (t_s = solidification time, tg α = rib wall inclination, b_n = rib thickness).*

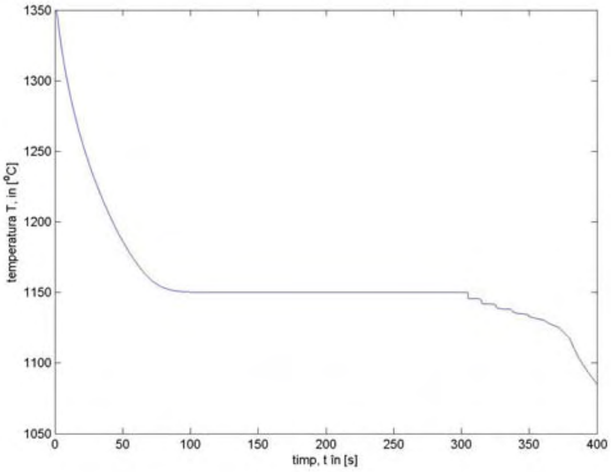

Fig. 17. *Temperature variation in the hot spot (coordinates x = 0 mm, y = 2.5 mm), part with a rib of b_n = 15 mm and inclination tg α = 1/60 (T = temperature; t = time).*

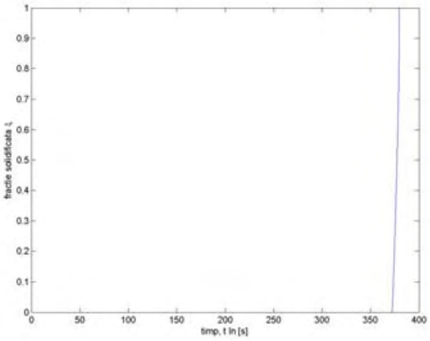

Fig. 18. *Variation of the solid fraction in the hot spot during solidification (coordinates x = 0 mm, y = 2.5 mm), part with a rib of b_n = 15 mm and inclination tg α = 1/60 (ξ = solid fraction).*

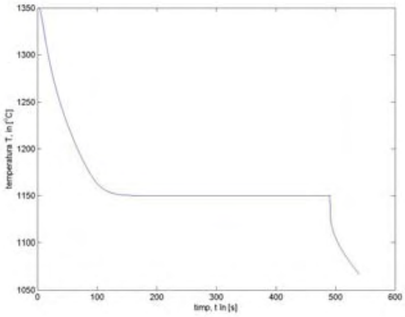

Fig. 19. *Temperature variation in the hot spot (coordinates x = 0 mm, y = 9.5 mm), part with a rib of b_n = 15 mm and inclination tg α = 9/60 (T = temperature; t = time).*

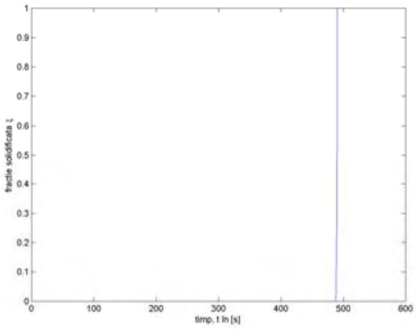

Fig. 20. *Variation of the solid fraction in the hot spot (coordinates x = 0 mm, y = 9.5 mm), part with a rib of b_n = 15 mm and inclination tg α = 9/60. (ξ = solid fraction).*

3. Conclusions

The following conclusions are yielded by the results of this study:

- in the case of ribs significantly thinner than the part wall (b_n = 3 mm; b_n = 5 mm) and for small inclinations of the lateral walls (tg α = 1/60 ÷ 6/60) the cooling effect of the rib is maintained; two hot spots are generated in the part wall, symmetrical in relation to the rib axis;
- with an increasing inclination of the rib lateral walls the two hot spots move closer to the rib axis, and for an inclination of tg α = 9/60 the two hot spots merge in a single one located on the rib axis (figure 6 and 10);
- in the case of ribs of thickness exceeding b_n = 15 mm, even for small inclinations a single hot spot is generated in the cast part, located on the symmetry axis of the part; with an increasing inclination the hot spot slightly moving along the y-axis (moving away from the part wall axis towards the rib);
- the solidification time of the hot spots increases to a relatively high degree in relation to the increase of rib lateral wall inclination; in the studied cases (ribs of thicknesses 3; 5; 15 mm), an increase of inclination from tg α = 0 to tg α = 9/60 determines an increase of solidification time by about 50%.

References

[1]. Ciobanu I., Monescu V., Munteanu S. I., Crişan A. – *Simularea 3D a solidificării pieselor turnate*, Editura Universităţii “Transilvania” din Braşov, Braşov, Ro, 2010, ISBN 978-973-598-678-0.

[2]. Ciobanu I., Ţuţuianu Diana – *Estetica, element valoric al pieselor turnate*, Metalurgia, no. 1, pag. 3-8, ISSN 0461/9579.

[3]. Ciobanu, I., Maşniţă, M., Monescu, V. *Cercetări privind solidificarea pieselor cu secţiune ”T”*, Metalurgia, nr.13, 2006.

[4]. Maşniţă M. – *Cercetări privind influenţa unor factori tehnologici şi constructivi asupra solidificării pieselor turnate*, Teză de doctorat, Universitatea Transilvania din Braşov, 2007**.**

[5]. Ţuţuianu Diana, Ciobanu I. – *Consideraţii privind implicaţiile tehnologice şi estetice ale înclinaţiilor de turnare şi ale razelor de racordare în cazul pieselor turnate*, Sesiunea de comunicări stiinţifice cu participare internaţională Terra Dacică - România mileniului trei. Acad. Forţelor aeriene Henri Coandă Brasov, 5-6 mai 2006, An VII, nr.1, CD - ISSN 1453 – 0139.

[6]. Zirbo G., Ciobanu I. – *Tehnologia turnării*, vol 1 & 2, Institutul Politehnic Cluj – Napoca, 1989.

THE ANNALS OF “DUNAREA DE JOS” UNIVERSITY OF GALATI.
FASCICLE IX. METALLURGY AND MATERIALS SCIENCE
N^{0}. 3 – 2010, ISSN 1453 – 083X

SCRAP QUALITY AND METALLURGICAL EFFECTS ASSOCIATED WITH COPPER AND TIN AS TRAMP ELEMENTS IN THE CASTING STEELS

Anisoara CIOCAN, Florentina POTECASU
“Dunărea de Jos” University of Galati
email: aciocan@ugal.ro, mihaela_potecasu@yahoo.com

ABSTRACT

The complex property requirements for steels make it essential that there is a thorough understanding of the influence of tramp elements on their properties. Surface aspects, metallurgical structure, mechanical properties (toughness, tensile strength hardness ...) and weldability are some examples of requirements for quality steels in correlation with these residual elements. An increased content of residual elements such as Cu, Ni, Sb, Sn, As… may deteriorate the final properties of steels.

These elements are introduced to steel using steel scrap in the steelmaking process. The recycled scrap can contain considerable quantities of impurities. For this reason the control of ferrous scrap is necessary in order to preserve the recycling rate at the current high level without sacrificing steel quality.

In this paper we discuss about copper and tin as particularly tramp elements in respect to their influence on the properties of the engineering steels and structure. For a lot of casting steels, we analyze these residual elements in respect to the tolerable contents. The possible synergic relations between other elements and these impurities are also considered. The sources and the effects of the residual elements were discussed as far as possible, in order to obtain accurate answers for practical situations.

KEYWORDS: tramp elements, copper, tin, scrap recycling, steel casts

1. General consideration

Copper and tin in steel are harmful to steel properties and for this reason these are called tramp elements.

The main source of copper and tin in the steelmaking processes is represented by metallic scraps.

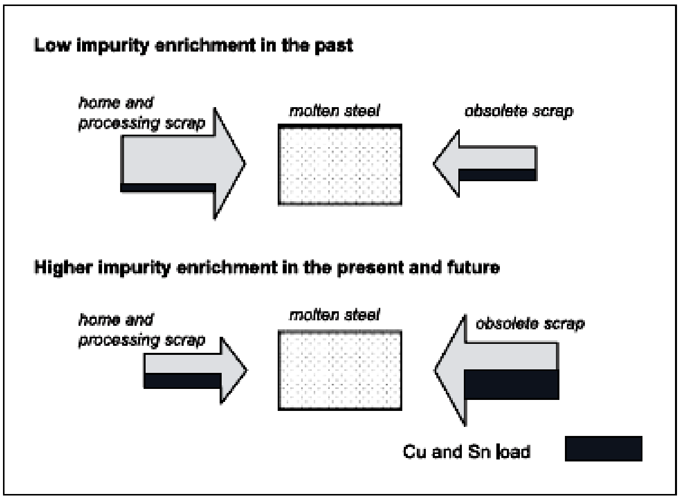

Fig.1. *Development of scrap material flow [1].*

Scrap becomes for the steel industry the single largest source of raw material because it is economically advantageous to recycle old steel into new steel. The impurity content largely determines the value of these resources.

Due to the disposal of a large amount of copper-containing steel scraps, the amount of copper-containing steel scraps is increasing day by day. Tin content in the steel circle increases at the same time. The development of material flow is schematically given in Figure 1.

Recently, the quantity of steel scraps such as waste automobiles and electronic appliances that contain copper wires, tin galvanized plate and other materials has spectacularly increased.

Moreover, over time they became part of the waste recycling cycle for the steel production without purification treatments. As result to these scraps recycling, the tramp elements accumulation in the scraps continuously increases. Also, in the steels that used these ferrous scraps, the content of these elements increases. Figure 2 shows the evolution of the copper content for the scrap and for the steels. This is the result of combining the technical information on the present purity of the scrap with an econometrical modelling.

Scrap	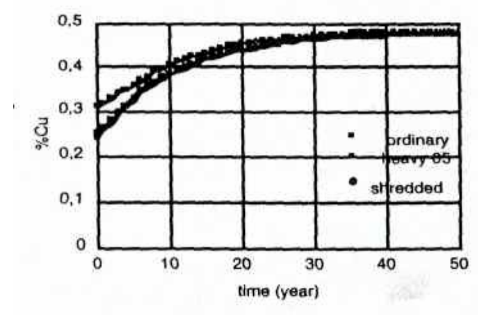
Steels	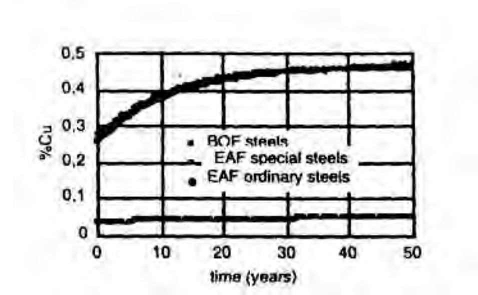

Fig. 2. *Evolution of scrap and steel quality at the time scale ranges over 50 years, 1995-2050 [2].*

Also, Figure 3 shows the results of projections of the level of copper and tin in obsolete scrap from 1985 until 2015 which are calculated in the case of Japan.

On the average, the copper level is expected to increase by 50 % over a 20-year period of time and the same conclusion applies to tin.

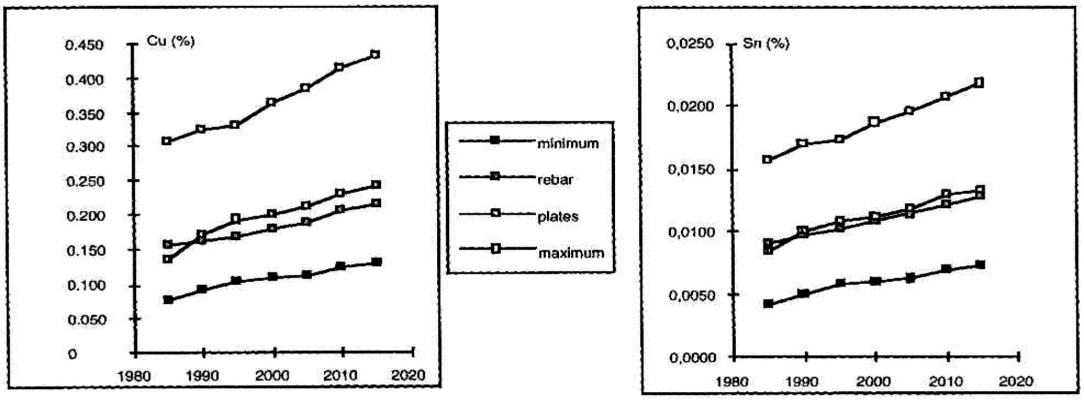

Fig.3. *Cu and Sn long term evolution in EAF steels as a result of tramp elements accumulation in the scrap deposit [3].*

The tendency of this evolution shows that the pollution of the scrap is inevitable. The steel quality is affected if the methods to remove copper and tin as tramp elements were not applied. The control and removal of copper and tin are necessary in order to preserve the steel recycling rate at the current high level without sacrificing steel quality. The methods for the purification of the scraps must be in accordance with the quality of the recycled scraps and the steelmaking process.

The techniques for eliminating the tramp elements can be divided into three groups: pretreatment of scrap by mechanical and chemical methods at different temperatures; elimination of the tramp elements during the preheating; elimination of the tramp elements on scrap melt or liquid steel. For the quality of the steels, the quality of scrap metal is an essential factor.

The input tramp elements reporting to the steel product must be severely restricted-especially for tin, copper, and zinc. This is essential because scrap, compared to other products, has specific characteristics. It has an unstable origin because it comes from a harvesting activity among a large number of producers, having very different structures, generally unknown to the consumer. Scrap is not a result of an industrial process [4].

On basis of the classical Quality Assurance Systems were established and imposed the scrap specifications.

The Romanian standard in relation with the quality of the steel scraps is SR 6058-1 from April 1999 „Ferrous materials for remelting” [5].

In the international standards, scrap quality is defined quite simply by two families of parameters, physical and chemical. The geometry and size of the scrap define the class of physical parameters. More important are the chemical parameters which are defined in terms of iron and tramp elements contents.

The value for the maximum allowable contents of tramp elements in recycled scrap is essential for the standard specifications. In the new European scrape code, impurity levels are specified for the different scrap families. The measurable criteria are used there for defining the residual elements like Cu, Ni, Cr, Mo, Sn. The limit value for copper that is established by European Steel Scrap Specification is ≤ 0.25 %wt for category E3 scrap and ≤ 0.4 %wt for category E1 scrap. More content (≤ 0.5 %wt) is specified for incinerated shredded scraps (category E46 scrap). Also the limit values for tin content are the following: ≤ 0.010 %wt for obsolete scraps (category E3 scrap) and ≤ 0.070 %wt for category E46 scrap [6]. There are two forms of copper that is present in the scraps: the copper as parts mixed with steel scrap and copper in the dissolved state. The contamination of the scraps with copper parts are specific for the obsolete scrap. The content of tramp elements in these scrap varies in a large scale, Table 1.

Table 1. *Typical composition of the obsolete scrap from varied source, %wt [7]*

Source	Shredded scrap	Urban incinerator	Cryo shredded
Cu	0.230-0.430	0.304-0.980	0.169-0.275
Sn	0.027-0.042	0.032-0.140	0.022-0.033

Usually, the obsolete scrap consists of iron and steel products discarded after the end of their service life. After their processing by shredding, a mix of steel and copper parts results. The presence of the copper in the metallic feeds of the steelmaking process is determined by incomplete separation of the components according to their nature. The second main source of copper is the scraps formed by high copper containing steels. In this case the copper is dissolved in the solid solution with the steel.

The sources of tin in the steelmaking processes are the coated components of the scrap. Tin is present as thin layers on the surface of the scraps such as beverage, cans and other packages.

2. Experimental method and materials

The variation of copper and tin content of the cast steel was studied. The samples were from varied steel grades used for the castings production at a Romanian steel foundry. An electric arc furnace is used for the steels making. In this paper we discuss about copper and tin as particularly tramp elements in respect to their influence on the properties of the steels. For a number of cast steels we analyze the content of these residual elements in respect to the tolerable contents. The possible synergic relations between other elements and these impurities are also considered. The sources and the effects of the residual elements were discussed as far as possible, in order to obtain accurate answers for practical situations.

3. Results and discussions

The copper and tin are tramp elements for the steels analyzed. These are not alloying elements. The level of copper and tin into cast steels was presented by graphs. The frequencies of the measured copper and tin contents are given in Figure 4.

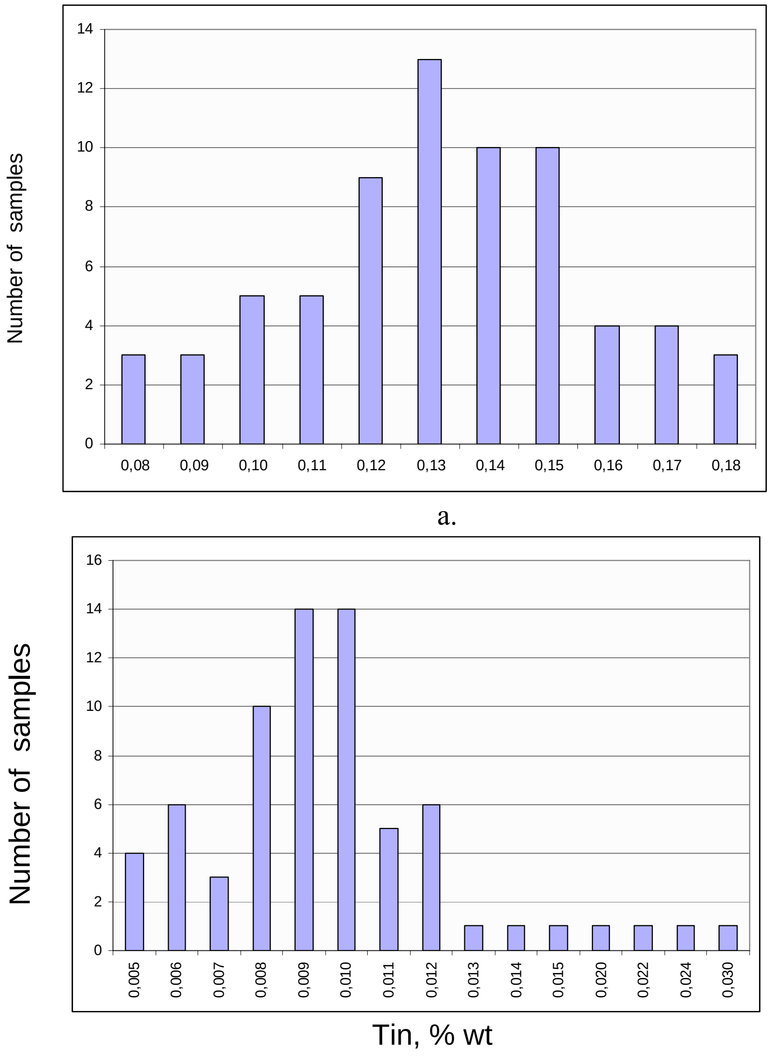

a.

b.

Fig. 4. *Tramp elements content of the cast steels: a. copper; b. tin.*

The origin of copper and tin in the steel samples are the scraps used into feeds for the steelmaking processes. In our cases, all feeds are composed of similar ferrous scrap. In the scrap yard of the foundry the scraps are not stocked or sorted after their composition. Also, it is not evaluated the steel scrap quality before feeding in the furnace. Only at the end of the melting period the chemical composition of the melting bath is determined. In this case, we can estimate that the quality of the ferrous scraps used as feeds for the steelmaking processes is comparable. As result, the copper and tin content for the steels analyzed varied in small scales. These are 0.08-0.18% for copper and 0.005-0.030% for tin.

Copper is wholly transferred to steel from scrap. Practically, copper is not found in steelmaking slag. The melting temperature of pure copper is much lower in comparison with steel (1083^{0}C). At typical steelmaking temperature which is over 1600^{0}C, the solubility of copper in the steel melt is practically unlimited. In comparison with iron, copper is characterized by a lower oxygen affinity. Accordingly, it is not removed by oxidation and transferred to the slag. Also, no essential copper content was found in the steelmaking dust. Unlike copper, tin is partially transferred to steel from scrap. Practically, tin is distributed between steel and dust. The melting temperature of tin is 232^{0}C. This is much lower in comparison with the temperature of the ferrous bath. In these conditions, most part of tin passes to the vapors form. This is found as oxides in the EAF dust. These are confirmed by the higher levels of tin (about 0.2…0.3% Sn) of the dust emitted in steelmaking processes [8]. Like copper, the solubility of tin in the steel melt is practically unlimited. As a result of the lower oxygen affinity, tin dissolved in the ferrous melting is not oxidized and transferred to the slag.

This element is not found in steelmaking slag. The average content of tin which is calculated for the steel samples analyzed is 0.01166%.

The values of copper and tin content must be discussed in relation to their influence on the properties and structure of the steels.

Copper and tin, like other residuals and alloying elements, can develop influence on metallurgical structure of the steels. In accordance with the type of the steel grade the elements develop varied micro- and macrosegregations: to grain boundaries, on free surface and to interfaces. As result of the structural modifications the copper and tin in steel are detrimental to various steel properties and these are tramp elements in relation to recycling steels. The effect of the contamination of the melt with tramp elements can be cumulative and irreversible. They can directly influence the mechanical properties of steel products.

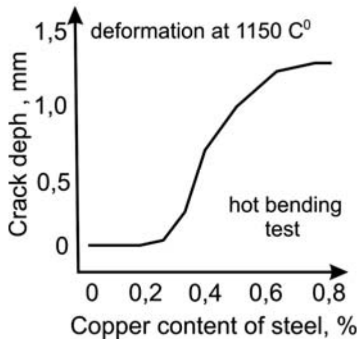

Fig. 5. *Relation between copper content and crack depth.*

The addition of some amounts of copper to iron based alloys during the smelting process is a well-known method of increasing their strength.

Upon heat treatment a fine structure of Cu precipitates in the iron matrix increased the strength of the alloy. Also copper contributes to the increasing of the corrosion resistance.

It is well known that small additions of alloying elements such as copper, chromium, nickel, phosphorus, and silicon lead to the development of adherent and protective rust on the steel during long-term atmospheric exposure.

However, copper is a key element related to surface defects which can appear during casting or hot rolling [1, 7]. The addition of copper to the steel cannot exceed 0.2% because it promotes cracking during the hot working process, Figure 5.

The surface cracks are in relation with the liquid phase that is formed at the grain boundaries above a certain temperature. With respect to its role in causing hot shortness (caused by a loss of hot ductility in the temperature range 1100-1300^{0}C), copper content should be kept below ≈0.1 %wt [1]. These conditions are in accordance with the solubility limit of copper in austenite or ferrite, Figure 6.

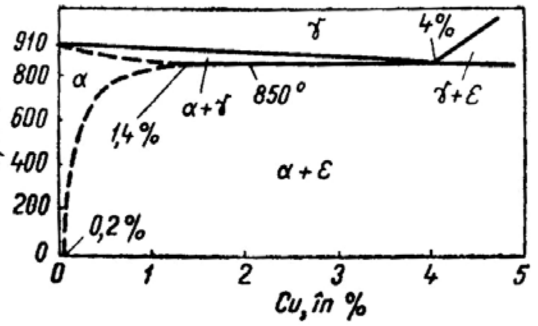

Fig. 6. *Diagram of the Fe-Cu binary system.*

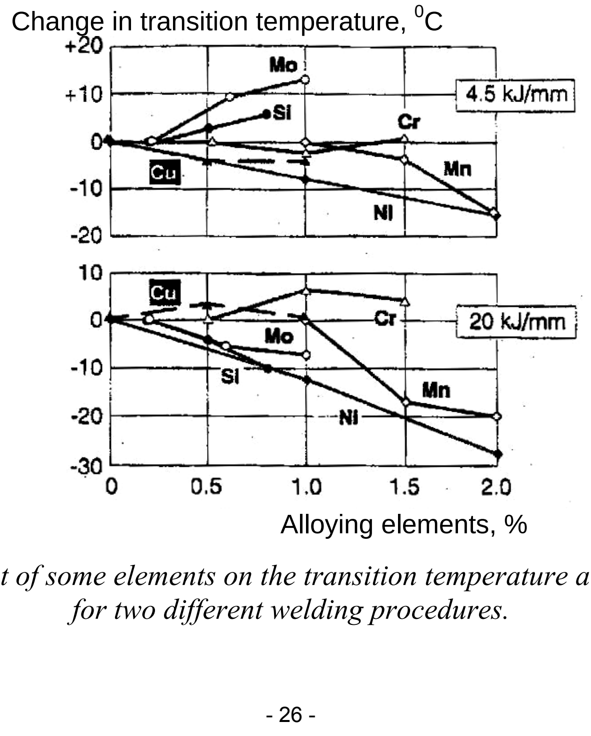

Fig. 7. *Effect of some elements on the transition temperature at fusion line for two different welding procedures.*

Copper has influences on the properties of the welded joints. This element impairs the toughness in heat affected zone or weld metal, Figure 7. Segregation of tin at grain boundaries has a more detrimental impact [7].

The copper, in the analyzed steel, does not exceed 0.2%: the maximum content is 0.18% and the average value is 0.1317%.

Sometimes, few fine cracking appeared on the surface of the steel castings in the critical zones at higher copper content and at the application of some thermal treatments.

The association of the elements in steel modifies the effect of copper: some elements amplify and others reduce or neutralize the negative effect of copper.

This is considered a synergism effect and is illustrated by empirical expressions called „copper equivalent” $Cu_{eq}=\%Cu+10\%Sb+5\%Sn+2\%As-\%Ni$. The synergism effect of copper and tin on the hot shortness (by lowering the melting point of the Cu-Sn enriched zones) can be expressed by following equivalence: 0.4% Cu in steel exerts the same influence as the sum $\Sigma(0.3\%Cu+0.02\%Sn)$.

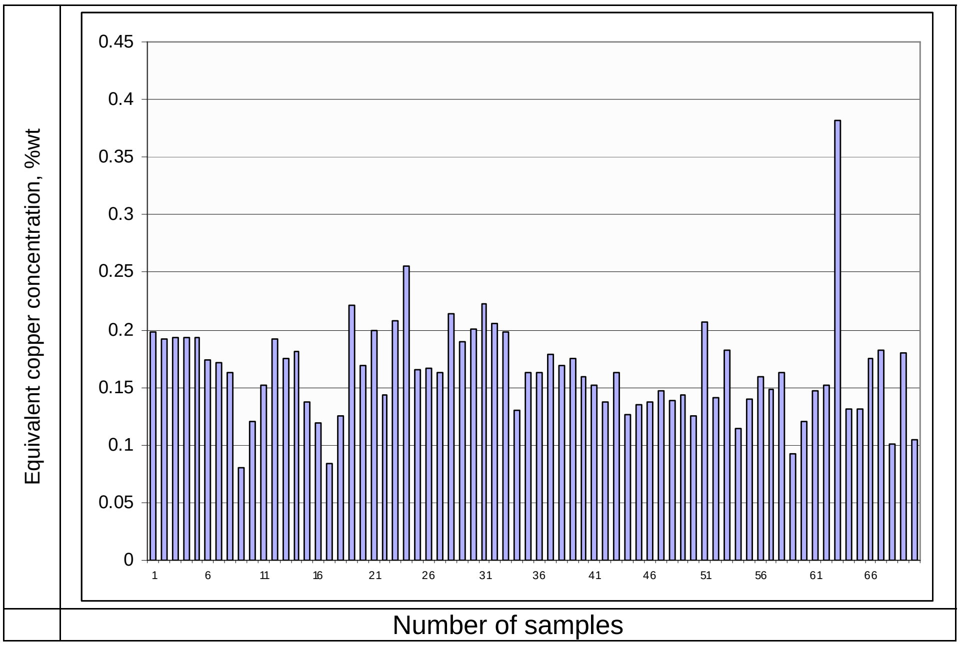

Fig. 8. *Variation of the equivalent copper of the steel samples.*

Also the sum $\Sigma(\%Cu + \%Cr + \%Ni + \%Mo)$ must be considered and restricted for the casting and hot rolling of the steels: to maximum 0.13% for bar steel and 0.80% for thin sheet. We calculated the „copper equivalent” for the steels samples. The evolution of the „copper equivalent” for the steels samples is given in Figure 8. The values of the equivalent copper for the steels samples do not exceed 0.4%. At these values the probability to promote cracking on casts surface is lower.

4. Conclusions

The copper and tin content for the steels analyzed is within the tolerable limits. Only three samples have the copper content near the maximum value which is restricted for prevention of the surface defects. The tin content is lower than the admissible limit value in accordance with the steel quality. For the preservation of the steel quality we recommended the utilization of the scrap with controllable quality. Especially the restrictions for the copper and tin are necessary. This is imperiously necessary because the scraps originated in various and uncontrolled suppliers. It is necessary to apply the advanced method to control the quality of the scrap. Also, the methods for the preparation and the pretreatment of the scrap must be applied.

References

[1]. Savov, L, Volkova, E., Janke, D. *RMZ-Materials and Geoenvironment,* Vol.50, No.3, pp.627-640, 2003.

[2]. Birat, J.P., Huin, D., Le Coq, X., Roth, J.L., Lemiere, F., *La Revue de Metallurgie-CIT*, April 1995, pp.477-486

[3]. Sato, S., Takeuchi, M., Mizukami, Y., Birat, J.P., *La Revue de Metallurgie-CIT*, April 1996, pp.473-483

[4]. Wulff, S.W., *La Revue de Metallurgie-CIT*, Oct 1998, pp.1202-1208

[5]. *** *„Ferrous materials for remelting*” ASRO-Romanian Stadard SR 6058-1, April 1999

[6]. Baillet, G., Birat, J.P., Bobrie, M., *La Revue de Metallurgie-CIT*, Nov. 1996, pp.1185-1200

[7]. Marique, C., *La Revue de Metallurgie-CIT,* Nov. 1996, pp.1378-1385

[8]. Ciocan, A., *Valorificarea deşeurilor metalurgice. Procese şi tehnologii,* Galaţi University Press, 2008.

THE ANNALS OF “DUNAREA DE JOS” UNIVERSITY OF GALATI.
FASCICLE IX. METALLURGY AND MATERIALS SCIENCE
N^0. 3 – 2010, ISSN 1453 – 083X

SOME CONSIDERATIONS ON ENVIRONMENTAL SAND CORES WITH INORGANIC BINDER

Tibor BEDŐ, Viorel ENE, Ioan CIOBANU
Faculty of Materials Science and Engineering,
Transilvania University of Brasov
email: bedo.tibor@unitbv.ro

ABSTRACT

Traditionally, complex sand cores are produced using organic binders such as phenolic and furan resins. These binders can create bad smelling fumes requiring complex and expensive ventilation equipment to fulfill environmental requirements. The increasingly more stringent environmental legislation forces the foundry industry to employ innovative and environmentally-compatible binder systems. The established organic binder systems have indeed been, and are still being, further developed with regard to their contents but it is questionable whether these will be able to fulfill the continuously increasing requirements of foundry neighborhoods and legislation. The Landshut magnesium and aluminum casting facility, which produces engine components, structural components and chassis parts for BMW, is expected to reduce its emissions of combustion residues by 98% with the implementation of the inorganic core binding system. The paper presents some considerations on environmental sand cores with inorganic binder.

KEYWORDS: sand cores, inorganic binder, foundry industry

1. Introduction

The use of modern moulds with high quality characteristics is required especially in the aircraft industry, military and engineering, under special circumstances.

In those cases are imposed strict quality characteristics on mould behavior at high temperatures, lack of responsiveness of mould components to metal alloy, dimensional stability and mechanical resistance of the mould.

"Most of what has to change is the core and mold making method," said Keith McLean, president of HA International LLC, Westmont, Ill. "Metalcasters are still mixing sand with a binder and still putting sand into a cavity.

What changes are sand preparation practices?

Sand reuse, cure speed, moldability and venting may all be significantly different and typically are not enhanced with inorganic. Larger operations might have to buy more equipment to maintain the production rate they are used to because of cure speeds."

Based on these considerations, researchers from worldwide, seek to obtain core sand recipes to meet all these requirements adequately.

2. Considerations on environmental sand cores with inorganic binder

Use of organic binders began to be restricted due to the high level of pollutants emitted during the moulding-casting-knock-out process.

A change to an inorganic system makes the foundry environmentally independent, especially for foundries which are located near a city or housing areas. A change to inorganic binder system can guarantee a foundry’s existence.

Inorganic binders have been generating more and more interest in recent years because of the advantages compared to commonly use organic binder systems. These include no emissions during the whole production process as well as better castings and less rejects.

Now all known binder producers have developed good inorganic binders, where slowly but surely, all disadvantages from the beginning are eliminated, so foundries can nowadays choose between several good inorganic binders on the market.

Every binder producer has their own patented formulation, each with its own characteristics. The binder systems can even be mixed by the foundries themselves with simple mixer equipments.

Since the early 90s, the combined effect of environmental regulations and fierce competition speed forced the manufacturers of castings to invest substantial amounts in research leading to acquisition of new technologies, combined with new types of sand cores, which fall whithin new environmental regulations and have the effect of cost reduction castings. The continuous growth of industry restrictions by environmental legislation requires casting industry to seek new green and core sand systems which have ecological properties. The binders used in the sand cores can be organic or inorganic, natural or synthetic, as shown in Table 1.

Table 1. *The binders used in the sand cores*

Binder type	***Natural binders***	***Synthetic binders***
Inorganic binders	Casting loam Bentonite	Sodium silicate Ethyl silicate Potassium silicate Colloidal silica Concrete Plaster Phosphates Sulfates
Organic binders	Alizarine oils Molasses Natural resins	Amine Phenolic resins Furan resins Polyester resins Polyurethane resins Cellulose resins

In this context, it is necessary to develop new inorganic binder systems to meet both the requirements of environmental legislation and of the economy and quality demanded by the explosive growth of competitiveness.

These requirements were the motivation for the aggregating, in 2002, three renowned German companies in the industry casting [1]:

- Johann Grihmann GmbH & Co. KG, Bisingen aluminium Foundry,
- Fritz Eichenauer GmbH & Co. KG, Hatzenbuhl, heating element manufacturer,
- Maucher GmbH Formenbau u. Kunststofftechnik & Co. KG, Markdorf began an extensive research project aiming to discover new inorganic binder systems for sand cores, which have high ecological properties.

Hydrobond project aimed at the development of an inorganic binders system which does not contain any organic substances, binders which are soluble in water and allowing the recirculation almost complete of the used sand.

Measurements showed that the use of water soluble inorganic binder systems results in an almost complete reduction of gas emissions in the production of castings.

Despite the advantages offered by the synthetic resins (high strength, good knock-out of moulds and sand cores regeneration) the use of the inorganic binders provides several advantages related to economic, labor hygiene and protection environment.

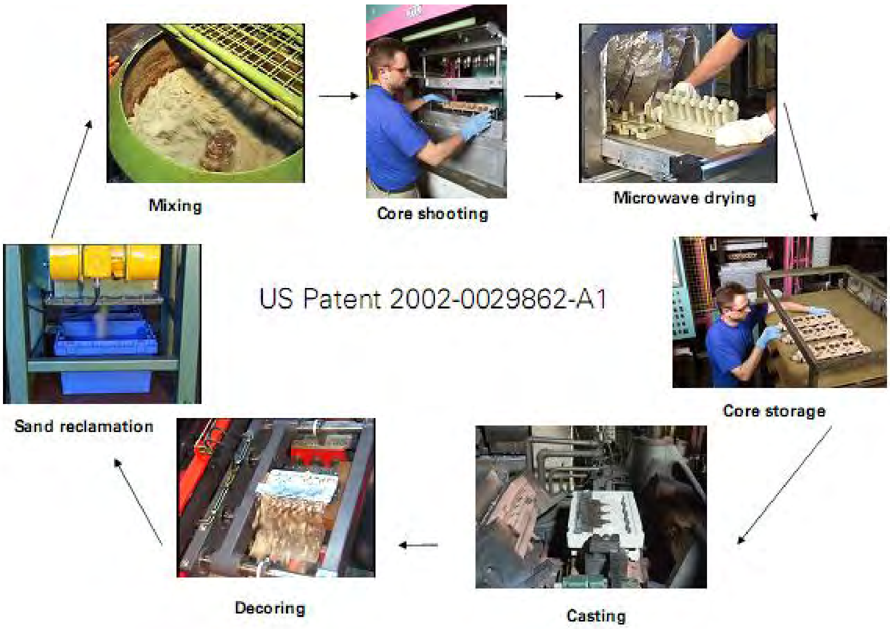

Fig. 1. *Castings production using the AWB process.*

A quality sand cores binder must law the sand particles together with sufficient force to produce a mold to keep the size and surface appearance when pouring molten alloy. The binder must also provide sufficient permeability of the mould, such as flue gases resulting from the casting to be removed without causing casting defects. During the casting process the mould must maintain integrity at high temperature avoiding the sand cores inclusions penetration in the metal weight, making the castings become scraps. Global experiments with inorganic binders have shown that these ensure the requirements of quality foundry binders.

In 2002 the United States AWB system was patented (U.S. Patent 2002-0029862-A1) to produce cores using an inorganic binder system and which has advantages for sand preparation that requires much lower power consumption compared to the organic binders systems, produces no toxic emissions during the technological process and storage or toxic combustion products are not necessary (Figure 1).

Inorganic binders, unlike the organic ones, are characterized in that, during thermal decomposition process, the gaseous emission is very low. The Beach Box process with LaempeKuhsBinder is based on the natural principle of certain minerals to bind and release water of crystallizations [2].

During core production the water of crystallization is driven off and the core or mould shows stability similar to concrete. However, the core breaks down in just a few seconds when making contact with water. De-coring problems and related damages of the casting are things of the past. The dry de-cored sand can be re-cycled repeatedly after adding water only.

When new sand is mixed with LaempeKuhsBinder, an envelope is formed around the sand grain, which is dissolved or consolidated by adding or withdrawing only water. In practice this means a substantial decrease in binder use.

The new core and mould production process developed by Laempe is, as the company claims, the most efficient method available as BAT (Best Available Technique) in foundries today. It can replace all known core production processes, particularly cold box, hot box, or warm box.

Laempe introduced a completely new <Beach Boxing> core production system to provide new solutions to solve environmental problems. Essentially it is using a binder based on magnesium sulfate mixed with sand and is subjected to heating to achieve strengthening (Patent WO/2003/013761, Method and device for the production of molds or cores for foundry purposes). The invention (Figure 2) relates to the production of molds or cores (2) for foundry purposes, wherein a mixture (3) of foundry sand and binder is produced and introduced into a mold or core tool (8), e.g. shot in a core shooter. A known binder or magnesium sulfate with and/or without at least one or additionally several crystallization waters are dispersed or dissolved in water and used as binder, which is then mixed with the foundry sand and introduced or shot into the mold tool or the core box (8).

For hardening purposes, the water and a fraction of the crystallization water are vaporized by heating and driven out by a gaseous medium, all of which can be carried out very rapidly.

To achieve a short curing time (10-40 sec.), only heated core boxes can be used at the moment. The type of heating system makes no big difference. An equal temperature distribution of 150-200°C should be achieved. Lower core box temperatures delay curing time and reduce the storage stability of the cores.

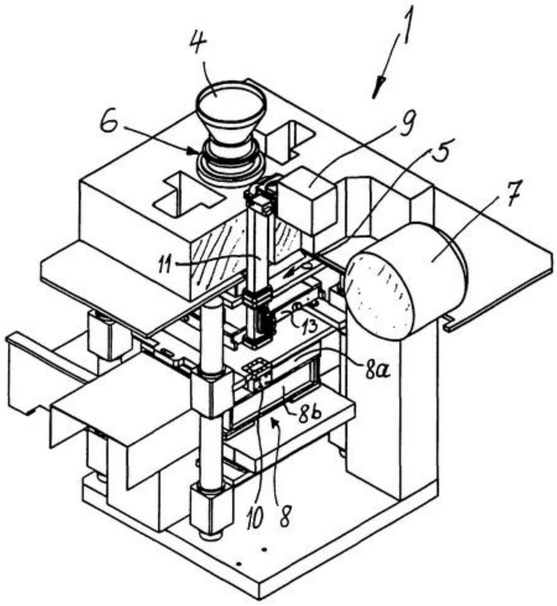

Fig. 2. *Method and device for the production of molds or cores for foundry purposes (Patent WO/2003/013761).*

Higher temperatures in the core box can give rough surfaces of the core due to binder additive reactions [3]. This is not a problem as most hot box machines supply a controlled temperature distribution.

The core production can be conducted on commonly used core shooting machines, as long they have a heated core box (Fig. 3). Commonly used hot box or shellcore machines work well without requiring any significant changes. However, a shooting pressure of 3-5 bars is needed. The shooting time should be held as short as possible, between 1-2 seconds, to avoid drying the sand in the shooting nozzle. Furthermore it is necessary to avoid heat transfer from the core box to the shooting nozzles and shooting head. This can cause drying of sand in the shooting head and blocked nozzles, especially when the machine is on standby.

The application of various inorganic binders was tested in the foundry of a German automobile manufacturer.

Instead of the expected bending strength of approx. 400 N/cm² the mixing process with an inorganic binder consisting of three liquid components by means of the STATORMIX resulted in approx. 540 N/cm² Consequently the binder consumption can be reduced considerably. Core sand containing less humidity can be better shot and the drying expenditure is reduced. The diagram illustrates the achieved bending strength depending on the added amount of binder (Figure 4).

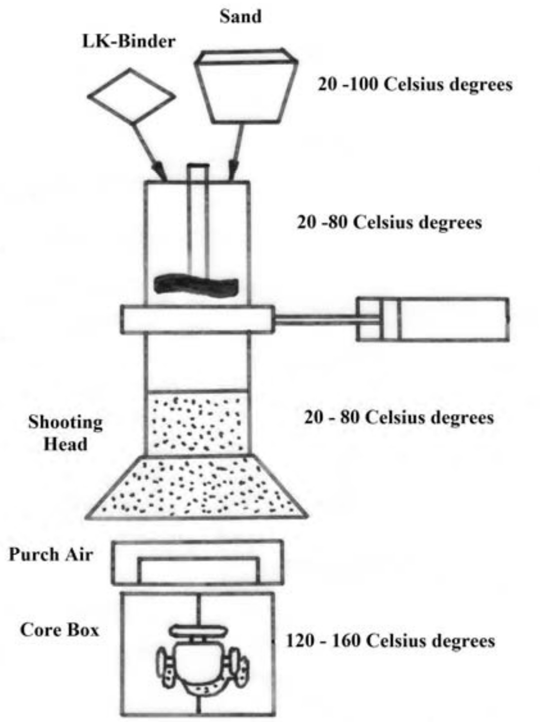

Fig. 3. *Making the moulds into the Beach Box [4]*

The Cordis process has meanwhile been available to the foundry binder market for more than 10 years. The process is based on an inorganic binder (silicate, phosphate and borate) one of the most environmentally compatible, low odor and smoke binders in existence.

Curing of the core in the core box takes place by means of water removal.

Cordis is an inorganic binder (silicat, phosphat and borat). Curing of the core in the corebox takes place by means of water removal.

The molding sand produced using this one-component system may also is cured with the aid of conventional ester-based hardeners.

The molding sand mix, made with AFS 55 silica sand, can be prepared in any commercial mixer. Depending on the geometry of the cores to be fabricated, the addition level of Cordis to sand is 2.0 - 2.5 parts by weight.

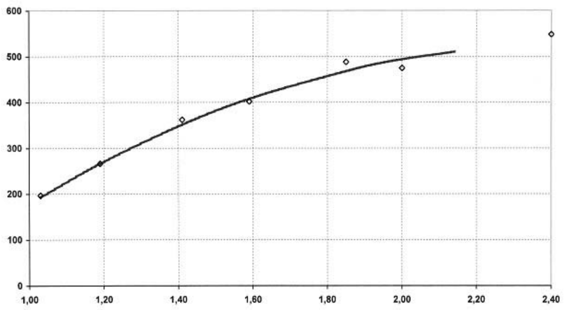

Fig. 4. *The achieved bending strength depending on the added amount of binder*

The sand mix is ready for use as soon as it leaves the mixer. The molding sand mix is very easy to process.

The coreboxes used for this process must be modified in such a manner that a large flow of warm air can be quickly and directly passed through the corebox. The corebox should be constructed of a material that can be heated to approx. 200 °C. Since - as previously mentioned - curing is critically influenced by the throughput of warm air, it is important to keep the temperature of the required air at 150 °C over the entire gassing period. The achieved gassing time for an intake manifold core would be of 30 seconds [5].

3. Conclusions

Using new types of inorganic binders is required as a necessity because it presents numerous advantages.

Advantages include:

- no emissions;
- no ash or products of combustion associated with decomposition of organic binder components;
- immediate stability comparable with cold box binder;
- dimensionally stable and accurate during storage, pouring, cooling;
- complete core breakdown in just a few seconds, allowing for gentle casting shake out;
- smallest orifices can be de-cored as the core sand is washed out with water;
- reduced cooling times by wet de-coring in water;
- no necessary coating, therefore no core wash drying required; extremely thin walled castings can be produced because of accurate and stable moulds and cores;
- sand with higher fines content can be used, producing a casting surface comparable to die-casting;

- core package process eliminates moisture problems attributed to green molding sand;
- minimal core production costs.

The large number of advantages justifies without any doubt the use of inorganic foundry binders, even if they show some minor drawbacks:

- binder shelf life of three months (for the Cordis inorganic binders);
- humidity/moisture reduce the storage life of the cores;
- sand crusting on the submerged nozzles.

These self-made inorganic binders reduce costs.

The core sand requires approximately 2.5% binder, which is much cheaper than any other organic system.

This makes the use of inorganic binder viable for small and medium sized foundries. Additional money can be saved, because no air cleaners are needed anymore, no thermal treatment, easy decoring, no condensation on the dies and easy reclaiming of the sand. Also, if the sand is not reclaimed, it is easily disposable as non-toxic land fill.

"It is absolutely not true that inorganic binders are too expensive," Furness said. "If that is the case, then why do so many major European [metal casting facilities] use low emission binders? When switching to low emission binders in green sand, a metal casting facility can save up to 20% of energy costs.

References

[1]. Helge Hansel – *An innovative inorganic binder system*, Casting Plant + Technology International, 2/2002

[2]. http://www.allbusiness.com/primary-metal-manufacturing/foundries/648620-1.html

[3]. http://kuhs-invent.com/3.html

[4]. http://www.epa.gov/ttn/atw/ifoundry/binders/laempe_reich10-26-05.pdf

[5]. http://www.huettenes-albertus.com.au/Cordis.1010.0.html

THE ANNALS OF “DUNAREA DE JOS” UNIVERSITY OF GALATI.
FASCICLE IX. METALLURGY AND MATERIALS SCIENCE
N^0. 3 – 2010, ISSN 1453 – 083X

INFLUENCE OF RIB LENGTH ON THE SOLIDIFICATION OF CAST PARTS

Ioan CIOBANU, Diana ŢUŢUIANU,
Tibor BEDŐ, Aurel CRIŞAN
Faculty of Materials Science and Engineering
„Transilvania” University of Braşov,
email: ciobanu_i_bv@yahoo.com

ABSTRACT

The ribs applied to the walls of cast parts are designed for enhancing both stiffness and aesthetics. The presence of ribs modifies the conditions of heat transmission and implicitly the solidification of the alloy in the joining area of the rib to the part wall. This is highlighted by the modified radius of the circles inscribed in the rib – wall joining area. The diameter of the circles inscribed in this area is greater than of those in the rest of the part wall. This leads to the assumption that the solidification of the alloy in this area is slowed. The paper presents the results of a study concerning the influence of rib dimensions (length) on the duration of cast part solidification and on the position of the hot spots. The study was conducted by computer simulation of solidification. The results have revealed that in certain situations (thin ribs compared to wall thickness) the ribs cause an acceleration of the solidification of cast parts. The length of thin ribs ensuring the maximum cooling effect is determined.

KEYWORDS: rib lenght, solidification, cast part, simulation

1. Introduction

While representing the technological elements required by the designer or manufacturing engineer, ribs, casting slopes and corner radii of the cast parts also have an aesthetic function. Generally ribs have the role of stiffening the walls of the cast parts. These technological elements (ribs, slopes, corner radii) influence the solidification of cast parts. Ribs determine a local thickening of parts in the rib – part wall joining area, as highlighted by the local increase of the circle radii inscribed in the part perimeter, as shown in Figure 1. Consequently it is to be expected that these technological elements determine a local increase of solidification time and hence the generation of hot spots, causing on their turn solidification-specific defects (porosity, shrinkholes, cracks, etc.). The paper presents the results of a study on the influence of rib length on the solidification of cast parts, and thus on the tendency of defect generation caused by solidification. The aim is to establish the magnitude of this influence and the opportunity of prevention measures. Research was conducted by computer aided simulation of the solidification process, by means of the dedicated „Sim-3D” software, developed at the Faculty of Materials Science and Engineering of the Transilvania University of Braşov.

2. Influence of rib length on the solidification of cast parts

There has been studied the rib length influence on the solidification of cast parts.

The test piece thickness was of a = 20 mm and had ribs of thickness b_n=3 mm and b_n=5 mm, respectively. Figure 2 shows the geometry and dimensions of the cast parts and casting mould included by the study.

The study was conducted on eutectic cast iron parts cast in silica sand moulds. Table 1 features the thermo-physical characteristics of the alloy and the mould used for simulation.

The study concerned the influence of rib length on the position of hot spots, on the solidification time, on temperature variation and on the solidified fraction in the hot spots.

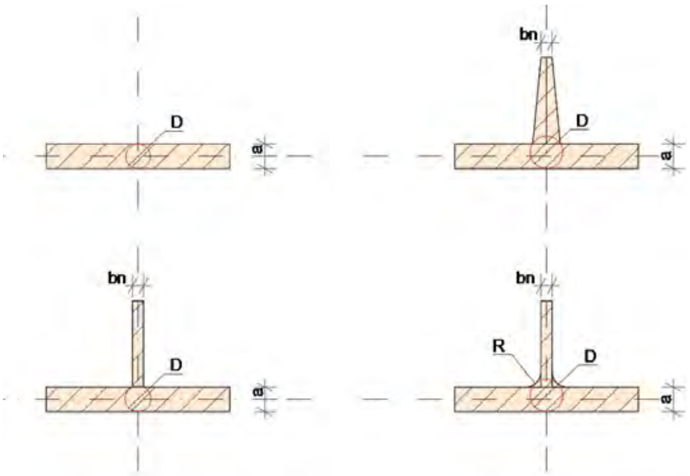

Fig. 1. *Influence of rib thickness, casting slopes and corner radii on the diameter of the circle inscribed in the contour of the cast parts.*

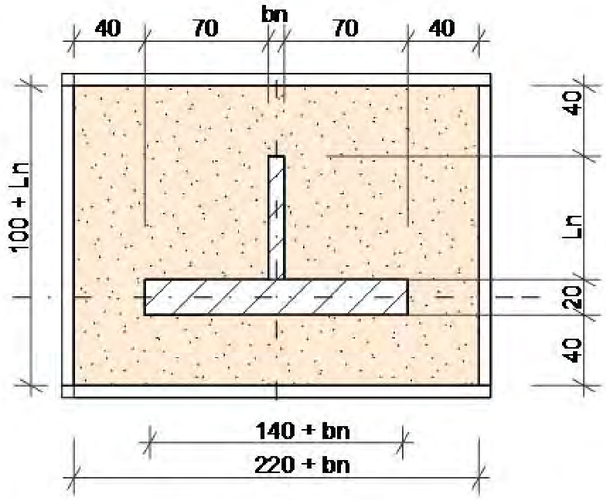

Fig. 2. *Geometry and dimensions of the part and mould.*

Table 1. *Values of the quantities used for simulation of solidification*

No.	Parameter	Physical symbol	Measure unit	Value
1	Mesh width of mould dividing	Δ	m	0,001
2	Time interval	τ	s	0,02
3	Environment temperature for the exterior of the mould	T_{ex}	^0C	20
4	Thermal exchange coefficient mould-exterior environment	α_{ex}	$W\cdot m^{-2}\cdot K^{-1}$	10,0
5	Solidus temperature of the cast alloy	T_{sme}	^0C	1150
6	Thermal conductibility coefficient of the mould	λ_{sfo}	$W\cdot m^{-1}\cdot K^{-1}$	0,85
7	Thermal conductibility coefficient of the solidified alloy	λ_{sme}	$W\cdot m^{-1}\cdot K^{-1}$	40
8	Thermal conductibility coefficient of the liquid alloy	λ_{lme}	$W\cdot m^{-1}\cdot K^{-1}$	30
9	Specific heat of the mould	C_{sfo}	$J\cdot kg^{-1}\cdot K^{-1}$	1170
10	Specific heat of the liquid cast iron	C_{lme}	$J\cdot kg^{-1}\cdot K^{-1}$	850
11	Specific heat of the solid cast iron	C_{sme}	$J\cdot kg^{-1}\cdot K^{-1}$	750
12	Mould density	ρ_{fo}	$kg\cdot m^{-3}$	1550
13	Alloy density	ρ_{me}	$kg\cdot m^{-3}$	6700
14	Specific latent heat of the cast alloy	L_{me}	$J\cdot kg^{-1}$	250000
15	Initial temperature of the mould	T_{0fo}	^0C	20
16	Initial temperature of the cast alloy	T_{0me}	^0C	1350

Figures 3 ÷ 8 show for a number of the studied cases involving ribs of thickness bn = 3 mm the distribution of the isotherms in the cast part and the mould at the moment of solidification of the hotspots. Figures 9 ÷13 present the isotherms for ribs of thickness b_n = 5mm. Tables 2 and 3 show the coordinates of the hot spots and their respective solidification times. The hot spot coordinates relate to a frame of reference corresponding to the symmetry axes of the cast part walls, as shown in Figure 14. Figure 15 shows the influence of rib length on hot spot solidification time.

Figures 16 ÷ 19 feature the variation curves of temperature and of the solid fraction in the hot spots for some of the studied cases, in order to the reveal solidification kinetics in those points.

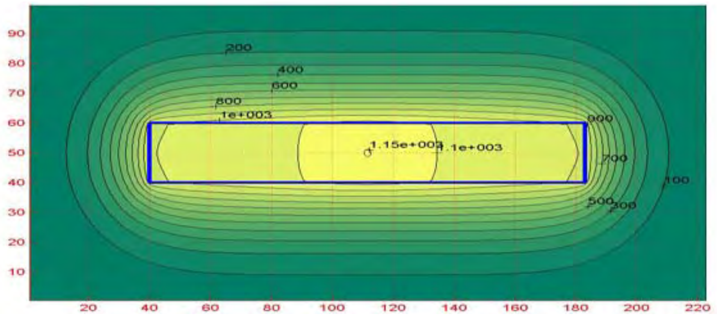

Fig. 3. *Isotherm outline for the ribless part (thickness a = 20 mm, width L = 140 mm) at the moment of solidification t = 302.70 s.*

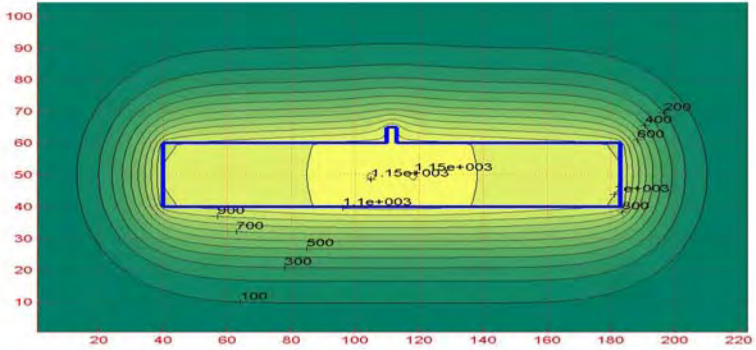

Fig. 4. *Isotherm outline for the part with a rib of thickness b_n = 3 mm and length L_n = 5 mm (at the time of solidification t_{sol} = 294.34 s).*

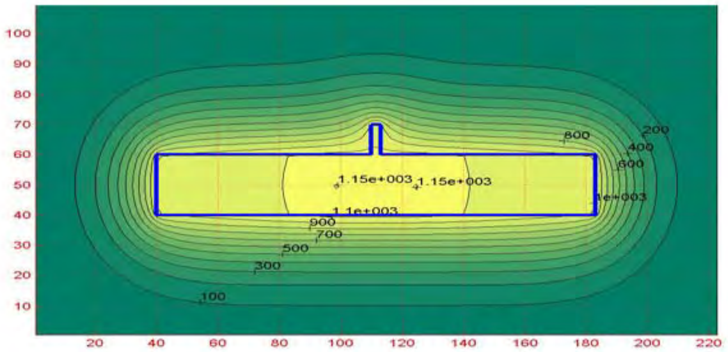

Fig. 5. *Isotherm outline for the part with a rib of thickness b_n = 3 mm and length L_n = 10mm (at the time of solidification t_{sol} = 283.02 s).*

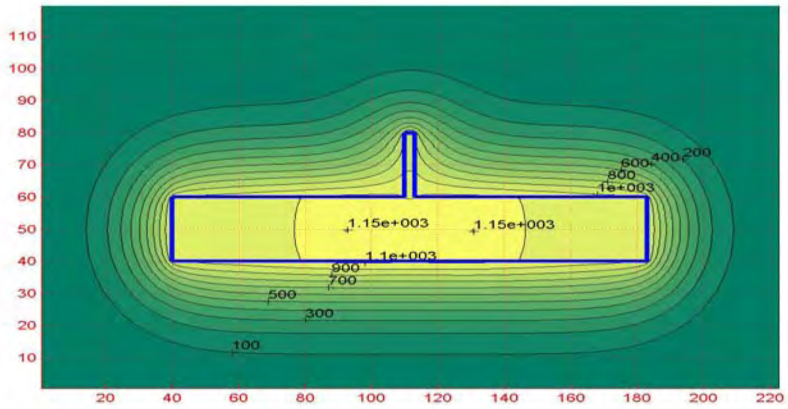

Fig. 6. *Isotherm outline for the part with a rib of thickness b_n = 3 mm and length L_n = 20mm (at the time of solidification t_{sol} = 268.06 s).*

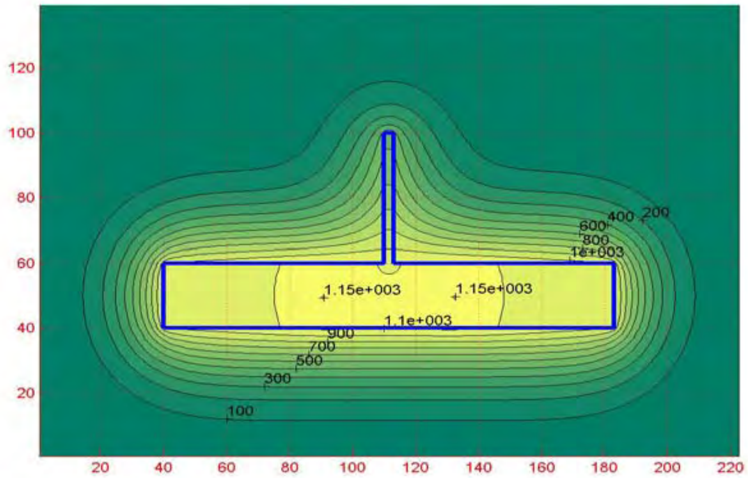

Fig. 7. *Isotherm outline for the part with a rib of thickness b_n = 3 mm and length L_n = 40mm (at the time of solidification t_{sol} = 262.24 s).*

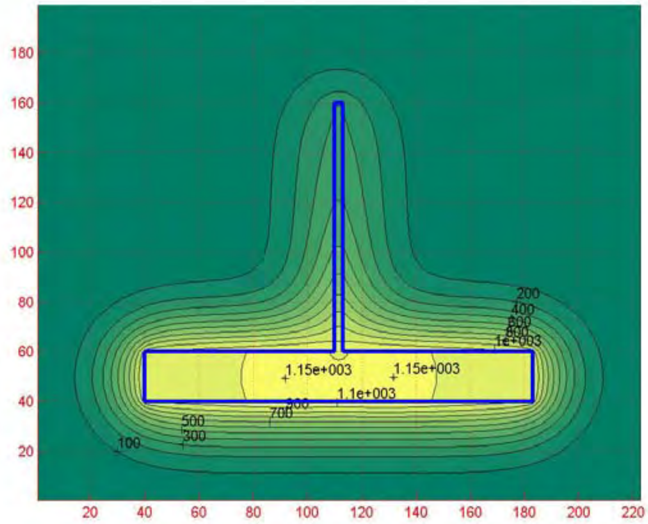

Fig. 8. *Isotherm outline for the part with a rib of thickness b_n = 3 mm and length L_n = 100mm (at the time of solidification t_{sol} = 264.08 s).*

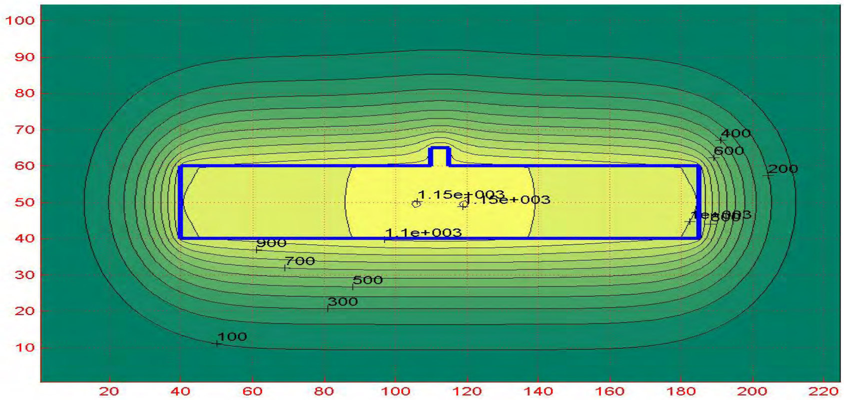

Fig. 9. *Isotherm outline for the part with a rib of thickness b_n = 5 mm and length L_n = 5 mm (at the time of solidification t_{sol} = 298.48 s).*

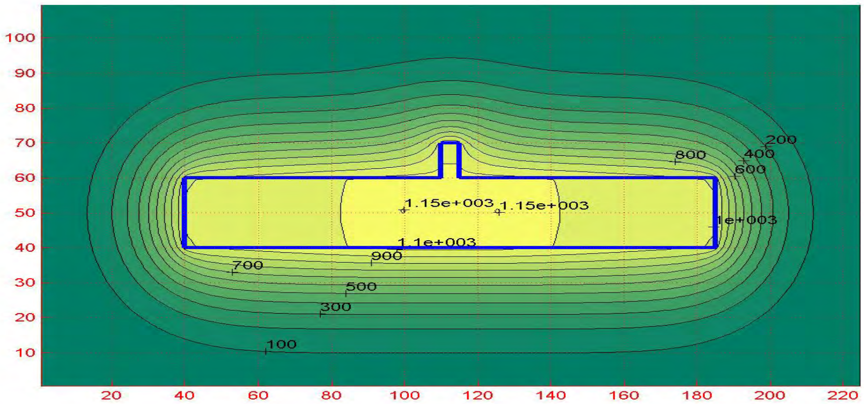

Fig. 10. *Isotherm outline for the part with a rib of thickness b_n = 5 mm and length L_n = 10mm (at the time of solidification t_{sol} = 289.00 s).*

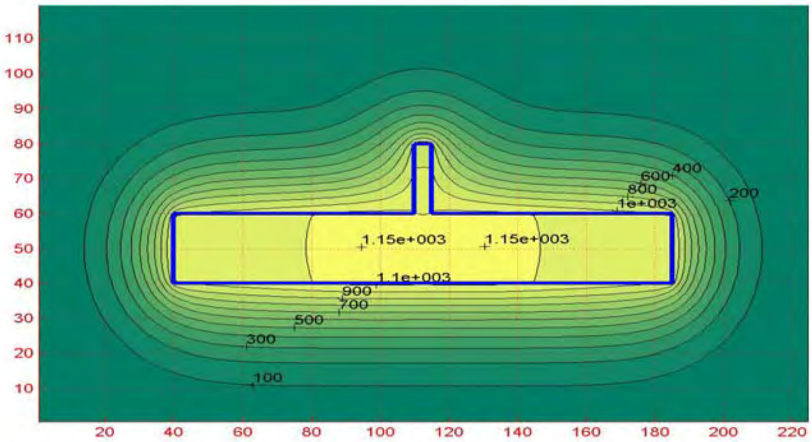

Fig. 11. *Isotherm outline for the part with a rib of thickness b_n = 5 mm and length L_n = 20mm (at the time of solidification t_{sol} = 275.30 s).*

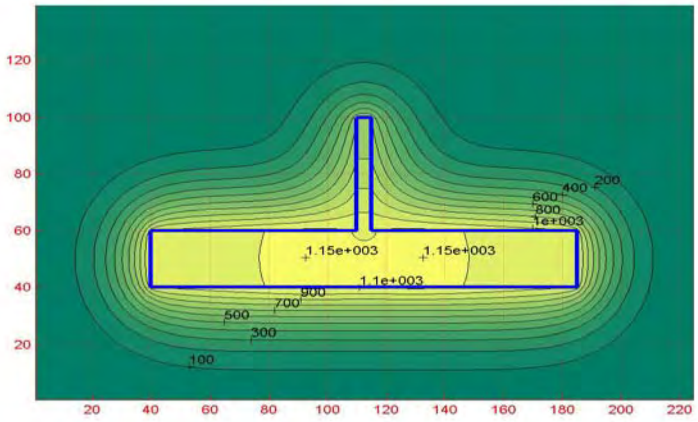

Fig. 12. *Isotherm outline for the part with a rib of thickness b_n = 5 mm and length L_n = 40mm (at the time of solidification t_{sol} = 269.62 s).*

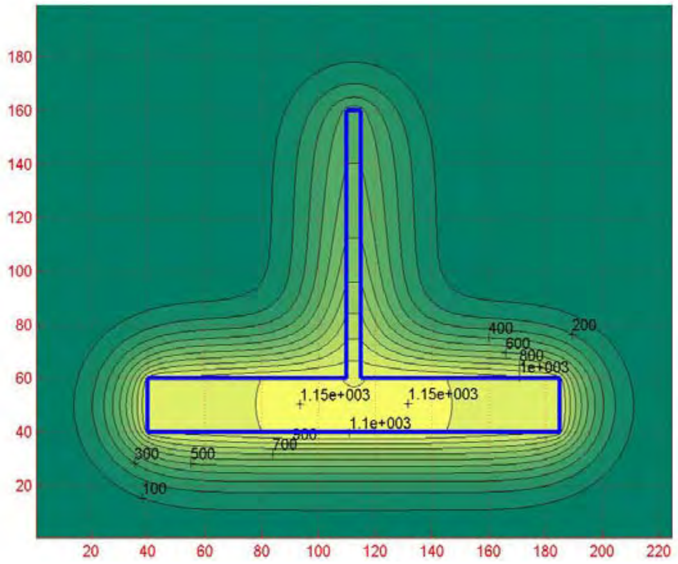

Fig. 13. *Isotherm outline for the part with a rib of thickness b_n = 5 mm and length L_n = 100mm (at the time of solidification t_{sol} = 273.98 s).*

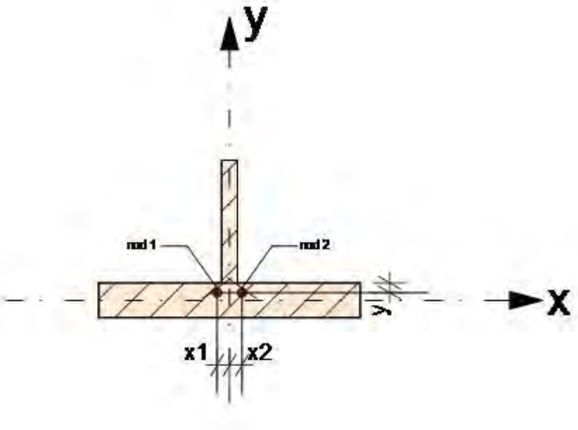

Fig. 14. *Coordinates of the hot spots.*

Table 2. *Coordinates of the hot spots and solidification time for ribs of thickness* $b_n = 3mm$

No.	**Rib lenght**	**No. of hot spots**	**Coordinates of hot spots**	**Solidification time**
Symbol	l_n	N_n	(x,y)	t_{sol}
u.m.	mm	-	(mm,mm)	s
1	0	1	(0;0)	302.70
2	5	2	(-7.0; -0.5) and (+7.0; -0.5)	294.34
3	10	2	(-13.0; -0.5) and (+13.0; -0.5)	283.02
4	20	2	(-19.0; -0.5) and (+19.0; -0.5)	268.06
5	30	2	(-20; -0.5) and (+20; -0.5)	263.00
6	40	2	(-21; -0.5) and (+21; -0.5)	262.24
7	50	2	(-21; -0.5) and (+21; -0.5)	262.58
8	60	2	(-20; -0.5) and (+20; -0.5)	263.08
9	70	2	(-20; -0.5) and (+20; -0.5)	263.52
10	100	2	(-20; -0.5) and (+20; -0.5)	264.08

Table 3. *Coordinates of the hot spots and solidification time for ribs of thickness* $b_n = 5mm$

No.	**Rib lenght**	**No. of hot spots**	**Coordinates of hot spots**	**Solidification time**
Symbol	l_n	N_n	(x,y)	t sol
u.m.	mm	-	(mm,mm)	s
1	0	1	(0;0)	304.12
2	5	2	(-7.0; -0.5) and (+7.0; -0.5)	298.48
3	10	2	(-13.0; +0.5) and (+13.0; +0.5)	289.00
4	20	2	(-18.0; +0.5) and (+18.0; +0.5)	275.30
5	30	2	(-20; +0.5) and (+20; +0.5)	270.14
6	40	2	(-20; +0.5) and (+20; +0.5)	269.62
7	50	2	(-20; +0.5) and (+20; +0.5)	270.50
8	60	2	(-19; +0.5) and (+19; +0.5)	271.58
9	70	2	(-19; +0.5) and (+19; +0.5)	272.58
10	100	2	(-19; +0.5) and (+19; +0.5)	273.98

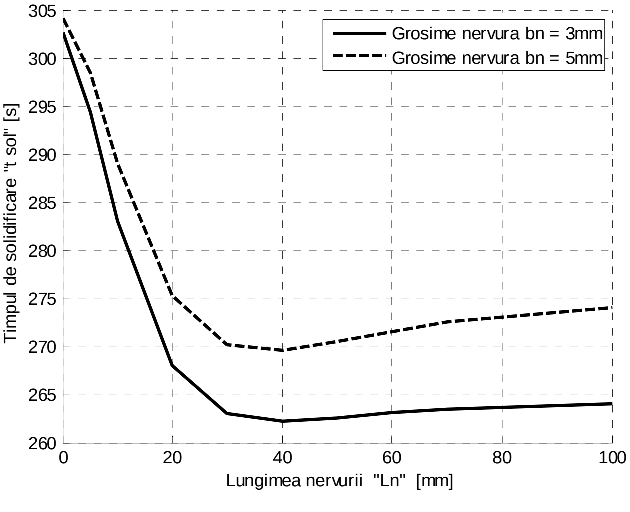

Fig. 15. *Influence of rib length "*L_n*" on the solidification time for a cast iron plate of thickness a = 20 mm (*b_n *= rib thickness;* L_n *= rib length).*

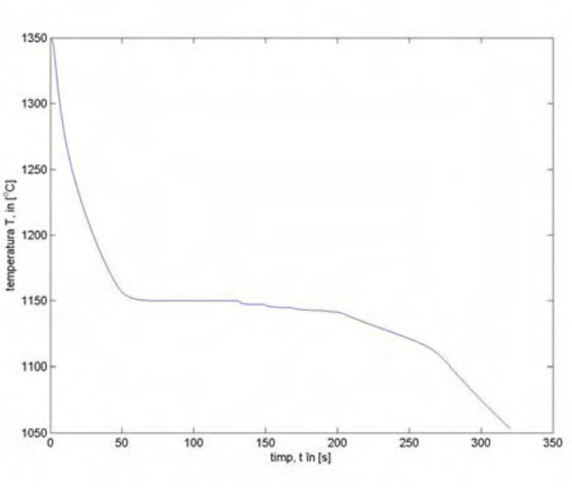

Fig. 16. *Temperature variation in the intersection of axes of symmetry of the walls part point of coordinates (x,y) = (0; 0.5), rib of thickness* b_n *= 3 mm and length* L_n *= 40 mm.*

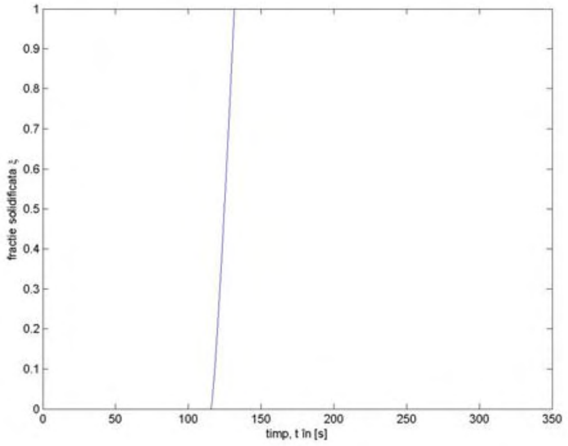

Fig. 17. *Variation of the solid fraction in the intersection of axes of symmetry of the walls part point of coordinates (x,y) = (0; 0.5), rib of thickness* b_n *= 3 mm and length* L_n*= 40 mm.*

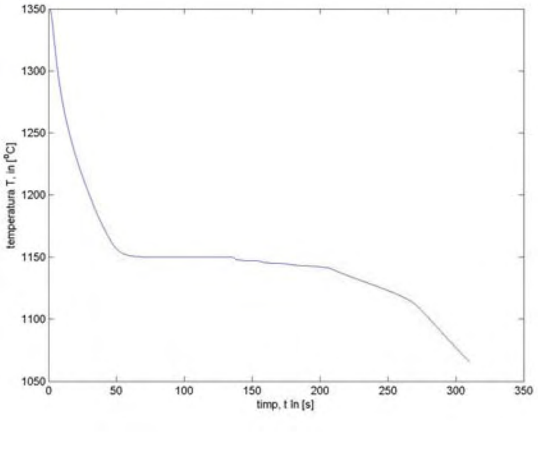

Fig. 18. *Temperature variation in the intersection of axes of symmetry of the walls part point of coordinates (x, y) = (0; 0.5), rib of thickness* b_n *= 3 mm and length* L_n *= 100 mm.*

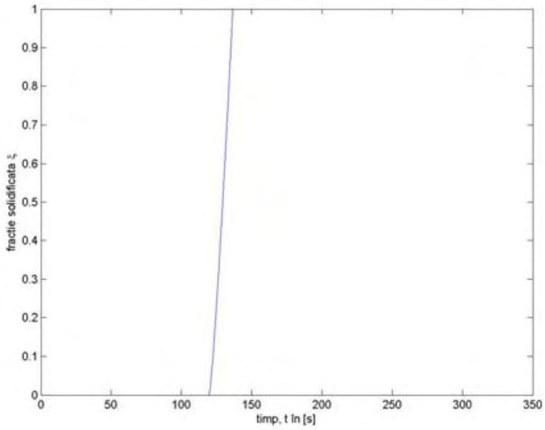

Fig. 19. *Variation of the solid fraction in the intersection of axes of symmetry of the walls part point of coordinates (x, y) = (0; 0.5), rib of thickness b_n = 3 mm and length L_n= 100 mm.*

•

3. Conclusions concerning the influence of rib length on solidification

The following conclusions are yielded by the results of this study:

- ribs significantly thinner than the wall of the cast parts have a cooling effect, causing the decrease of solidification time compared to that of a ribless part;
- the cooling effect (or wing effect) is stronger in the case of thinner ribs;
- the maximum effect of the cooling caused by the ribs is observed (in the case of the studied parts, part of thickness a = 20 mm, rib of thickness b_n = 3mm and 5mm) for a rib length of L_n = 40 mm (L_n = 2a), that is the double of the cast part wall thickness);
- the cooling effect of the ribs intensifies significantly with the increase of their length from 0 mm to 40 mm;
- the increase of rib length over L_n = 40 mm determines a small increase of the cast part solidification time, revealing a slight damping of the cooling effect;
- in the studied cases (part of thickness a =20 mm and ribs of thickness b_n = 3 mm and 5 mm) the maximum decrease of solidification time (compared to the ribless part) is of times 1.13 - 1.15, illustrating the small influence of rib length on part solidification;
- in the case of the b_n = 3 mm rib, the solidification time of the part decreases from 302.70 s in the case of the ribless part to 262.24 s for the part with a rib of length L_n = 40 mm. In the case of a rib of thickness b_n = 5 mm the solidification time decreases from 304.12s to 269.62 s (for a rib of length L_n = 40 mm);
- figures 16 ÷ 19 show that in the case of very thin ribs, the length has no visible influence on the temperature variation curves and on solidification kinetics in the rib-wall joining area.

References

[1]. Ciobanu I., Monescu V., Munteanu S. I., Crişan A. – *Simularea 3D a solidificării pieselor turnate*, Editura Universităţii “Transilvania” din Braşov, Braşov, Ro, 2010, ISBN 978-973-598-678-0.

[2]. Ciobanu I., Ţuţuianu Diana – *Estetica, element valoric al pieselor turnate*, Metalurgia, no. 1, pag. 3-8, ISSN 0461/9579.

[3]. Ciobanu, I., Maşniţă, M., Monescu, V. *Cercetări privind solidificarea pieselor cu secţiune ”T”*, Metalurgia, nr.13, 2006.

[4]. Maşniţă M. – *Cercetări privind influenţa unor factori tehnologici şi constructivi asupra solidificării pieselor turnate*, Teză de doctorat, Universitatea Transilvania din Braşov, 2007**.**

[5]. Ţuţuianu Diana, Ciobanu I. – *Consideraţii privind implicaţiile tehnologice şi estetice ale înclinaţiilor de turnare şi ale razelor de racordare în cazul pieselor turnate*, Sesiunea de comunicări stiinţifice cu participare internaţională Terra Dacică - România mileniului trei. Acad. Forţelor aeriene Henri Coandă Brasov, 5-6 mai 2006, An VII, nr.1, CD - ISSN 1453 – 0139.

[6]. Zirbo G., Ciobanu I. – *Tehnologia turnării*, vol 1 & 2, Institutul Politehnic Cluj – Napoca, 1989.

THE ANNALS OF “DUNAREA DE JOS” UNIVERSITY OF GALATI.
FASCICLE IX. METALLURGY AND MATERIALS SCIENCE
N^0. 3 – 2010, ISSN 1453 – 083X

NEW ACHIEVEMENTS IN MANUFACTURING OF CHURCH BELLS

G. FLOREA, C. OANCEA, C. GHEORGHIES
L. GHEORGHIES
“Dunarea de Jos” University of Galati
email:gflorea@ugal.ro

ABSTRACT

Analysis, modelling and design of the bells are a topical issue for manufacturers of bells, in general, and for church bells manufacturers in particular. The transition from manual design of a bell to that achieved with the computer led to fabrication of bells capable to produce sounds of bells controlled close to those of musical instruments. It is mentioned a number of specialized software such as AUTODESK, for sizing profile of a bell; RESHAPE for analyzing and adjusting tones and WAVANAL for processing issued sound. The performances of a bell are closely related to the material used, casting technologies, possibly heat treatment and their grinding, processes that can be controlled automatically by computer.

KEYWORDS: bell, sound, software

1. Introduction

Nowadays, most foundries use computer for design bells. With the help of specialized software, the future of bell geometry is achieved, starting from the bell section. Analyzing vibrations bell, bell sound, mechanical and metallurgical properties of bell, wearing bell, the tension states during its working. It also studied the degree of impact of bell tong on the bell and is make simulation of the bell movement and bell sounds. Making a perfect bell both in terms of design, especially in terms of sound, involves collaboration between musicians, acoustic engineers, IT engineers, whistleblowers, and experts in casting bells.

Figure 1 shows cross-sectional profile of a bell (a) and possible instantaneous position of the bell and his tongue (b) during oscillation movement.

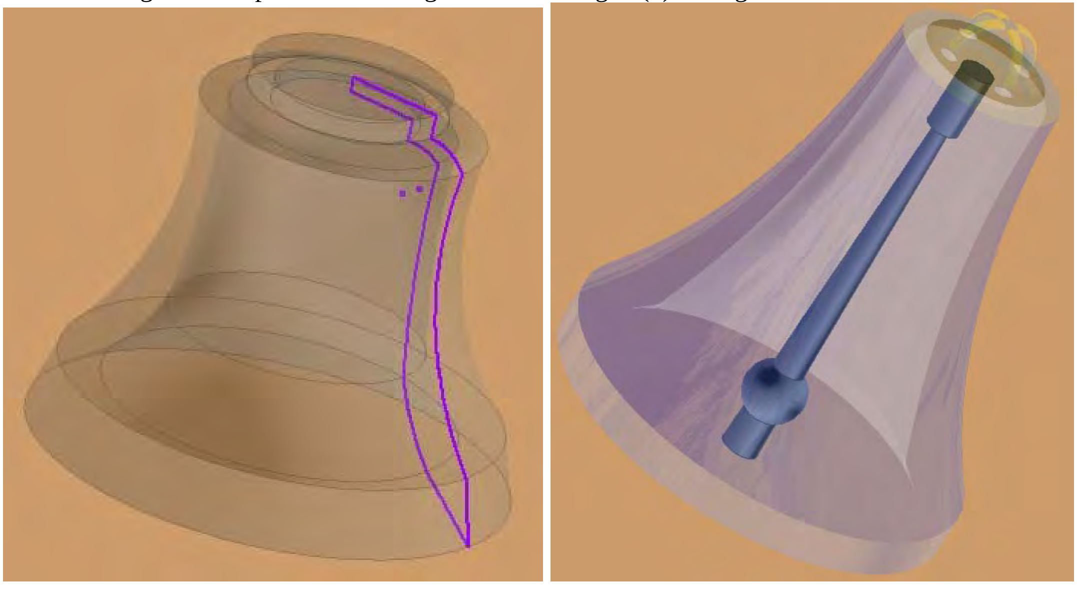

Fig. 1. *Cross- sectional profile (a) and instantaneous position of the tongue (b) of a bell.*

2. Profile Design bell

Figure 2 shows the bell shape design created with Autodesk software starts by profiling and sizing bell profile. Autodesk is a world-leading supplier of engineering software, providing companies with tools to experience their ideas before they are real. By putting powerful Digital Prototyping technology within the reach of mainstream manufacturer, Autodesk is changing the way manufactures think about their design processes and is helping them create more productive workflows.

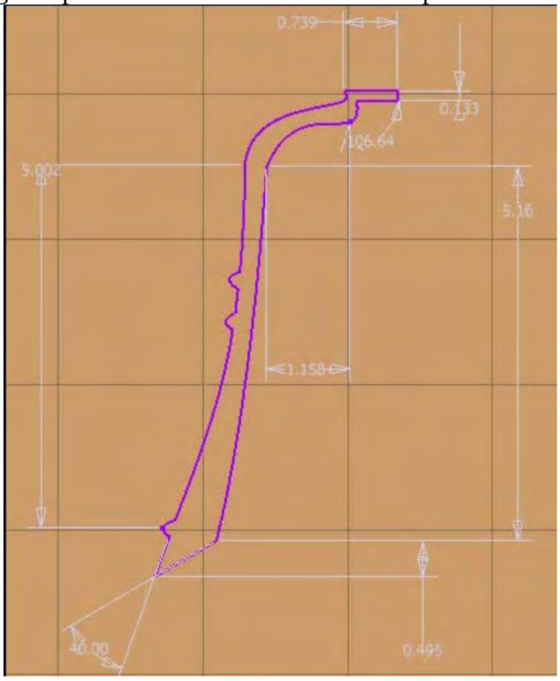

Fig. 2. *Bell shape and size obtained by Autodesk.*

Figure 3 shows the 3D image of the bell made based on two-dimensional profiles, shown in Figure 2. Bell may have very different forms from one manufacturer to another, depending on foundry tradition, the purpose of which the bell will be used or the desired sound.

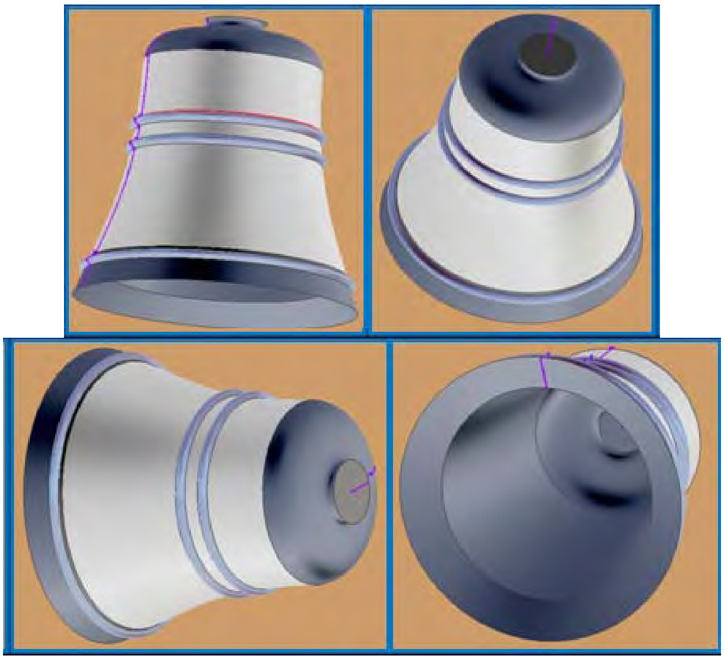

Fig.3. *3D images from 2D images of the bell, using Autodesk Inventor software.*

An important role in designing a bell is played by its own tongue. Its shape and size are the defining elements of the acoustics of a bell. In Fig. 4 the 2D profile elements of language (a) of a bell, and its size (b), both are closely related to the dimensional constructive of the bell elements.

Based on the 2D image of the bell tongue, Autodesk Inventor gets 3D image, as shown in Fig. 5.

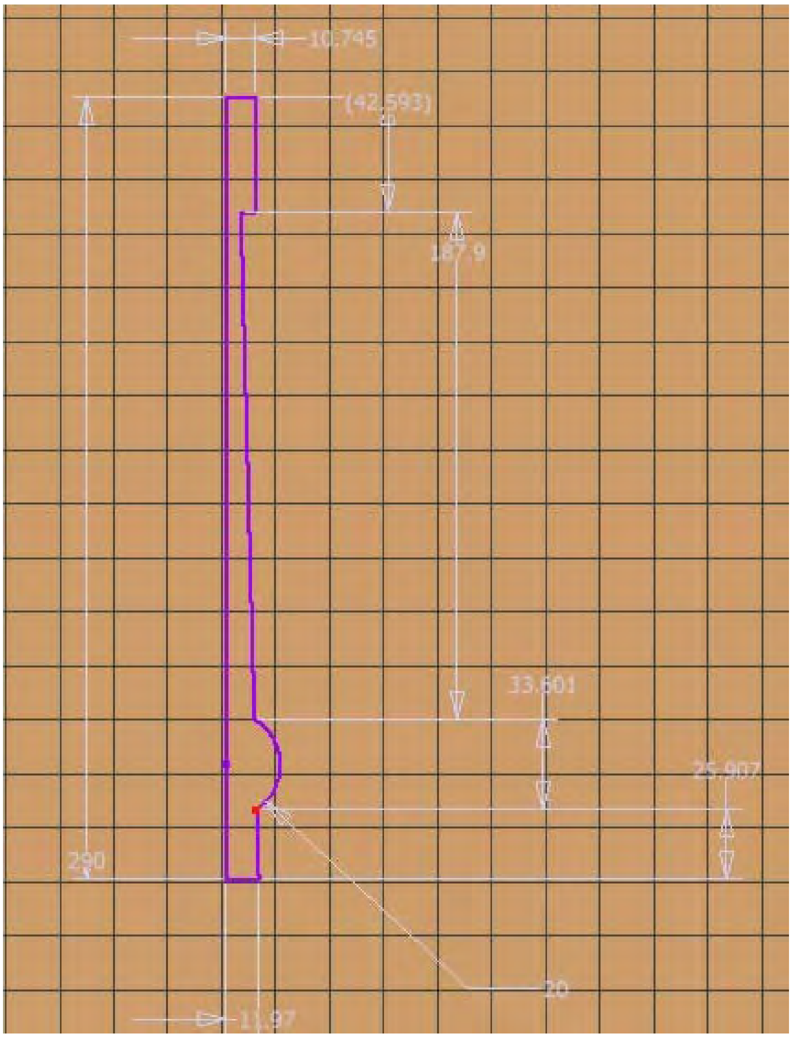

Fig. 4. *2D and tongue size bell obtained by Autodesk Inventor software.*

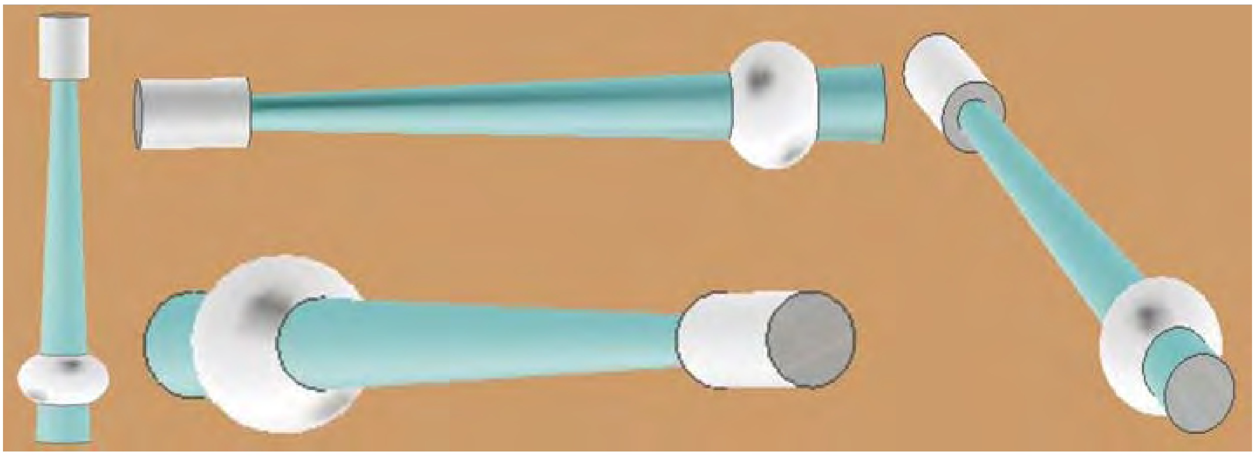

Fig. 5. *3D images obtained for bell tongue with Autodesk Inventor software.*

Composer Neil McLachlan [1] and sculptor Antonn Hassel [2] have managed to build a much better cup design using computer technology for the bells. Neil McLachlan said that this technology would create many opportunities for musical performances. A bell that can mimic the harmonic sequence of the human voice can produce an ear pleasing very smooth sound. Before its discovery technology, created by Western, bells were not really part of the orchestral instruments. Carilon bells, which are used in music does not require a tuning.

Complex profiles generated by computer modeling are either laser cut into steel thick sheets, allowing manufacturing of casting molds for larger bells, either are designed to have a high tolerance for manufacturing of smaller bells.

In Fig. 6 presents the 3D image of a bell, which allows spectral analysis of the sound, eventually achieving, later, a tuning thereof.

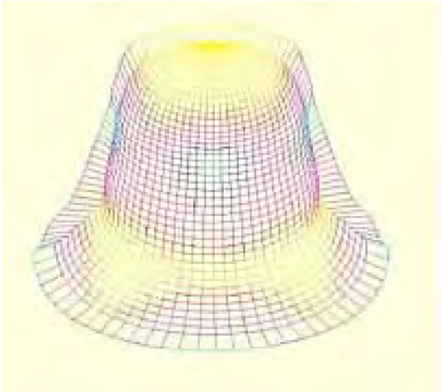

Fig. 6. *3D image of a bell with its elastic deformation.*

The sensitivity of human ear can perceive differences of sounds bell wall thickness of 50 microns and they can be detected in small bells. Australian harmonic bells are so detailed computer modeling, that the observed differences of up to 10 microns can be produced repeatedly with CNC lathes. Bells greater than 400 mm in diameter often require fine-tuning after casting them.

This process occurs on a manually operated vertical lathe.

Parties of bell that must cut are calculated by computer modeling.

By the '80s, few improvements have been made, when the engineers of Dutch companies have started to use finite elements computerized analyzers, creating three-dimensional models to determine some mechanical properties of an object.

Using this method, engineers tuned bell, the sound improves, but decreases its harmony.

3. Software used in the design and analysis of sounds

Some programs may be used in bells computerized analysis. The following software can be mentioned: Wavanal which analysis the tuning, by using pre-recorded sounds; Rounds is used to convert the tinkle of a bell in many tinkles in changing and can also use in tuning, and the Pitcher is a simple program that can check the height of a bell sounds. A comprehensive profile of the bell made by RESHAPE software in Fig.7 is presented.

The grid shows the elements that compound the bell. The blue profile was the basic profile for this stage of design (drawing at different scales). It can see the “lace" on the inner wall that was added by the computer at this stage of design. A complex form can be observed at "foot" bell.

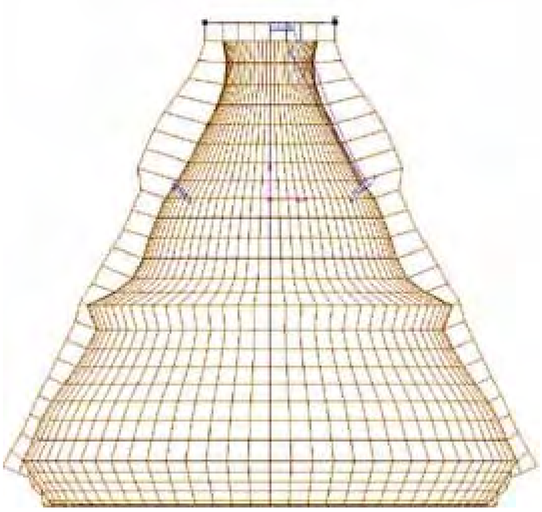

Fig. 7. *3D image of a bell made software RESHAPE software.*

The frequency spectrum for a Japanese temple bell in Kyoto in Fig. 8 is presented. The recorded spectrum by using a microphone when the tongue touches a bell in Fig. 8 is shown. There are three heights of the bell sound that take 2.5 seconds. The apparent temporal variation in the intensity of sounds emitted during the emission can be observed.

The high frequency is perceived due to presence of a very strong single component. The sharp peak at about 1.5 seconds is caused of reductions of the low frequency compound that masks a part of tone when the tongue strong beats. Average frequency that is perceived increases whiles others partial frequencies decrease.

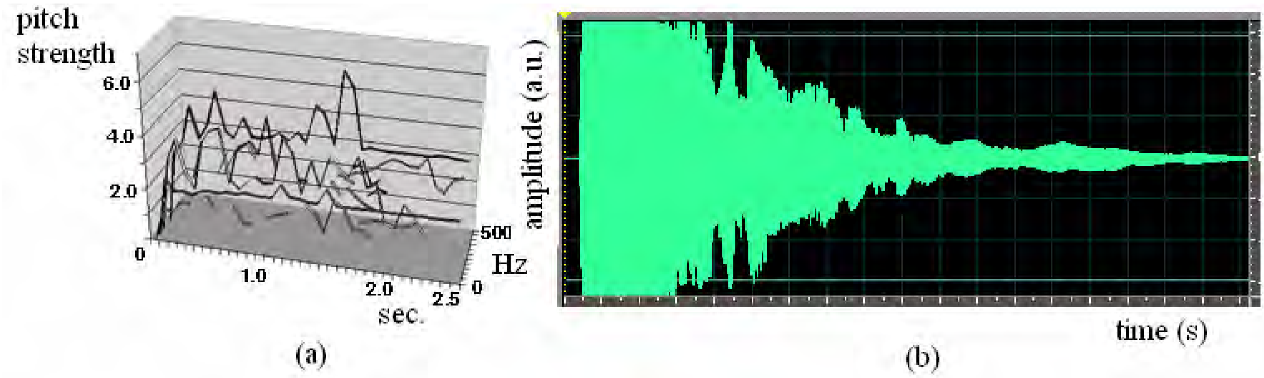

Fig.8. *Sound spectrum of a bell from a temple in Kyoto.*

The emitted sounds by a bell can be registered by multiple devices, among which the most important is the microphone. The most important criteria in selecting a microphone are quality microphone, frequency stability of the device, automatic control compared to the manual control.

4. Conclusion

For the analysis, modeling and design of bells advanced technologies are used bells, allowing their manufacturing with high accuracy. It went from manually design to that carried out by means of a computer, creating special software providing vibrational characteristics of the bell based on bell profile or alloy, such as software Autodesk – for sizing profile of a bell, software Reshape – for analyzing and adjustment of bell models or music software - like Wavanal software. Researchers in manufacturing bells field pursuit improvement of their performance starting from casting bells technology.

References

[1]. McLachlan, Neil, *Acoustic Quality in Musical Instrument Design, Sounds Australian:* Journal of the Australian Music Centre, no. 62, 2003, pp. 34-36.

[2]. Hasell, Anton and Neil McLachlan, *The Secular Bell,* in Acoustic Ecology: An International Symposium, World Forum for Acoustic Ecology, Melbourne, 19-23 March, 2003.

THE ANNALS OF "DUNAREA DE JOS" UNIVERSITY OF GALATI.
FASCICLE IX. METALLURGY AND MATERIALS SCIENCE
N^0. 3 – 2010, ISSN 1453 – 083X

HISTORY OF FABERGE EGGS

Gheorghe CROITORU[1], **Ion RUSU**[2]
[1]„INCERCOM", Chişinău, Rep. Moldova
[2]„Universitatea Tehnica din Moldova", Chişinău, Rep. Moldova
email: gcroitoru@mail.ru, irusu@mail.md

ABSTRACT

Faberge's primary source of inspiration came from works of previous centuries. Translucent enameling was a valued technique in the nineteenth century that required several coats of applied enamel and the "firing" of the object in an oven after each coat. However, only a small number of colors were used in the nineteenth century, and so Faberge took it upon himself to experiment and soon came up with over 140 shades. Technique used by Faberge included guilloche, a surface treatment that could make waves and striations in the design and could be done by machine or by hand. Faberge used natural stones often found in abundance in the area.

Fifty six Imperial eggs were made, forty-four of which have been located today and another two that are known to have been photographed. Another twelve Easter eggs were commissioned by Alexander Ferdinandovich Kelch, a Siberian gold mine owner.

However, the Imperial Easter egg collection commissioned by the last of the Russian Tzars is the most celebrated. Fabergé was given carte blanche in creating the Imperial eggs, the only requirement being that each must be unique and each must contain a surprise.

KEYWORDS: *technique, surface treatment, egg collection*

1. Introduction

Born in 1846 Peter Carl Fabergé, would become the most famous goldsmith of his time. Son of jeweler Gustav Fabergé, owner of a small silver and jewelry shop in St. Petersburg, Carl Fabergé was well-trained in the jeweler's art by apprenticeships in the major centers of the European decorative arts.

***Fig.1.** The young Fabergé.*

By the time Carl was twenty, he had also received a solid foundation in economics and commercial affairs. When Carl took over his father's jewelry firm in 1872 at the age of twenty-four, it was not much different from several other workshops catering to the upper classes of St. Petersburg. But the young Fabergé (Figure 1) was determined to distinguish the family name.

Jewelry and the decorative arts of the day had previously been valued by the size and weight of the precious stones and metals. In a departure from such gaudy ostentation, and with the help of his younger brother Agathon, a talented designer and valued advisor, Fabergé eagerly formulated a new aesthetic, which he hoped would capture the fancy of the Russian aristocracy.

According to Fabergé collector Christopher Forbes, "His feeling was that it should be creativity and craftsmanship rather than carat-content that dictated the appreciation of a piece – and he certainly had a wonderful sense of humor. So his pieces caught the attention of Alexander III, who admired them as examples of Russian genius."

"And here you see the shrewd man, the businessman," says author and Fabergé expert, Géza von Habsburg.

"He worked for an institution called the Imperial Cabinet, which was in charge of all the treasures of the Tzars in the Hermitage. And he worked there free-of-charge and repaired things, appraised things, and so on." Having earned the recognition of this prestigious organization by virtue of his expertise in the task of restoring its collections, Fabergé was invited in 1882 to participate in the Moscow Pan-Russian Exhibition, where he earned a gold medal and a good deal of press for his innovative work. It was at this event that Tzar Alexander III and his wife, Maria Fedorovna, became acquainted with the House of Fabergé, captivated by the exquisite display of jewels and *objects de luxe*

In 1885, Fabergé's hard work, meticulous standards and shrewd positioning paid off when he was given the highest honor possible for a jeweler: an appointment as "Supplier to the Court of His Imperial Majesty" (Figure 2).

That same year he received the now famous order from the Tzar to create the first Imperial Easter egg for the Tzarina [1].

Fig. 2. *Russian Imperial Court.*

In 1885 Fabergé won the Gold Medal at an exhibition in Nuremberg for his replicas of the antique treasures of Kerch. It was also in 1885 that the first Imperial egg was produced.

The beautifully simple egg opened up to reveal a yolk. Inside the yolk was a golden hen and inside the hen was a diamond miniature of the crown and a tiny ruby egg.

1.1. House of Fabergé

"Once you were one of the approved suppliers to the Crown, it was a very lucrative source of business," says Fabergé expert Christopher Forbes. "Every time the Tzar went on a visit or received another head of state, there was an exchange of gifts. Also Russia was growing as an industrial power, and Fabergé was catering to this whole class of nouveau riche Russians.

The Imperial eggs were his loss leaders to give him the cachet. But the cash was all coming from these newly minted millionaires in Russia". Author Géza von Habsburg continues: "And when the Tzar and Tzarina traveled, they traveled with suitcases full of Fabergé, which were presented here and there to people in thanks. By 1896, the year of the coronation of Nicholas II, virtually all the major presents came from Fabergé"[2].

But ironically, the man who conceived of and hand-delivered these incredible pieces had little to do with their actual fabrication. According to Christopher Forbes: "Fabergé was the head of the firm.

Fig.3. *House Fabergé in Moskau.*

Fig.4. *Carl Fabergé.*

He had the best designers, the best goldsmiths, the best jewelers, the best stonecutters, the best miniaturists all working for him. At the top of the success of the firm he had over five hundred employees, four shops in Russia, one shop in London and a catalogue operation.

He provided the taste and the direction, and he was the genius that got all these artists and artisans to work together to produce these incredible fantasies."

These men were organized into autonomous workshops under master craftsmen hand-picked by the Fabergé brothers. "The head workmasters were the key persons in the realm of Fabergé," says author Géza Von Habsburg. "They stood at the apex of the pyramid immediately under Fabergé, and they controlled the entire output of the workshops. The inventions came from Fabergé.

These were discussed with the head work masters, and then taken to the design studio."

The process of making the eggs usually took about one year. After the preliminary period of detailed and meticulous planning, sketches and models were prepared. Discussions were held among the goldsmiths, silversmiths, enamellers, jewelers, lapidary workers and stonecutters who would contribute their talents to the finished creation. Then the parts were farmed out to the various Fabergé workshops.

Fig.5. *Fabergé workshops.*

"Fabergé had his mechanisms made in Switzerland, and he had the portrait miniatures either done by Russians or Germans or Scandinavians, "adds Forbes". He used the best available craftsmen from wherever he could find them to create these objects. But most of the eggs, as far as we know, were made in the workshops of either Michael Perkhin or Henry Wigstrom, who were sort of the head craftsmen. And they had whole teams of people working under them". (figure 3,4,5)

Fabergé refused to be limited by nineteenth century goldsmith techniques. If methods did not exist to execute his ideas, he required that his craftsmen invent them. In the field of enameling, they developed and perfected techniques that far surpassed those of the competition: "Creating the eggs with the tools that they had, by hand, and making them look as though they were just some miracles that had occurred, is actually an enormous feat of technology," explains author Lynette Proler". Fabergé used an extraordinarily complicated enameling process, a technique that cannot be duplicated, even today.

The House of Fabergé actually buried their own documents, and his formulas and techniques have been lost. They're secreted away someplace, and ware hopings one day that somebody will find them." While his competitors used a standard palette of whites, pale blues, and pink, Fabergé took it upon himself to experiment. He created resplendent yellows, mauves, salmon and all shades of greens – over one hundred forty new colors in all [3].

"Fabergé wrote to his clients saying that everything he produced was one-of-a-kind, guaranteed," adds Von Habsburg. "Anything that was unsold at the end of the year – this was real salesmanship at that time – would be destroyed. So shopping at Fabergé's must have been the ultimate experience, because everything was unique. This is the greatest thing about Fabergé and the reason I admire him most of all. He never repeated himself. Imagine producing 150,000 different objects without repeating yourself!"

Faberge's primary source of inspiration came from works of previous centuries. Translucent enameling was a valued technique in the nineteenth century that required several coats of applied enamel and the "firing" of the object in an oven after each coat. However, only a small number of colors were used in the nineteenth century, and so Faberge took it upon himself to experiment and soon came up with over 140 shades. The most prized of these was oyster enamel which varied in color depending on the light. Materials used by Faberge included metals - silver, gold, copper, nickel, palladium - that were combined in varying proportions to produce different colors. Another technique used by eighteenth century French goldsmiths and again Faberge involved a simple tinting of the completed work using stones and enamel. Another technique used by Faberge included guilloche, a surface treatment that could make waves and striations in the design and could be done by machine or by hand. Faberge used natural stones often found in abundance in the area. These included jasper, bowenite, rhodonite, rock crystal, agate, aventurine quartz, lapis lazuli, and jade (nephrite mostly although he would sometimes use jadeite). Precious stones including sapphires, rubies and emeralds were used only for decoration, and when used they were en cabochon (round cut). Diamonds were typically rose-cut. Semi-precious stones including moonstones, garnets, olivines, and Mecca stones were used more often en cabochon. Fifty six Imperial eggs were made, forty-four of which have been located today and another two that are known to have been photographed. Another twelve Easter eggs were commissioned by Alexander Ferdinandovich Kelch, a Siberian gold mine owner. However, the Imperial Easter egg collection commissioned by the last of the Russian Tzars is the most celebrated.

Fabergé was given *carte blanche* in creating the Imperial eggs, the only requirement being that each must be unique and each must contain a surprise. Concealing his plans – even from the Tzar – Fabergé would spend nearly a year meticulously designing and crafting appropriate surprises. "And we're told these eggs were, at that time, conversation pieces. And even the Tzar would ask, 'What's the surprise going to be in the next running?' But Fabergé would only say, 'Majesty will be satisfied.' So it was the best-kept secret in St. Petersburg."[4].

2. The history of the eggs

When an egg was complete, it was brought to the palace and presented to the Tzar in person by Fabergé, while the anxious craftsmen remained at their workstations, waiting until Fabergé returned to assure them of its safe delivery.

The **Lilies of the Valley egg (1898)** is a translucent pink-enameled treasure covered with gold-stemmed flowers made of pearls, diamonds and rubies. One flower, when turned, releases a geared mechanism inside to raise the fan of tiny miniatures from the top – portraits of the Tzar and his first two daughters, Olga and Tatiana. Every spring, Alexandra had the rooms of the palaces filled with beautiful floral bouquets. Fabergé knew that pink was the favorite color of the Empress, and lilies of the valley her favorite flower.

The jade **Alexander Palace egg (1908)**, Figure 6, contains a perfect replica of their favorite royal residence in the country – only two and one half inches long. And sailing on the clear rock crystal sea of the **Standart egg (1909)**, is a replica of their royal yacht – reproduced to the last detail – where many happy days were spent together (Figure7).

Fig.6. *A. Palace egg.*

Fig.7. *Standart egg.*

"I think that was where Fabergé differed so much from all the other jewelers of the period," adds author Lynette Proler. "Where they were only interested in large gemstones, Carl Fabergé was interested in the ultimate effect that a piece would have, a lasting effect so that every time you looked at a particular object, you would have this great sense of sheer enjoyment and pleasure from it."

Fabergé knew both the joys and sorrows of the Romanovs. According to Proler, "It wasn't very well known, of course – the Imperial family kept it very quiet – that the Tzarevich had hemophilia. He was dying; he was very close to death, so close that the Imperial Court had already written out his death notice. But Alexei survived, and Fabergé designed a special tribute. The **Tzarevich egg (1912)** was Alexandra's most cherished (Figure 9).

In 1900, the railway that would link European Russia with the Pacific coast was near completion, an accomplishment that brought Nicholas great satisfaction and the support of his country. Fabergé devised an ingenious offering to celebrate the event.

Etched on a belt of silver encircling the **Trans-Siberian Railway egg (1900)** is a map of the railway line, the stations marked in precious stones. And inside there is a little train just one foot long (Figure 9) [5].

"It's made out of gold and platinum, and its headlights are diamonds, and its rear lights are rubies, and the coaches are individually labeled for gentlemen, for smoking, for ladies.

There was a restaurant car, and at the end there was the traveling church, which was appended to the Imperial train. It winds up, and I've tried it myself," says author Géza von Habsburg.

"The mechanism is a bit rusty, and it moves slowly, but it's like a sort of old 'dinky toy" [6].

Fig.8. *Tzarevich egg.*

Fig.9. *Trans-Siberian.*

Railway egg

But most Russians had no time for toys. The zeal to expand the empire led to a disasterous war with Japan and further demoralized the country.

Hopeless wars, famine, disease and despair were unraveling the fabric of faith the Tzar's people once had in the divine right and benevolence of the monarchy. Choosing to believe in the unfailing devotion of his people, Nicholas became a prisoner of his self-delusion.

2.1. Outrageous opulence

With every egg, Fabergé outdid himself in technique, detail or complex mechanics. Some of the world's best examples of handcrafted automata are hidden in the jeweled shells of the Imperial eggs. At the stroke of the hour, a ruby-eyed rooster emerges crowing and flapping its wings from the top of the elaborately designed **Cockerel egg (1900)**. Fabergé was known to have worked on the mechanism of the Peacock Clock in the Winter Palace, and his familiarity with that famous automaton no doubt inspired the creation of this egg. "Fabergé, who had traveled a lot, had absorbed all the currents, the various artistic currents, in Paris, in Florence, in Dresden, in London," says author Géza Von Habsburg. "He could go back to this memory bank and select objects from it.

Fig.10. *Bay Tree egg.*

For instance, the Bay Tree egg in the Forbes Magazine Collection is based on an 18th century mechanical orange tree, a French automaton, which was a fairly well-known object which Fabergé must have seen during his travels.

Other eggs that Fabergé made were based on objects he saw in the imperial treasury and used as prototypes for his first eggs. The **Bay Tree egg (1911),** Figure 10**,** is laden with gemstone fruits set among carved jade leaves. Turning one of the fruits opens the top of the egg as the tiny bellows inside producing the sweet song of a feathered bird.

As if to bolster the Tzar's self-image during his most trying times, Fabergé presented Nicholas with a series of eggs commemorating achievements of the Romanovs. In lavish Rococo style, the **Peter the Great egg (1903)** celebrated the two-hundredth anniversary of the founding St. Petersburg; the **Napoleonic egg (1912)** honored the Motherland's victory over the French general and his armies, Figure 11,12[7].

Fig.11. *Peter egg.*

Fig.12. *Napoleonic egg.*

In 1913, the three-hundred-year rule of Russia under the House of Romanov was recorded in the portraits encircling the **Tercentenary egg (1913)** – from the founder, Mikhail Fedorovich, to Catherine the Great, and Nicholas himself, Figure 13.

Fig.13. *Tercentenary egg.*

The white enameled shell of this egg is nearly obscured by over eleven hundred diamonds and golden symbols of royal order. Inside, a globe of burnished steel inlaid in gold displays the frontiers of Russia in 1613 and the vastly extended borders of Russia under Nicholas II.

Two Eggs presented to the Dowager Empress Maria Fedorovna – the **Winter egg (1913)** and the **Grisaille egg (1914)** – may best represent the height of Fabergé's career, expressions in miniature of the life of Imperial privilege. Both were kept at Maria's favorite Anichkov Palace: one inspired by the serene surroundings in winter; the other by the opulent embellishments of the palace interior, where many of the ceilings are painted *en grisaille*.

At that time, there was great hope that Russia would yet prevail in the war, and Fabergé was asked to continue the tradition of Imperial Easter eggs. But to match the solemn mood of the nation and reflect the noble efforts of the family, Fabergé wisely altered the tone of the Easter gifts that year [8].

Inside the **Red Cross egg (1915)** given to the Dowager Empress Maria, are portraits of the Romanov women dressed as Sisters of Mercy, Figures 14,15.

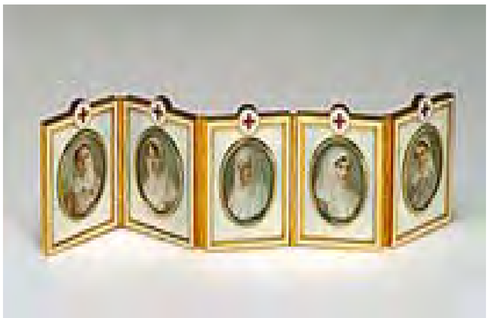

Fig.14. *Romanov women.*

Inscribed inside are the words, "Greater Love hath no man than this, to lay down his life for his friends."

Fig.15. *Red Cross Egg.*

Fig.16. *Image of Nicholas.*

In 1915, the Tzar appointed himself "Supreme Commander of the Army," displacing one of the top generals. For this act, he was awarded the Order of St. George, given for outstanding military bravery or achievement. "Nicholas had decided to take over from his cousin, Grand Duke Nicholas Nikoliovich, this tall giant of a man, beloved by his soldiers, who had been at the head of the armies. And this was maybe, for the Tzar, the high point of his reign," says author and Fabergé expert, Géza von Habsburg. "He could do no wrong at that time, and the war went very favorably at first for Russia."

Believing as many did that now the Tzar would overcome the difficulties, Fabergé designed two eggs to applaud the event. For the Tzarina, he painted an image of Nicholas consulting with his officers at the front (Figure 16).

Resting on the points of four miniature artillery shells, the **Steel Military egg (1916)** makes up in sober significance what it lacks in ornamentation, Figure 17.

Fig.17. *Steel Military egg.*

According to Von Habsburg: "Fabergé had to close down his workshops because his craftsman were all at the front. He was unable to continue to make these objects of art. He had no more precious materials.

Gold and silver were no longer allowed to be handled by jewelers at that time so it was steel and brass and copper that they were using. And the imperial family could also not be seen ordering expensive things from Fabergé at a time when Russia was bleeding to death." The simple **Order of St. George egg (1916)**, given to the Dowager Empress Maria that year, was another gesture to wartime austerity.

Away from St. Petersburg supervising Red Cross activities in the south, she wrote to her son: "I thank you with all my heart for your lovely Egg, which dear old Fabergé brought himself. It is beautiful. I wish you, my darling Nickya, all the best things and success in everything. Your fondly loving old Mama."

2.2. The fate of the eggs

In 1918, after the death of the Romanovs, the House of Fabergé was nationalized and ransacked by the Bolsheviks. Fabergé and members of his family (Figure 18) left Russia on what was to be the last diplomatic train to Riga, not realizing that they would never be able to return to their beloved Russia again.

Fig.18. *Fabergé and members of his family.*

According to author Géza von Habsburg: "When Fabergé saw that all was lost – all of the members of the Imperial family on Russian soil had been murdered – he decided that was it, his whole world had collapsed, and he fled to Switzerland, where he died in 1920 of (I would say) a broken heart." Soon after the revolution, the contents of the Romanov palaces were confiscated by the Bolsheviks. Most of the Fabergé eggs, along with masses of Imperial gold, silver, jewels and icons were inventoried, packed in crates and taken to the Kremlin Armoury. Several eggs disappeared during the looting and pillaging of the palaces. The only egg not found at the time was the Order of St. George egg, which the Dowager Empress had managed to save, along with other valuables, when she was evacuated from Yalta to England aboard the British battleship Marlborough.

"All the other jewelry and the eggs were sent, by order of Lenin, to Moscow and stayed there," says Von Habsburg.

"They were lost in some dark passage in the Kremlin Armoury storerooms; nobody knew where they were." There the crates containing the eggs remained, unopened, guarded by Kremlin staff. But Lenin's efforts to preserve Russia's cultural heritage were undermined when Joseph Stalin came to power. Stalin began trading the Russian Imperial legacy for desperately needed Western currency to support his new regime. "The treasures were rediscovered somewhere around 1927. For the communists, there was the idea at the back of their minds that these things might actually be sold for the good of the new Bolshevik government, to finance their economic plans. So these things were taken out of safekeeping, appraised, and offered to the West." (Von Habsburg).

Recognizing that the treasures of a dynasty were being swept into oblivion, the eminent businessman and socialist sympathizer brought ten of the eggs to America in the early 1930's. Hammer set up business and heavily marketed and promoted the sale of these riches, but during the Depression years, even the most stable American fortunes had faltered. A friend of Hammer's ironically observed that while the Fabergé eggs were indisputably beautiful, they were not, in fact, edible [9].

According to Géza von Habsburg: "Hammer arrived here in New York in 1931 with thousands of Russian works of art to be sold on behalf of the Soviets. At the time there was no money... deepest Depression... nobody was interested... until he struck on the idea of marketing these things through department stores. And he took them through North America, from the East coast to the West coast, stopping at department stores in every major city and touting these things, lecturing about how he discovered these things. And they caught on."

There were five major collectors in the early days here in the United States: Matilda Geddings Gray, Lillian Thomas Pratt, Marjorie Merriweather Post, India Early Minshall and Malcolm S. Forbes.

Though some Imperial eggs originally were sold at auction for as little as four or five hundred dollars, it took several decades for the eggs to gain recognition as magnificent works of art. Now they are valued in the millions.

3. Conclusion

- The technique used by Faberge included guilloche, a surface treatment that could make waves and striations in the design and could be done by machine or by hand.
- Faberge used natural stones often found in abundance in the area.

References

[1]. Tatiana Fabergé, Lynette G. Proler, Valentin V, Skurlov. *The Fabergé Imperial Easter Eggs* (London, Christie's 1997)

[2]. The History of the House of Fabergé according to the recollections of the senior master craftsman of the firm, Franz P. Birbaum (St Petersburg, Fabergé and Skurlov, 1992)

[3]. Henry Charles Bainbridge, Peter Carl Fabergé - *Goldsmith and Jeweller to the Russian Imperial Court* - His Life and Work (London 1979, Batsfords - later reprints available such as New York, Crescent Books, 1979)

[4]. A Kenneth Snowman, *The Art of Carl Fabergé* (London, Faber & Faber, 1953-68)

THE ANNALS OF "DUNAREA DE JOS" UNIVERSITY OF GALATI.
FASCICLE IX. METALLURGY AND MATERIALS SCIENCE
N^0. 3 – 2010, ISSN 1453 – 083X

QUALITY ASSURANCE OF CYLINDRICAL CASTED PARTS WITH SMALL THICKNESS

**Nicolae CANANAU, Alexandru CHIRIAC,
Vasile BRATU**
"Dunărea de Jos" University of Galati
email: ncananau@ugal.ro

ABSTRACT

The casting of the cylindrical parts with great diameter and small thickness and intermediary flange is difficult because of the great values of the forced contraction. Thus the value of the tensile stress is very great and can determine the fracture of the part in zone of the thermal knot. For assurance of the quality of these parts some technological solutions are necessary. The paper shows the analysis of this aspect and presents practical solutions.

KEYWORDS: casting, solidification, small thickness, flange

1. Introduction

The casting is a very good technological method for obtaining complex engineering parts.

The parts with great diameter and length and very small thickness when have intermediate flange present a thermal knot (Fig.1).

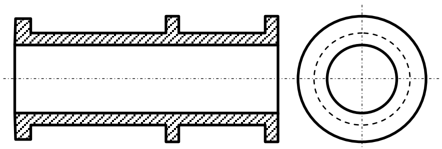

Fig. 1. *Example of a part with thermal knot.*

The thermal knot has a great influence on the solidification process and on the quality of the casted part. This can determine a contraction hole (shrink hole) in the case of the metallic material with great contraction coefficient at the solidification.

In the case of the metallic material with fragility (in the casted state) and great thermal contraction coefficient, cracks can be developed.

Under the practical condition, cracks appear with a relatively great frequency.

In this paper we develop the study in the aim of analyzing the casting and solidification processes for eliminating the causes that can determine the appearance of cracks in zones of the thermal knot.

2. Analysis of the solidification process

We will consider that the solidification process begins immediately, in the certain point, when the casting process is finished. We admit that the material of the cast form (mould) is homogeneous and uniform. Under these conditions, the heat flux from the casted material to the casting mould, at the beginning of the solidification process, is constant.

In the following stage the thermal flux is different in the different geometrical points of the thermal knot.

Admitting a macro-element with the volume V and surface area A, we get of the equation of heat flux [1]:

$$\overline{\alpha} A\left[T(t)-T_0\right]=V\dot{Q}_{gen}-V\rho c\frac{dT}{dt} \qquad (1)$$

Where:

$$\dot{Q}_{gen}=\rho_s \Delta H_f \frac{\partial f_s}{\partial t} \qquad (2)$$

The function f_s has the form:

$$f_s=a+bT$$

and, after the integration, using the initial condition, we obtain the time t_s of solidification of the parts defined by equation:

$$t_s=-\frac{\rho c V}{\alpha A}\left(1-\frac{b}{c}\Delta H_f\right)\ln\left(\frac{T_f-T_0}{T_i-T_0}\right) \qquad (3)$$

In the above equations we have:

$\overline{\alpha}$ -mean heat transfer coefficient, ρ-density, c-specific heat, ΔH_f- latent heat of melting, T_f-melting temperature, T_i-casting temperature, T_0- temperature of the mould.

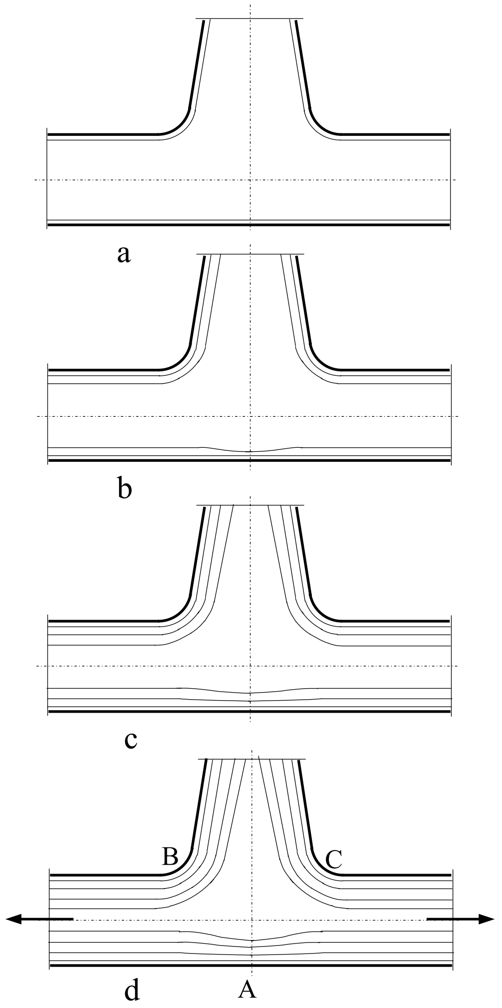

***Fig. 2.** Evolution of the solidification front.*

The equation (3) proves that the solidification time is greater when the local volume is greater. Therefore the greatest solidification time is in the centre of the thermal knot.

The solidification front, in the thermal knot, at various moments of the solidification process is represented in Figure 2.

In the first phase of the solidification process, the intensity of the heat transfer is constant and, consequently, the solidification front is uniform in the entire contour of the form walls (Fig. 2a).

In the following phase (Fig. 2b), the intensity of the heat transfer decreases in the points B and C because of the peak form of the mould. Consequently the thickness of the solid layer in these points is smaller than in the points of the uniform thickness of the part.

In the point A, because of the great quantity of the melt metallic material, the thickness of the solid layer is small, too.

When solidification finishes, without the thermal knot, the two solidification fronts meet in the middle of the part wall.

In the thermal knot rests an important quantity of liquid metallic material. The thickness of the solid phase is variable with minimum value at the point A.

Simultaneous with the solidification process, the thermal contraction of the solid phase is developed, because the cast part has flanged at the both its heads. The part has a great length and, consequently, the absolute value of the free contraction is great.

Because we have forced contraction, the tensile stress in zone A can be greater than the strength of the material, in the given conditions, and the crack appears.

In the practical conditions, we found the cracks at the interior surface of the cast parts at the label of the point A.

3. The solution of the problem

The solving of the objective, the elimination of the cracking rescue, entails the control of the solidification process by the control of the heat transfer in the junction of the walls.

We consider the solidification module defined by the expression:

$$M = \frac{V}{S} \tag{4}$$

In this relation, V is the volume of the melting material and S is the surface of the heat transfer.

The solidification time is correlated with the solidification coefficient through the relation:

$$t = k \cdot M^2 \tag{5}$$

Definitely, in the above relations it is supposed that the intensity of the heat transfer is constant on the interface cast material-mould. In the real conditions, the heat transfer intensity has dynamic character and the evaluation of the correct value of the local intensity of the heat transfer is necessary.

For ensuring the control of the solidification time, respectively a correct value of the solidification module in the thermal knot, it is chosen one of the following methods:

- changes in the local form and thickness of the cast part,
- use of cooling elements,
- use of thermo-insulating sleeves included in the mould walls,
- modification of some mould walls by the forced heating or cooling.

Through the use of cooling elements in the construction of the casting mould, the real partial solidification modules change. For the calculus of the real solidification modules, in this case, the knowledge of the cooling coefficient k_i for the surfaces with the cooling elements or thermo-insulating sleeves is necessary. In this aim is used the equation that describes the heat quantity extracted by the mould from the cast part through unity of contact surface mould-cast part, in function of temperature gradient liquid alloy – mould and time, used by Chvorinov, at the definition of the exterior geometric solidification module, for the multiplication of real solidification module with the factor n in the conditions of the given thermo-physical characteristics of the available materials.

In Table 1 the thermo-physical characteristics of the various materials are showed. They are materials with small and great values of thermo-physical characteristics.

Table 1. *Thermo-physical characteristic of some materials*

Material	**Density** kg/m^3	**Specific heat** J/(kg K)	**Thermal conductivity coefficient** W/(m K)	**Heat accumulating coefficient** Ws/m K
Mould mixture (95% quartz sand + 5% sodium silicate)	1700	1312	1.5	1856
Mould mixture (97.8% quartz sand + 1.8% furfurol + 1% ortophosphoric acid)	1700	1356	1.35	1761
55.6% quartz powder + 22.8% quartz sand + 16.6% ethyl–silicate and catalyser	1600	1232	1.12	1579
46% zircon powder + 39% zircon sand + 16.6% ethyl–silicate and catalyser	2700	968	1.35	1881
Raw mould mixture (quartz sand and bentonite)	1800	1050	0.29	740
Dried mould mixture (quartz sand and bentonite)	1700	840	0.17	492
Low carbon steel	7850	840	50"	18157
Medium carbon steel	7850	800	46	16996
Cast iron	7200	540	40	12470
Siluminum (86-89% Al + 14-11% Si)	2600	880	160	19133
Bronze (90% Cu + 10% Sn)	8760	360	42	11508
Copper	8900	440	380	38575
Diatomite (brick)	550	840	0.17	280
Vermiculite	300	830	0.14	186

It is observed that the metallic materials, used as cooling elements, have the heat accumulating coefficient 10-30 times greater then of the mould mixture, and thermo-insulating materials have the heat accumulating coefficient 2-10 times smaller of than the mould mixture.

The exterior cooling elements for the casting of steel parts are worked frequently from steel (sheet or rod), in case of the complex form they are cast form cast iron, and in very complex form, the cooling elements form magnesite mixture are used.

The forms of the metallic cooling elements are showed in Figure 3.

Solving the problem is possible through the use of exterior or interior cooling metallic elements.

The interior cooling element can be used, but is important to establish very exactly its volume for ensuring complete melting. Otherwise the part may be rejected.

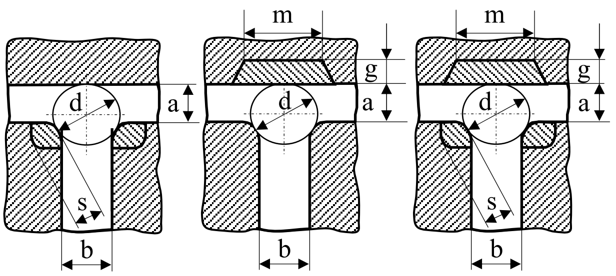

Fig. 3. *Forms of the exterior cooling elements.*

***Table 2**. Dimensions of the cooling elements*

Cooling mod	**Dimensions of the cooling space,** mm		**Dimensions of the cooling elements,** mm		
	a	*b*	g	s	*m*
Thermal knot cooled with two elements	from 20 from 20 to 20 to 20	to 20 from 20 to 20 from 20	-	0.5-0.6 *d* 0.3-0.4 *d* 0.5-0.6 *d* 0.3-0.4 *d*	-
Thermal knot cooled with one element	from 20 to 20 to 20	to 20 from 20 to 20 from 20	0.5-0.6 *a* 0.5-0.6 *a* 0.6-0.8 *a* 0.6-0.8 *a*	-	2.5-3 *b* 2-2.5 *b* 2.5-3 *b* 2-2.5 *b*
Thermal knot cooled with three elements	from 2 from 20 to 20 to 20	to 20 from 20 to 20 from 20	0.4-0.5 *a* 0.4-0.5 *a* 0.5-0.6 *a* 0.5-0.6 *a*	0.4-0.5 *d* 0.3-0.4 *d* 0.4-0.5 *d* 0.3-0.4 *d*	2.5-3 *b* 2-2.5 *b* 2.5-3 *b* 2-2.5 *b*

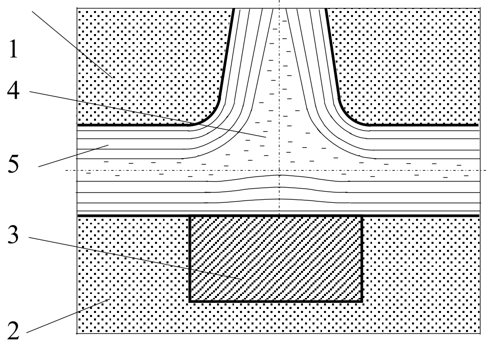

***Fig. 4.** Solidification with cooling element: 1-casting mould, 2-mould kernel, 3-cooling element, 4-liquid phase, 5-solid phase.*

The exterior cooling element, included in the mould kernel (Fig. 4), is the favorable method for intensifying of thermal flux in zone of the metal agglomeration.

The heat transfer between the cast metal and the mould is intensified, in the metal agglomeration zone, because the heat conduction coefficient increases.

Here it makes heat transfer through thermal conduction metal-metal more intense of thermal conduction metal-casting mould mixture. Consequently, the evolution of the solidification front is reversed in comparison with the before case mentioned.

As a result, the thickness of the solid phase in the point *A* is greater than the one in zones of the uniform thickness of the part walls. The dimensions of the cooling element are established in function of the dimensions of the part wall and intermediary rib.

Thus, for *a* equal of 25mm and *b* equal to 30mm, we must use a cooling element with dimensions: m=60-75mm and g=12.5-15mm.

4. Conclusions

The casting process of the parts with great diameter and length and small thickness, relatively, two marginal flanges and one intermediary flange is difficult because of three reasons:

- firstly it occurs a great thermal contraction after the solidification of the part,
- secondly the great fragility of the steel in the cast state,
- thirdly small value of the solidified crust.

As a result, these can appear a crack in the plan of the intermediate flange, in the thermal knot of the cast part.

This rescue may be diminished or eliminated by using exterior metallic cooling elements assembled in the kernel of the mould.

The dimensions of the cooling element are calculated in function of the characteristic dimensions of the part in zones of the thermal knot.

References

[1]. Stefanescu D.M. - *Stiinta si ingineria solidificarii pieselor turnate*, Ed. AGIR, Bucuresti, 2007.

[2]. Flemings M.C. - *Solifification Processing,* McGraw-Hill, 1974.

[3]. Ciobanu I., Munteanu S.I., Crişan A. - *Un nou concept în turnătorie: modulul de solidificare real al pieselor turnate*.- Revista de turnătorie, nr. 1-2, 2005, pag 27 - 33

[4]. Ciobanu I., Munteanu S.I., Crişan A. - *Modulul de solidificare al barelor cu secţiune U.Partea I: Modulul de solidificare ideal*.- Revista de turnătorie, nr. 3-4, 2005, pag3-7

[5]. Ciobanu I., Munteanu S.I., Crişan A. - *Modulul de solidificare al barelor cu sfecţiune U.Partea II:* -Modulul de solidificare real.- Revista de turnătorie, nr. 5-6, 2005, pag 9 -16, ISSN 1224-21-44

[6]. Ciobanu I., Munteanu S.I., Crişan A. - *Caracterizarea solidificării pieselor turnate prin modulul de solidificare real* .- Metalurgia, nr.5, 2005, pag. 15- 25, ISSN 0461/9579.

[7]. Chvorinov N. - *Teoria solidificării pieselor turnate.* - Giesserei 17 mai 1940, pag.177-186, Giesserei 31 mai 1940, pag.201-208, Giesserei 17 iunie 1940, pag. 222-225.

[8]. Defretin G. - *Calcul des modules de solidification apparents des pieces de fonderie.* - Fonderi 384, decembrie 1978, pag. 355-361.

[9]. Siegel A., Howell J.R. - *Thermal Radiation Heat Transfer*, Hemisphere Publ. Co., New York, 1981.

THE ANNALS OF “DUNAREA DE JOS” UNIVERSITY OF GALATI.
FASCICLE IX. METALLURGY AND MATERIALS SCIENCE
N^0. 3 – 2010, ISSN 1453 – 083X

A SETUP FOR PREPARATION OF GLASS-CARBON COATINGS ON TiO_2-Nb_2O_5 INTENDED FOR HIP JOINT PROSTHESES

Jordan GEORGIEV[1], Stefan STEFANOV[1],
Dimitar TEODOSIEV[2], Lubomir ANESTIEV[1]
[1] Institute of Metal Science, Bulgarian Academy of Sciences, Sofia, Bulgaria
[2]Space Research Institute, Bulgarian Academy of Sciences, Sofia, Bulgaria
j.georgiev@ims.bas.bg

ABSTRACT

A setup for preparation of glass-carbon coatings on TiO_2-Nb_2O_5 ceramic materials, intended for implants for surgery of hip joint prostheses, is described. The setup described consists of vacuum tight ceramic chamber; programmable high temperature furnace and a system for controlled introduction of inert gas into the chamber.

The setup allows working with temperatures up to 1350^{o}C, controlled heating rates from 1 to 15^{o}C/min and chamber pressures down to 10^{-2} mmHg.

KEYWORDS: ceramics, glass- carbon coating, coating setup

1. Introduction

There exist several materials used for production of endoprostheses: biocompatible stainless steels, pure titan or its alloys, cobalt alloys, some polymers, inert bio-ceramics (e.g. Al_2O_3, ZrO_2), glass-carbon etc. All these have their strong and weak sides but all of them have one common quality, namely, they are biocompatible and comply with the ISO 5832-1 standard, stating the requirements for the materials used for bio-implants.

One, still unsolved, problem at the utilization of biomaterials for production of hip joint prostheses is their limited life span, which at present is less or around 20 years. Obviously, the increase of the life span of these materials is highly desirable, especially when these are intended for implantation in relatively young patients.

In a series of papers Jordanova et al. studied the synthesis of a composite material based on Rutile ceramics TiO_2-0.3-10 mol.% NbO_5 [1,2].

This composite material depends strongly on the structure and reactivity of the ceramics. The same authors found that the composite prepared by coating of the TiO_2-NbO_5 ceramics with amorphous carbon is not rejected from the human body and is thus suitable for preparation of human implantants.

The glass carbon is an amorphous modification of the crystalline carbon, not found in the nature. Compared to the crystalline carbon the amorphous (glass) carbon is lacking the characteristic for crystalline substances long distance ordering of the atoms. It should be noted, that the glass carbon modification is unstable and that it tends to transform to crystalline form, during coating process. Therefore, to obtain the desired glass carbon modification and keep it stable during the subsequent deposition on the TiO_2-Nb_2O_5 ceramic's surface, it is required a specialized setup for preparation of glass-carbon and its deposition on ceramics.

The aim of the present paper is to describe such experimental setup, designed and constructed in the BAS, and its tuning to working conditions.

2. Description of the equipment

The setup designed (see Fig.1), consists of: vacuum tight ceramic chamber, which is a ceramic tube with a 120mm diameter and length of 1500mm, furnished with vacuum tight flanges; programmable high temperature ceramic Silit-furnace, allowing reach temperatures up to 1350^{o}C and controlled heating rates from 1 to 15^{o}C/min; a vacuum system, allowing pressures down to 10^{-2} mmHg, consisting of rotational vacuum pump **2DS-2**; and a system for controlled introduction of inert gas into the chamber, made around needle-valve, allowing controllable gas flow through the chamber.

Fig.1. *Photo of the setup for deposition of glass carbon coatings.*

Obviously, the production of the desired carbon coating requires application of predetermined temperature regimes inside the chamber. Fig.2 shows the block-scheme of the furnace and the temperature controlling unit. The thermal block of the setup consists of: thermo-chamber with Silit heaters (1) and computer-model-selected positions for positioning of the specimens; temperature controller (2); power electronics block (3); and PC-based system for collecting and storing of data.

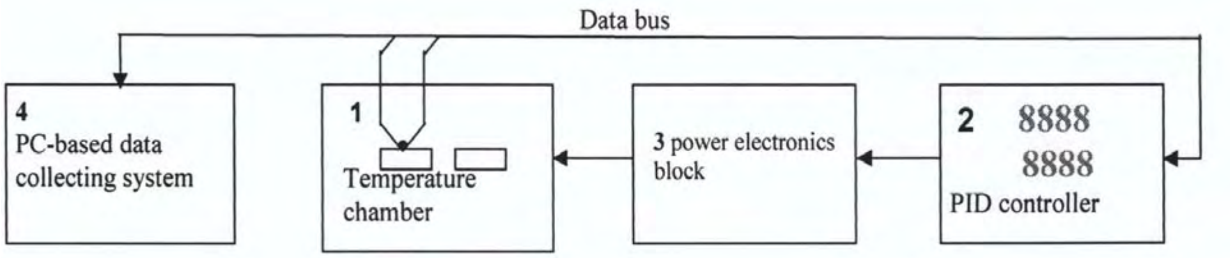

Fig. 2. *Block-scheme of the furnace, the temperature controlling and data collecting units.*

The data collecting procedure during the coating process is as follows: the specimens, to be coated with glass-carbon, are placed into the chamber (1) and are submitted to a pre-selected temperature regime, monitored by the PC-system (4). The desired temperature regime, i.e. the electric current to the Silit heater, is controlled by the controller (2) via the power electronics block (3). During the coating experiments carried out, it was found that a quality coating is obtained only if the temperature-time regime inside the furnace closely follows the one preset by the operator. This imposes certain requirements to the controller, such as ability to keep a linear interpolation between two preset points on the coordinate system temperature-time. The circumstances above predetermined the choice of the controller.

It is well known that the most suitable for the requirements imposed are the universal PID (proportional–integral–derivative) controllers. The PID controller calculates an "error" value as the difference between a measured process variable and a desired set-point. The controller attempts to minimize the error by adjusting the process control inputs. In the absence of knowledge of the underlying process, which is actually the case here, PID controllers are the best choice. However, for best performance of the controlled item, the parameters of the specific PID device used must be tuned according to the nature of the controlled system, in our case the furnace. Since the design of the furnace is unique the parameters controlled by PID would be also unique and would depend on the specific system.

In other words, a successful controlling of the temperature regimes desired would depend on successful tuning of the PID controller unit.

$$y(t) = P.x(t) + I.\left[\int_0^t x(t)dt\right] + D.\left(\frac{dx(t)}{dt}\right) \qquad (1)$$

The PID control scheme is named after its three correcting terms, whose sum constitutes the manipulated variable *y(t)* see Eq.(1).

Here: ***P***, ***I*** and ***D*** are the tuning parameter termed, respectively; Proportional gain, Integral gain and Derivative gain.

For the specific case here, controlling of the temperature inside the furnace, an eight channel PID controller "**COMECO-RT1800**" type is used.

All eight channels of the controller allow pre-programmable temperature-time profiles of the type "initial temperature - plateau - final temperature" with linear temperature-time laws for heating and cooling.

The tuning of the PID controller above was carried by heating the furnace on its maximal power without back feed up of the controlling system. From the results obtained, the time constant τ, absolute delay d and amplification coefficient K, have been graphically determined. The tuning parameters of the controller were graphically calculated from the **S**-curve, $T= f(t)$ shown in Fig.3, using the dependencies:

$$\mathbf{P=1,2.T/K.d;\quad I=0,6.T/K.d2\quad D=0,6.T/K} \qquad (2)$$

according to Ziegler-Nichols PID tuning Rules [3, 4]. The concrete temperature profile used for the tuning procedure and obtaining of the PID parameters for the COMECO-RT1800 controller is shown in Fig.4.

Fig. 5 shows a selection of glass-carbon coated ceramics produced with the setup described.

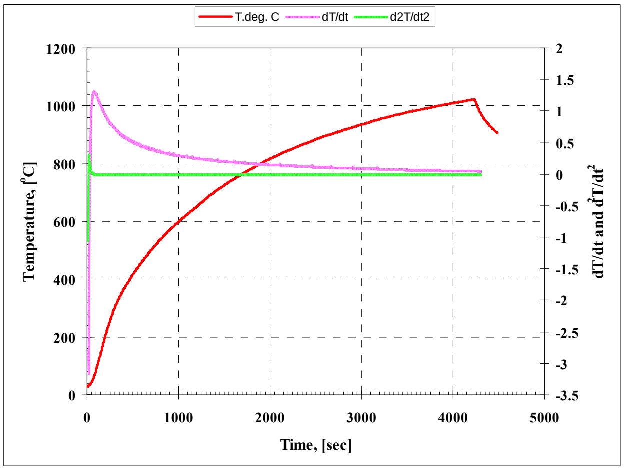

Fig. 3. *Temperature-time dependencies used for tuning of the* ***COMECO-RT1800 PID*** *controller.*

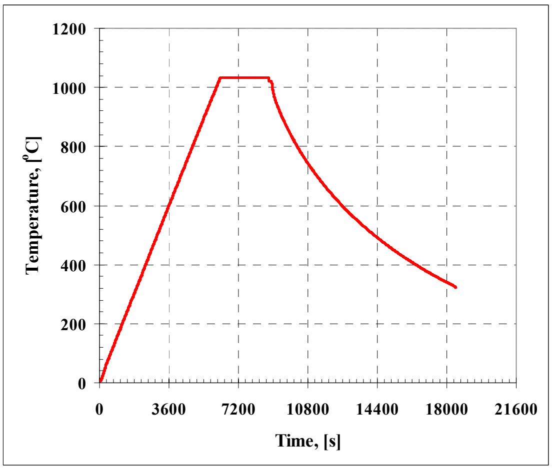

Fig. 4. *Temperature profile used for the tuning procedure and obtaining the parameters for the COMECO-RT1800 PID controller.*

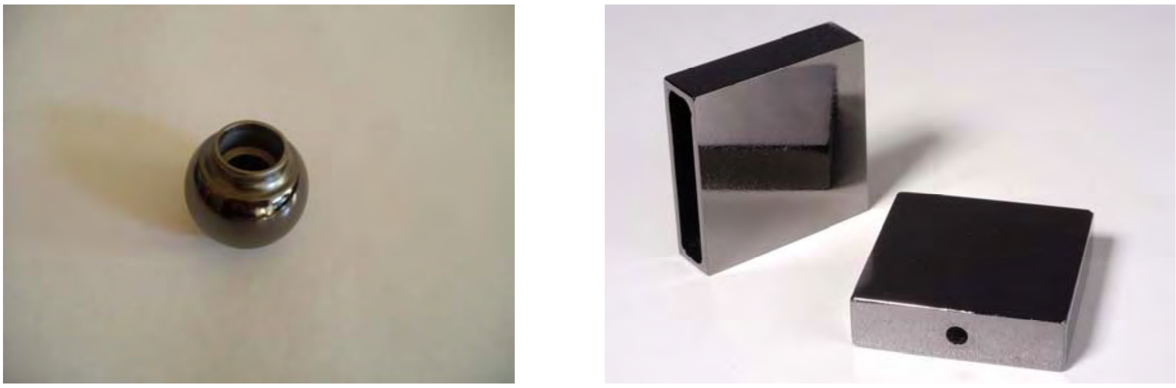

Fig. 5. *A selection of glass-carbon coated ceramics produced with the setup described.*

3. Conclusion

Based on the experience gained by using the setup for preparation and deposition of glass-carbon coatings on ceramics it could be concluded that the controller, selected and used in the setup, allows:

Maximum flexibility at preprogramming of different temperature regimes depending on the coating applied and the substrate ceramics used.

The obtained PID parameters keep the controlled parameters well within the desired limits, required for production of high quality coatings, respectively, for a successful practical application of the glass-carbon coating setup.

The designed and constructed setup allows development of new technologies for coating of different materials.

Acknowledgements

The authors are grateful to National Science Fund of Bulgaria for the financial support of this work by projects DO 02-234/2008 and BRS-11/2007.

References

[1]. Jordanova M., D. Teodosiev, J. Georgiev *„Composite ceramic materials based on vitreous carbon as transplantation materials in the human organism – Obtaining and structure,* Acta morphologica et antropologica, vol. 6, 2001, pp. 64-69.

[2]. Jordanova M., D. Teodosiev, J. Georgiev *„Composite ceramic materials based on vitreous carbon as transplantation materials in the human organism* – Basic structural and functional tests, Acta morphologica et antropologica, vol. 6, 2001, pp. 70-75.

[3]. Copeland, B. R., *The Design of PID Controllers using Ziegler Nichols Tuning,* Department of Economics University of British Columbia, March 2008.

[4]. McMillan, G. K., *Good Tuning,* ISA Measurement and Control, Volume EMC 27.01.

THE ANNALS OF “DUNAREA DE JOS” UNIVERSITY OF GALATI.
FASCICLE IX. METALLURGY AND MATERIALS SCIENCE
N^0. 3 – 2010, ISSN 1453 – 083X

RESEARCH ON THE EFFECT OF TEMPERATURE AND DURATION OF IMMERSION ON THE LAYER THICKNESS OF ZINC COATING OBTAINED IN MICROALLOYED ZINC MELTS

Tamara RADU, Lucica BALINT, Viorel DRAGAN
„Dunărea de Jos” University of Galaţi
email: tradu@ugal.ro

ABSTRACT

This paper aims to establish the influence of temperature and duration of immersion on the thickness of zinc layer deposited through a thermal process, in correlation with the chemical composition of melted zinc. Layers obtained in microalloyed zinc with nickel, bismuth, tin, lead, aluminium, at different times of immersion and temperature, are analyzed. In terms of layer thickness, melted zinc microalloyed with bismuth and / or lead to coating to increase the content in these elements has thicknesses of increasingly small effect given the increasing fluidity of the melt in their presence. Decreased thickness of the layer is enhanced by increasing temperature and decreasing the duration of immersion. Best results are obtained at a temperature of 460^{0}C and 5 seconds of immersion time.

KEYWORDS: duration of immersion, layer thickness, microalloyed zinc

1. Introduction

The thickness layer resulted from zinc coating of steel is an important characteristic of the galvanized product. Thick layer of hot dip galvanizing process varies with temperature and immersion time and depends on the chemical composition of melt [1]. Elements of microalloying change the fluidity and surface tension of zinc melt and consequently drainage (leakage) of zinc when support is extracted from the melt [2, 3].

Immersion temperature affects both quality and quantity of zinc deposited on the surface of bands and produce ash, slag and dross. The melting temperature of zinc is of approximately 420^{o}C and zinc layer deposited at temperatures above 420^{o}C increases to 470^{o}C (Fig. 1.)

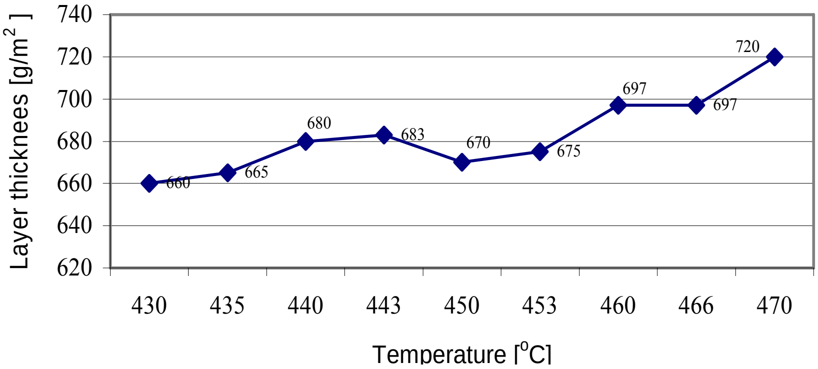

***Fig.1.** Influence of temperature on the thickness of zinc coating on steel sheet by a maintenance period of 90 seconds.*

The usual working temperature in the galvanizing process is chosen between 450-460^{o}C. At lower temperatures it is a more difficult adhesion between zinc and steel and at higher temperatures (over 470^{o}C) when the layer thickness starts to decrease, Fe-Zn alloys begin to break passing interface in the melt and form a large amount of dross [4].

Time of immersion. Duration of immersion is determined by the thickness of steel sheet and desired thickness of the layer [4]. For a given temperature, a given composition to melt and the same work speed, increasing the duration of immersion leads to a corresponding increase in deposit weight.

The optimal duration is determined by technology.

The short amounts of time lead to defective adhesion and uniformity, and too long lead to a strong attack, large layer of Zn-Fe alloy and the emergence of such compounds in the melt (matt, ash), [5].

2. Experimental research

Steel sheet has been galvanized to its chemical composition according to Table 1, in zinc melts whose chemical composition is shown in Table 2.

Table 1. *The chemical composition of steel support*

C	S	Mn	P	S	Al	Ti	V	Cu	Ni	Cr	Mo	As
[%]												
0.025	0.015	0.210	0.013	0.010	0.046	0.002	0.001	0.005	0.008	0.025	0.001	0.004

Table 2*. The chemical composition of experimental zinc melts*

Alloy sample	**Chemical composition,** [%]						
	Ni	Bi	Sn	Cd	Pb	Al	Zn
Zn- Ni-Bi-Sn-Cd	0.16	0.71	2.95	0.26	0	0	remaining
Zn- Ni-Pb-Sn	0.16	0	2.88	0	0.72	0	remaining
Zn- Ni- Pb-Bi-Sn	0.16	0.41	3.49	0	0.43	0	remaining
Zn-Bi I	0	0.27	0	0	0	0	remaining
Zn-Bi II	0	0.36	0	0	0	0	remaining
Zn-Bi III	0	0.52	0	0	0	0	remaining
Zn-Bi-Sn-Al	0	0.44	0.86	0	0	0.33	remaining

Presences of microalloying elements influence layer thickness by altering the characteristics of zinc melt. It was applied microalloying with lead and bismuth elements that increase the fluidity [6] and favour the leakage of zinc and lead toobtaining layers with small thicknesses. Tin and nickel slow reactions between zinc and iron favour the formation of a substantial layer of zinc. Microalloying with nickel, bismuth, tin, cadmium and lead was directly made, using metallic elements, finely crushed, followed by mechanical mixing. At microalloying with nickel, it was applied a maintenance at 700^{0}C.

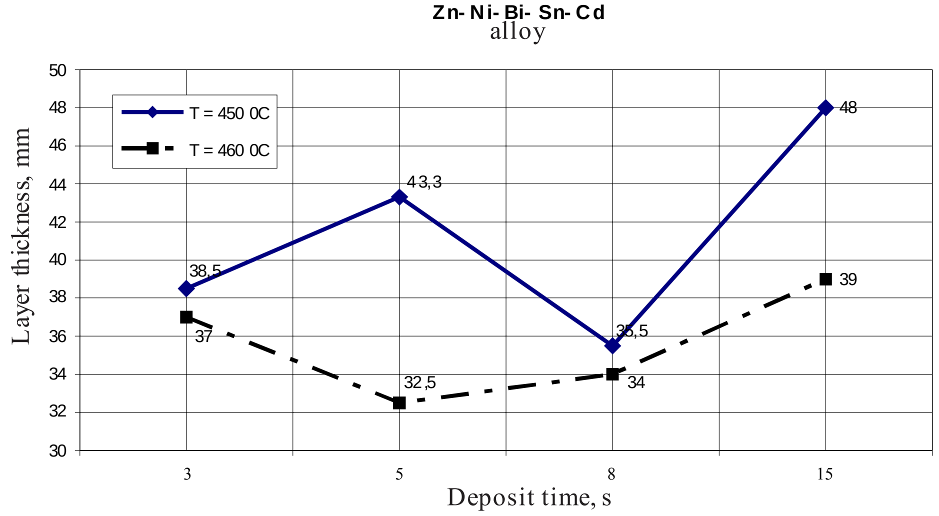

Fig.2*. Layer thickness variation depending on temperature and duration of immersion, (Microalloyed Zn with Ni-Bi-Sn-Cd).*

In the experiments, there wasn’t applied any control and uniformity process, coating thickness resulting in a free flow of zinc from the sample. Experimental immersion times were 3, 5, 8, 15 seconds. Layer thicknesses were measured with a special X-ray device.

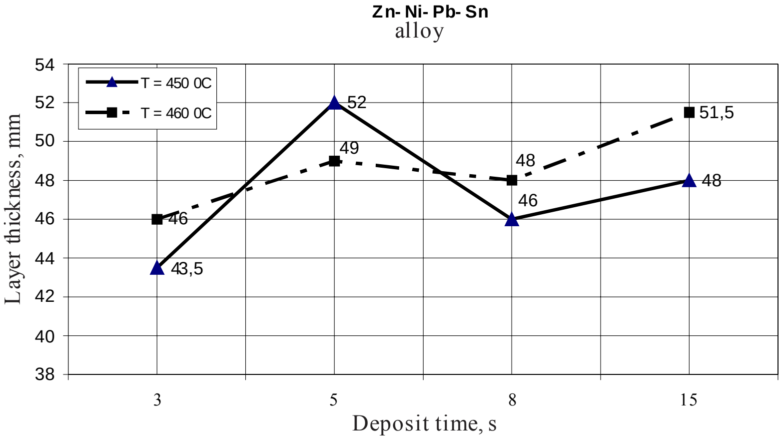

Fig. 3. Layer thickness variation depending on temperature and duration of immersion, (Microalloyed Zn with Ni-Pb-Sn).

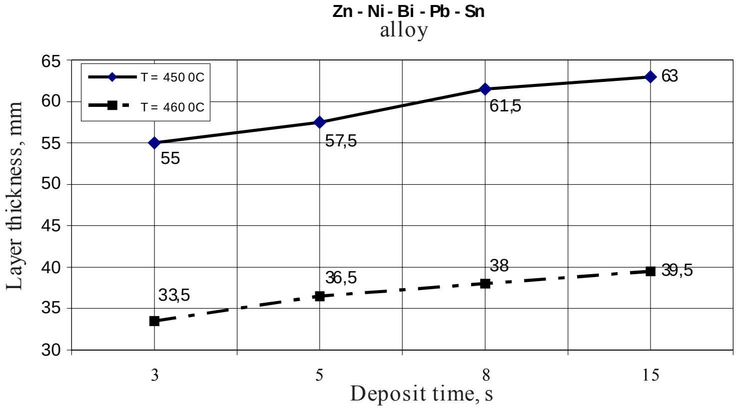

Fig.4. Layer thickness variation depending on temperature and duration of immersion, (Microalloyed Zn with Ni-Pb-Bi-Sn).

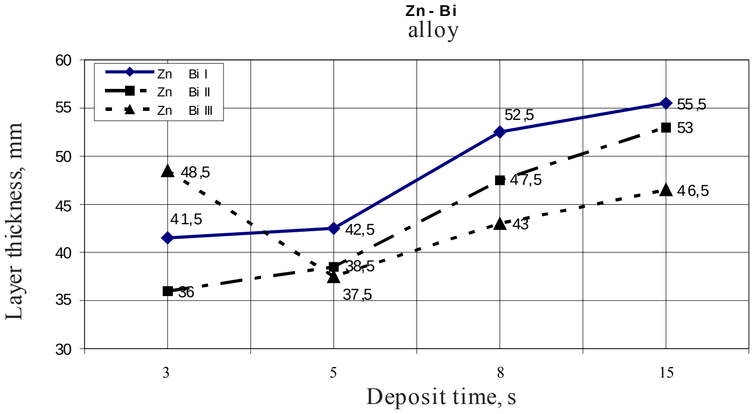

Fig.5. Layer thickness variation on duration of immersion, (Microalloyed Zn with Bi, T= 450^{o}C).

Laboratory experiments at the microalloying zinc melts were performed in the temperature range typical galvanizing processes, working at 450-460^{0}C.

By analysing the changes in layer thickness of the composite coatings obtained from microalloying with nickel (and elements for improving fluidity and structure) shown in Figures 2, 3, 4 at 450^{0}C, is observed a poor uniformity and high values of thickness, and compared to the 460^{0}C operating temperature of the melt. After the trials for these types of coatings, it is proposed a technological temperature of 460 ^{0}C and a maintenance period of 3-5 seconds. The finest layers were obtained in microalloyed zinc melt with tin, bismuth and aluminium at the temperature of 450 ^{0}C and 5-8 seconds duration of immersion (Fig. 6).

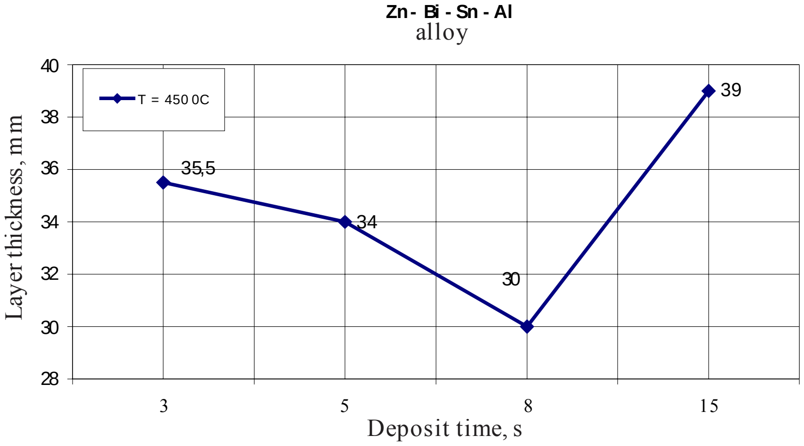

***Fig. 6.** Layer thickness variation on duration of immersion, (Microalloyed Zn melt with Bi-Sn-Al, T= 450^{o}C).*

3. Conclusions

1. All types of coatings growth analyzed over eight seconds of immersion time lead to a significant increase in the thickness of the layer.

2. For coatings obtained in microalloyed Zn melts with nickel (and elements to improve the fluidity and structure: bismuth, tin, lead, cadmium) the appropriate indicate the temperature is 460^{0}C and the maintaining time is 3-5 seconds. At the temperature is 450^{0}C; it results a large and uneven layer thickness.

3. Regarding the thickness of the layer, microalloyed zinc melt with bismuth leads to decreasing layer thickness. This effect is given by the increased melt fluidity in the presence of bismuth.

For all three types of microalloyed Zn melts with bismuth appropriate the temperature is 450 ^{0}C and the duration of immersion is 5 seconds.

4. The finest layers were obtained in microalloyed zinc melt with tin, bismuth and aluminium at the temperature of 450 ^{0}C and 5-8 seconds duration of immersion.

References

[1]. Radu T. Constantinescu S. Balint L. *Materiale metalice rezistente la coroziune*, Ed. IFR. Buc. 2004

[2]. John Zervoudis, Graeme Anderson, *A Review of Bath Alloy Additives and their Impact on the Quality of the Galvanized Coating*, p. 4, Teck Cominco Metals Ltd. 120 est, Suite 1500 Toronto, Ontario, Canada

[3]. Bo Zhang, *Development of Corrosion Resistant Galvanising Alloys*, Metallurgy and Materials School of Engineering The University of Birmingham, July 2005.

[4]. Tamara Radu, Vlad Maria, Mitoseriu Olga, *Prevention and reduction of wastes in the hot dip galvanizing steel sheet*, conf int. Technology and Quality for Sustained Development TQSD 2008 Buc. P. 59 - 64, ISSN 1844 – 9159, AGIR Publisher HOUSE, Editors Univ. Polith. Bucharest.

[5]. Lucica Balint, Tamara Radu, Conferinţa Internaţională Transfrontalieră: *Integrated monitoring of environmental media(air, water, soil) in the Lower Danube Euro region*, Galati-Cahul area, Galati, 19 noiembrie 2009, Editura Fundatiei universitare „Dunarea de Jos"Galati, ISBN 978-973-627-455-8 pag. 218-222.

THE ANNALS OF “DUNAREA DE JOS” UNIVERSITY OF GALATI.
FASCICLE IX. METALLURGY AND MATERIALS SCIENCE
N^0. 3 – 2010, ISSN 1453 – 083X

STRUCTURAL ASPECTS OF ANTIFRICTION PROPERTIES BRASS

Alexandru CHIRIAC, Gheorghe Florea, Marian NEACSU,
Ioan SARACIN, Olimpia PANDA
“Dunărea de Jos” University of Galati
email: sandu.chiriac@yahoo.com

ABSTRACT

$a + \beta'$ brass types with antifriction properties belong to the category of high-tensile brass, alloys which besides Cu and Zn also contain certain alloying materials introduced in order to obtain some special characteristics. It is known that these elements change the limits of the equilibrium diagram, widening or narrowing the phase existence areas.

KEYWORDS: antifriction, properties brass

If one part of zinc is replaced by another alloying element, the quantity ratio of the solid solutions a and p' is changed, although the copper content remains the same; depending on the metal added, it is likely to occur a greater or smaller quantity of solid solution α.

Thus it was established a zinc equivalence of the most important alloying elements - equivalence factors known as Guillet coefficients, which can be used to calculate beforehand the structure that the alloy will have (Table 1). This paper aims to analyze the structural aspects of the antifriction brass for manufacturing synchronous rings and mobile cones for Dacia Logan cars (Fig. 1).

The chemical composition of this quality brass contains as alloying elements: aluminum, manganese and silicon (Table 2).

Table 1. *Equalization coefficients by Guillet [1]*

Element	Ni	Mn	Fe	Pb	Sn	Al	Si
t [% Zn]	-1.3	0.5	0.9	1	2	6	10

Table 2. *The chemical composition of brass parts for the manufacturing of antifriction marks*

Chemical composition, %					**Maximum of impurities allowed,** %	
Cu	**Al**	**Mn**	**Si**	**Zn**	**Pb**	**Fe**
57-60	1.5-2	2-4	0.6-0.9	remaining	<0.35	<0.25

Due to their high equivalence coefficients, aluminum and silicon reduce the amount of the α alloy phase. Aluminum increases the tensile breaking strength, the yield strength and the hardness of the material, without lowering the values of tenacity; it also improves resistance to corrosion and oxidation. Manganese increases the creeping resistance, the yield strength, the relative elongation and especially the corrosion resistance against sea water. Silicon increases the tensile strength and the hardness without reducing the plasticity and also improves weldability. As a rough guide, the manufacturing technology of mobile cones includes: alloy elaboration, ingot casting, profiled pipe extrusion and mobile cone stamping (Fig. 1).

The chemical composition of the batches produced in the induction furnaces under charcoal layer varied little from the one presented in Table 3.

Table 3. *The chemical composition of the batches produced*

Chemical composition, %					**Impurities, %**			
Cu	**Al**	**Mn**	**Si**	**Zn**	**Pb**	**Fe**	**Sn**	**P**
59.31	1.6	2.58	0.663	*remaining*	0.035	0.028	0.002	0.006

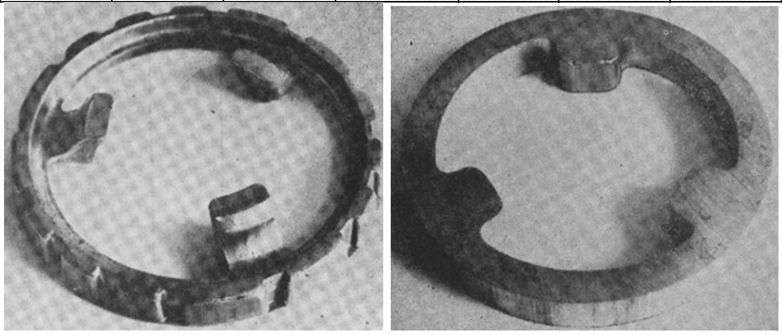

Fig. 1. *Synchronous rings and mobile cone*

The presence of manganese and silicon in the alloy is reflected by the formation of the compound Mn5Si3, macrostructurally highlighted (Fig. 2. a, b) and confirmed by the analysis of the Mn and Si distribution made with electron microscope (Fig. 3. a,b, c).

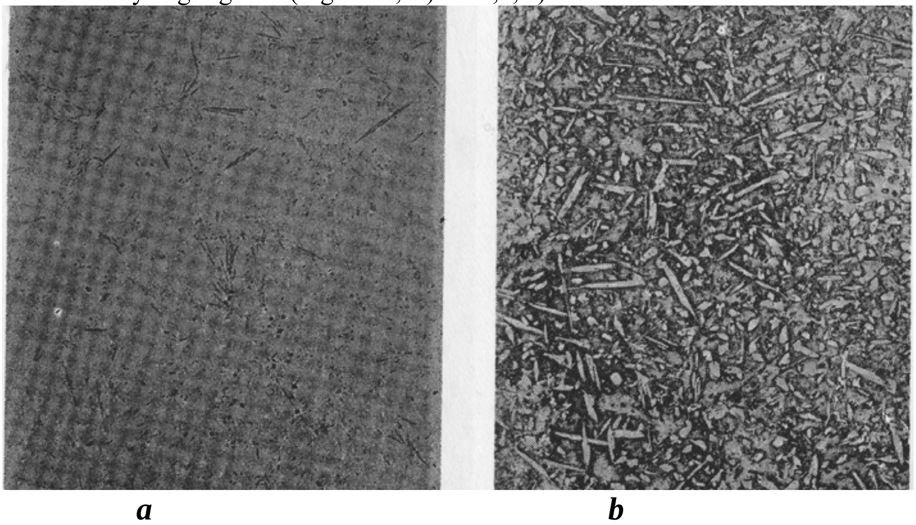

a ***b***

Fig. 2. *Microstructure of a sample taken from the molten raw material:*
a – Mn5Si3 compound is observed. Open to challenge (X 100); b - mass and solution (dark) is observed solution crystals request α to coloured Light,
Attack: FeCl5, (X 100).

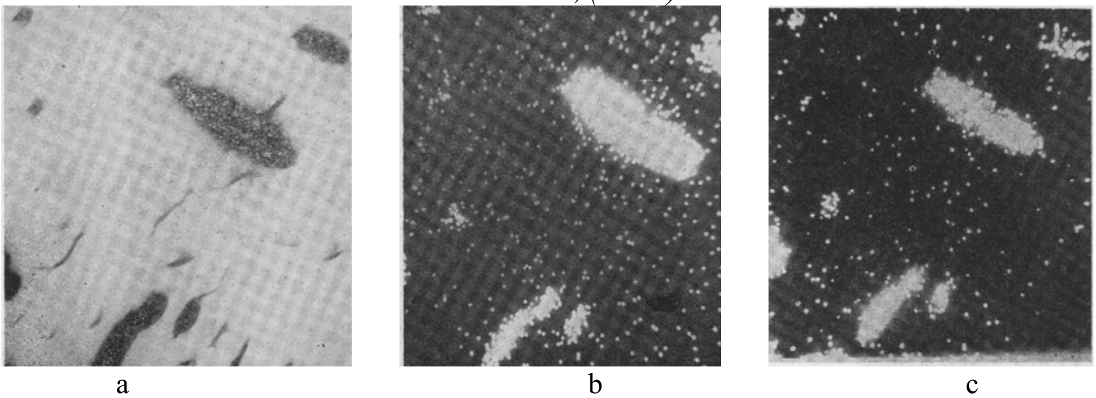

a b c

Fig. 3. *Mn and Si distribution made with electron microscope.*

The morphology and distribution of the Mn5Si3 compound can be seen in higher magnifications, as shown in Figure 4 a, b. The two phases *(a* + β') have different mechanical properties, phase *B’* is hard and less ductile, while the phase *a* is less hard and very ductile. The microhardness of these phases in the molten material are HV 0.01 = 35.4 for phase β' and HV 0.01 = 29.5 for phase α.

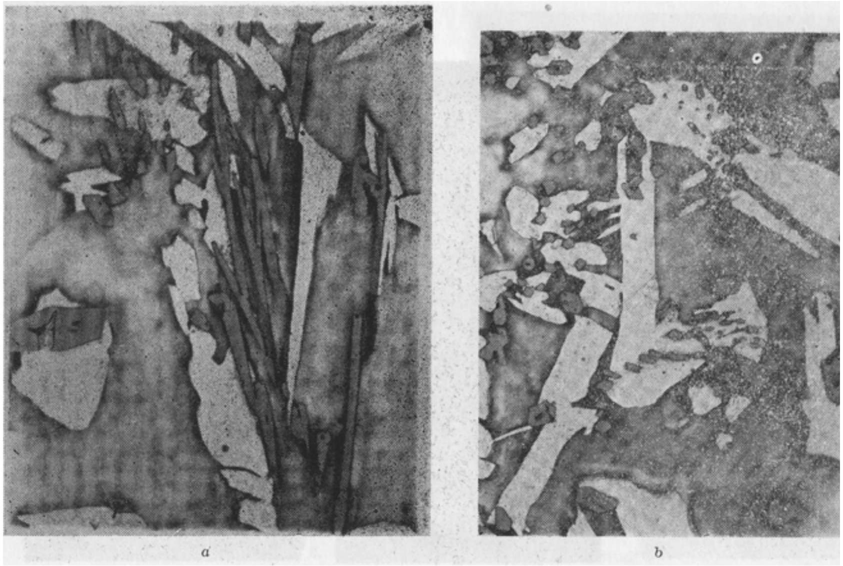

Fig. 4. *a, b Morphology and distribution of the Mn$_5$Si$_3$ compound in the cast material. The needle-shaped compound Mn Si$_3$ (grey) is distributed in the solid solution a (light colored) as well as in the solid solution (dark). Attack; FeCls, (X 1000).*

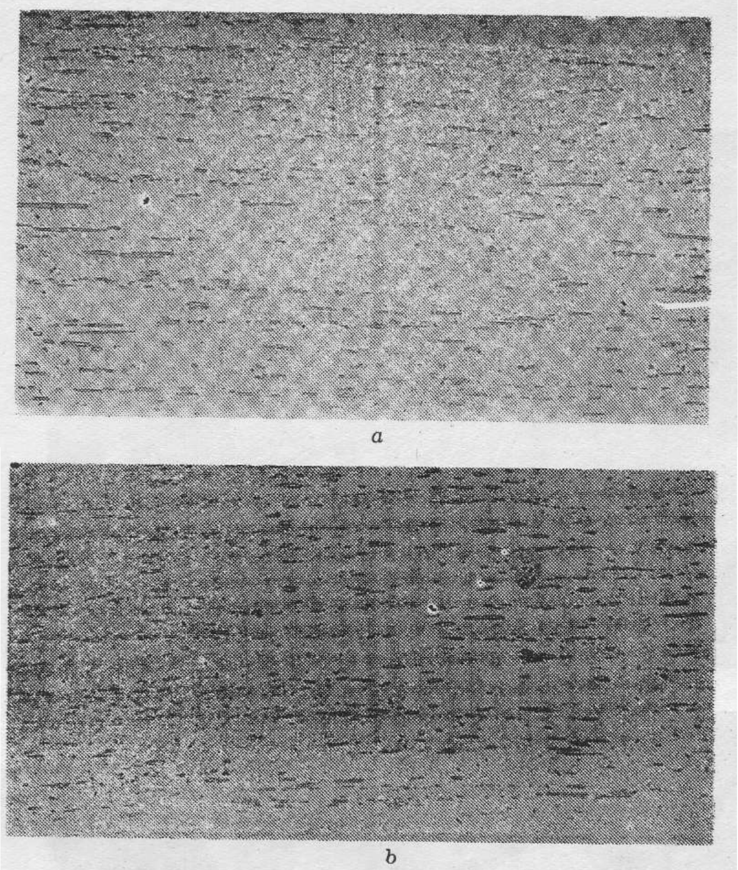

Fig. 5. *Microstructure of extruded semi-product*
a-beginning of extrusion, b-middle of extrusion, c- end of extrusion.

The mechanical properties of the cast material are presented in Table 4. After extrusion, the Mn_5Si_3 compound structures themselves in rows in the flowing direction of the alloy.

Table 4. *Mechanical characteristics of the alloy in cast state*

No.	**$Rp_{o,2}$.** N/mm^2	**R_m,** N/mm^2	**A_5,** %	**HB**
1	245	476	7.6	156
2	255	476	7.8	156
3	242	490	7.6	157

Because of the metal cooling, during extrusion there is a certain modification in the structure of the material on the workpiece length, as shown in Figures 5. a, b, c and 6. a, b. Table 5 shows the hardness variation along the length of the extruded semi-product.

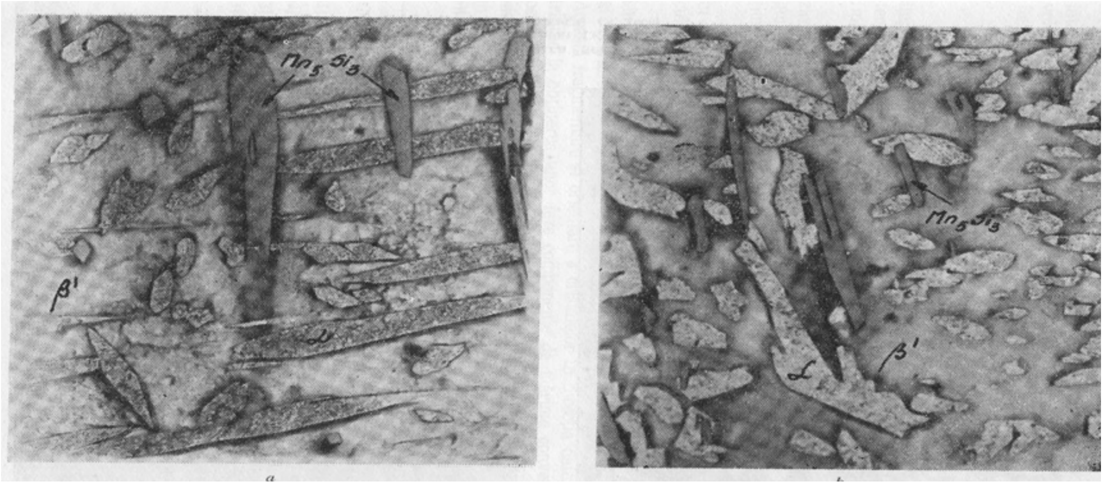

Fig. 6. *Microstructure of extruded semi-product a- beginning of extrusion, b- end of extrusion.*

Table 5. *Hardness variation along the length of the extruded semi-product*

Distance from the top end of extrusion, mm					
30	400	800	1300	1600	1900
162	170	174	174	176	179
163	174	174	174	178	177
163	175	174	172	177	176

From the data presented in the table it appears that the alloy cooling during extrusion does not strongly influence the mechanical properties of the material. From figures 7 a, b showing the microstructure of the semi-product hot stamping it appears that the moulding operation does not lead to radical structural changes in the material, the only change being the fragmentation of the Mn5Si compound.

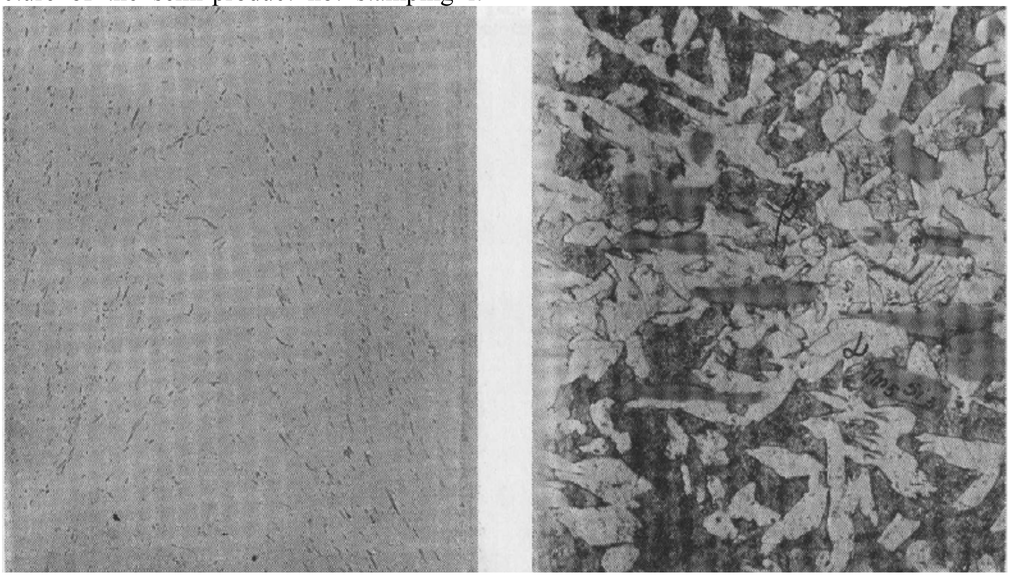

Fig. 7. a, b. *Microstructure of mold semi-product: a - unattacked (x 1000) b-attacked: FeCl3 (x 1000).*

During plastic deformation (extrusion, stamping), residual internal tensions appear, which are the result of the non-simultaneous volume changes; in order to eliminate these tensions, the mould semi-products were subjected to a tension release treatment at 400-420°C.

Conclusions

1. The structural analysis of the experimental material has shown the importance of the alloy structure for the imprinting of the mechanical characteristics and of the antifriction properties of the finished product.

Thus, the molten material has specific phases of a biphasic brass ($\alpha + \beta'$) with needle crystallization. This eutectoid structure provides excellent mechanical characteristics but not antifriction properties.

2. From a structural standpoint, the presence of manganese and silicon in the alloy is reflected by the appearance of the needle-shaped compound Mn_5Si_3 evenly distributed in the mass of material.

3. It is considered that in the case of the studied brass the antifriction properties are ensured by hot plastic deformation. At the extruded and mold material, a fragmentation of all component phases could be noticed. This fragmentation and the crystal orientation in the deformation direction contribute to the obtaining of convenient size phase components, dispersed uniformly throughout the mass, structure which improves the mechanical features and antifriction properties, characteristics which are absolutely necessary in the process of synchronization, wear and friction during mobile cones operation.

References

[1]. Schumann, H. - *Metalurgia fizică.* (Physical Metallurgy) Bucureşti, 1962.

[2]. Kurt, Dies - Cupru şi aliajele de cupru în tehnică. (Copper and copper alloys in engineering) Berlin. 1997.

[3]. Jo1obov, V.V., Zverev, G. I. — *Pressovanie mctallov.* Moscova, 1991.

[4]. * * * - Îndreptar. Kovka i ştampovka ţvetnîh metallov. Moscova, 1992.

THE ANNALS OF “DUNAREA DE JOS” UNIVERSITY OF GALATI.
FASCICLE IX. METALLURGY AND MATERIALS SCIENCE
N^{0}. 3 – 2010, ISSN 1453 – 083X

INFLUENCE OF SiC/Ni NANOCOMPOSITE COATINGS ON SRB ATTACHMENT AND BIOFILM FORMATION

Lidia BENEA[1], Alina CIUBOTARIU[1],
Bernard TRIBOLLET[2], Wolfgang SAND[3]
[1]Dunarea de Jos University of Galati, Competences Center Interfaces –Tribocorrosion and Electrochemical Systems (CC-ITES), Galati, Romania.
[2]Laboratoire Interfaces et Systemes Electrochimiques, Université Pierre et Marie Curie, Paris France.
[3]University of Duisburg-Essen, Biofilm Centre, Aquatic Biotechnology, Duisburg, Germany.
email: Lidia.Benea@ugal.ro

ABSTRACT

Bacteria adhesion is a very complicated process affected by many factors: bacterial/material properties and environment. Materials characteristics and chemistry of surfaces are the most important factors in bacterial adhesion and biofilm growth. Cells initially attach by physico–chemical interactions or extracellular matrix protein secretion to form a cell monolayer, in which cells express pili and have twitching motility and/or the ability to undergo chemotaxis. Cells proliferate in the monolayer and other microbes attach to form an active biofilm, the development and distortion of which is influenced by environmental factors such as hydrodynamic and mechanical stress. Cells in the mature biofilm are motile and undergo chemotaxis, which leads to spreading of biomass and an increased rate of horizontal gene transfer. As cells die, active bioconversion and/or biodegradation leads to solute transfer to or from the bulk liquid which results in eventual biofilm detachment.

The work was focused on performing surface modifications studies by co-deposition of dispersed nano particles with metals in order to observe the influence of materials structure (nano-structured coatings prepared) on bacteria cells (Sulphate Reducing Bacteria) attachment. Sessile bacteria on coupons were stained with 4, 6-diamidino-2- phenylindol (DAPI) and visualized by EFM as well as AFM. These types of bacteria are well known as very corrosive for metals in natural seawater.

KEYWORDS: biofilm, bacteria attachment, surface modification, electrodeposition, nanocomposite coatings, sulphate reducing bacteria.

1. Introduction

Many microorganisms in the natural environment exist in multicellular aggregates generally described as biofilms, associated with solid surfaces and in intimate contact with other microbial cells [1–3]. Cells adhere to surfaces and each other through a complex matrix comprising a variety of extracellular polymeric substances (EPS) including exopolysaccharides, proteins and DNA. Biofilm configurations range in complexity from flat, relatively featureless films, to tightly clustered aggregates, to complex heterogeneous cellular arrangements such as towers and streamers. Cells within biofilms are physiologically distinct from the same cells grown in dispersed culture [4-6]. Biofilm cells respond to nutrient and waste product diffusion gradients, modulate their metabolism as a function of their position within the biofilm, contact adjacent cells, and engage in cell–cell communication. Adherent populations exhibit elevated antimicrobial tolerance as a consequence of biofilm structure and physiological adaptation [3]. Biofilms have tremendous practical importance in industrial, medical and agricultural settings, exhibiting both beneficial and detrimental activities. The biofims are formed by microbial aggregates and extracellular polymeric substances (EPS). The EPS creates a microenvironment for sessile bacteria and allow the development of synergistic relationship. Their main components are not only polysaccharides, but also proteins, lipids and nucleic acids in minor proportion [3]. The biofilms are involved in both beneficial and detrimental effect. One beneficial aspect is their potential use as biosurfactancts in tertiary oil production and their capacity to trap heavy metals; as detrimental effect, biofouling, increase friction resistance, and produce changes in metallic surface properties (hydro phobisity, roughness, color etc.); finely biofilms participate in biocorrosion by bind with metal ions [4]. Microbiologically Influenced Corrosion, MIC refers to corrosion that is influenced by the presence and activities of microorganisms and/or their metabolites (the products produced in their metabolism). Bacteria, fungi and other microorganisms can play a major part in bio corrosion [3-8]. Spectacularly rapid corrosion failures have been observed due to microbial action and it is becoming increasingly apparent that most metallic alloys are susceptible to some form of MIC. The mechanisms potentially involved in MIC are summarized as:

-Cathodic depolarisation, whereby the cathodic rate limiting step is accelerated by micro-biological action

-Formation of occluded surface cells, whereby microorganisms form "patchy" surface colonies. Sticky polymers attract and aggregate biological and non-biological species to produce crevices and concentration cells, the basis for accelerated attack.

-Fixing of anodic reaction sites, whereby microbiological surface colonies lead to the formation of corrosion pits, driven by microbial activity and associated with the location of these colonies.

-Underdeposit acid attack, whereby corrosive attack is accelerated by acidic final products of the MIC "community metabolism", principally short-chain fatty acids.

Certain microorganisms thrive under aerobic conditions, whereas others thrive in anaerobic conditions. Anaerobic conditions may be created in the micro-environmental regime, even if the bulk conditions are aerobic. The pH conditions and availability of nutrients also play a role in determining what type of microorganisms can thrive in a soil environment. Microorganisms associated with corrosion damage are classified as follow:

-Anaerobic bacteria that produce highly corrosive species as part of their metabolism.

-Aerobic bacteria that produce corrosive mineral acids.

-Fungi that may produce corrosive by products in their metabolism, such as organic acids. Apart from metals and alloys they can degrade organic coatings and wood.

-Slime formers that may produce concentration corrosion cells on surfaces.

Microorganisms pervade our environment and readily "invade" industrial systems wherever conditions permit. These agents flourish in a wide range of habitats and show a surprising ability to colonize water rich surfaces wherever nutrients and physical conditions allow. Microbial growth occurs over the whole range of temperatures commonly found in water systems, pressure is rarely a deterrent and limited access to nitrogen and phosphorus is offset by a surprising ability to sequester, concentrate and retain even trace levels of these essential nutrients.

Many engineers continue to be surprised that such small organisms can lead to spectacular failures of large engineering systems. The microorganisms of interest in Microbiologically Influenced Corrosion (MIC) are mostly bacteria, fungi, algae and protozoan.

Bacteria are generally small, with lengths of typically under 10 μm, collectively, bacteria tend to live and grow under wide ranges of temperature, pH and oxygen concentration. Carbon molecules represent an important nutrient source for bacteria.

Fungi can be separated into yeasts and molds. Corrosion damage to aircraft fuel tanks is one of the well-known problems associated with fungi. Fungi tend to produce corrosive products as part of their metabolisms; it is these by-products that are responsible for corrosive attack. Furthermore, fungi can trap other materials leading to fouling and associated corrosion problems.

Protozoan are predators of bacteria and algae and therefore potentially mitigate microbial corrosion problems.

MIC is responsible for the degradation of a wide range of materials. Bacteria can exist in several different metabolic states. Those that are actively respiring, consuming nutrients, and proliferating are said to be in a "growth" stage. Those that simply exist, not growing because of unfavourable conditions, are said to be in a "resting" state.

Some strains, when faced with unacceptable surroundings, form spores that can survive extremes of temperature and long periods without moisture or nutrients, yet produce actively growing cells quickly when conditions again become acceptable.

The latter two states may appear, to the casual observer, to be like death, but the organisms are far from dead. Cells that actually die are usually consumed rapidly by other organisms or enzymes.

When looking at an environmental sample under a microscope, therefore, it should be assumed that most or all of the cell forms observed were alive or capable of life at the time the sample was taken.

Microorganisms can be categorized according to oxygen tolerance.

Sulphate reducing bacteria (SRB) are anaerobes that are sustained by organic nutrients. Generally they require a complete absence of oxygen and a highly reduced environment to function efficiently. Nonetheless, they circulate (probably in a resting state) in aerated waters, including those treated with chlorine and other oxidizers, until they find an "ideal" environment supporting their metabolism and multiplication. SRB are usually lumped into two nutrient categories, those that can use lactate and those that cannot. The latter generally use acetate and are difficult to grow in the laboratory on any medium. Lactate, acetate, and other short chain fatty acids usable by SRB do not occur naturally in the environment. Therefore, these organisms depend on other organisms to produce such compounds. SRB reduce sulphate to sulphide, which usually shows up as hydrogen sulphide or, if iron is available, as black ferrous sulphide. In the absence of sulphate, some strains can function as fermenters and use organic compounds such as pyruvate to produce acetate, hydrogen, and carbon dioxide. Many SRB strains also contain hydrogenase enzymes, which allow them to consume hydrogen. Most common strains of SRB grow best at temperatures from 25° to 35°C. A few thermophilic strains capable of functioning efficiently at more than 60°C have been reported. SRB have been implicated in the corrosion of cast iron and steel, ferritic stainless steels, 300 series stainless steels (also very highly alloyed stainless steels), copper nickel alloys, and high nickel molybdenum alloys. They are almost always present at corrosion sites because they are in soils, surface water streams and waterside deposits in general. Their mere presence, however, does not mean they are causing corrosion.

The key symptom that usually indicates their involvement in the corrosion process of ferrous alloys is localized in corrosion filled with black sulphide corrosion products. Sulphate Reducing Bacteria are responsible for extreme damage to piping and support equipment in many industries. Sulphate Reducing bacteria are a group of anaerobic bacteria (Do not need air or oxygen) that generate hydrogen sulphide (H_2S). H_2S can cause a number of significant problems in water.

Problems range from “rotten egg” odors to the blackening of equipment, slime formations, and extensive corrosion. SRB microorganisms are difficult to detect because they are anaerobic and tend to grow deep down within biofilms (slimes) as a part of a microbial community.

Our knowledge of the mechanisms behind these interactions is limited because they are complex, and because we lack suitable model systems to study the interactions.

Our paper is a part of a big project concerning the nanocomposite coatings obtained by electrodeosition of nano SiC with nickel on different surface materials in order to improve their corrosive and wear properties [7-8]. This part will present few results about SRB attachment and biofilm formation on nanostructured SiC/Ni surfaces compared topure Ni coatings, by Atomic Force Microscopy (AFM) and Epifluorescence Microscopy (EFM).

In an attempt to determine the relative importance of nano SiC included in the nickel during electrodeposition, experiments were designed to evaluate the electrochemical corrosion [9] and the relationship between SRB bacteria and two types of protecting coating on steel:

i) Nano-structured composite coating with SiC (20nm) embedded during nickel electrodeposition from a disperse nickel plating bath

ii) Pure nickel coating electrodeposited at the same thickness from a sulphate -chloride plating bath.

Biofouling has been recognized as a widespread problem in design and operation of processing equipment such as heat exchangers, cooling water systems and food processing equipment. The objective of this work is to study the influence of SiC/Ni nanocomposite coatings on biofilm formation compared to pure nickel coatings.

2. Experimental set-up

For the SRB biofilm investigations on SiC/nickel nanostructured coatings cold rolled steel panels (20mm x 100mm) were coated with the following combinations:

i) SiC (20 nm) + nickel with two coating thicknesses:

1) 54 μm Ni+SiC
2) 28 μm Ni+SiC

The content of SiC nano particles was determined by EDX analysis on electronic microscope and was found to be between 12 and 13 as volume percent of SiC particles inside the nickel matrix.

ii) pure nickel with two coating thickness:

1) 54 μm Ni
2) 28 μm Ni

In the bacteria attachment and biofilm formation, the Sulphate Reducing Bacteria was used. SRB cells were prepared in University of Duisburg Essen Biofilm Centre. The pH of all solutions with cells suspension was 6.2.

Attachment of cells was made in the following steps: putting a drop from the prepared solution with cells on the surface of coatings; waiting to dry (15-20min); incubation in bacterial suspension of SRB (about 10^9 cells / mL) for 24h to allow attachment and biofilm formation with 2,5% glutaraldehyde. Subsequently, they were stained with 0.01% (wt/vol) DAPI for 10min and visualized at the EFM. AFM imaging was performed by contact mode in air.

Biofilms and attached cells on pure nickel and SiC/Ni nanostructured coatings samples were investigated with combined AFM and EFM. A NanoWizardII atomic force microscope (JPK Instruments, Germany) and an upright epifluorescence microscope (AxioImager A1m; Zeiss, Germany) were combined using the BioMaterialWorkstation (JPK Instruments). Throughout the present study the prototype of this new system was used. The key feature of the BioMaterialWorkstation was a shuttle stage that carried the actual sample precisely fixed on a glass slide. This shuttle stage could be transferred between the atomic force microscope and the epifluorescence microscope, giving a precise positioning of the stage on both microscopes. Furthermore, a precision sample clamp guaranteed a tight and accurate fixation of the sample to the shuttle stage, thereby allowing the retrieval of the same sample location with AFM and EFM with an error of no more than 3 µm to 5µm. For sequential investigations, this shuttling could be repeated as often as required without losing position. For a successful combination of both microscopes, meaning the visualization of the same sample location, the variable position of the AFM cantilever had to be aligned to the static optical axis of the epifluorescence microscope in order to match the AFM scan region with the epifluorescence microscope's field of view.

3. Results and discussions

3.1. Structural aspects of SiC/Ni nano composite coatings

Micrographies presented allow comparison between a nanostructured composite surface (Fig. 1) and pure nickel surface (Fig. 2). The pure nickel deposit has a rather regular surface, whereas the composite coating develops in a nodular disturbed surface structure.

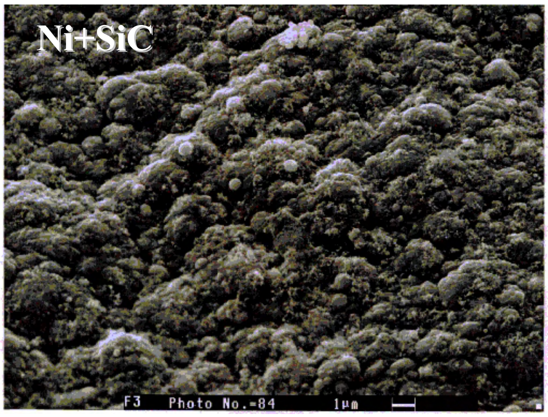

Fig. 1. *SEM surface morphology of SiC/Ni nano-structured composite coating.*

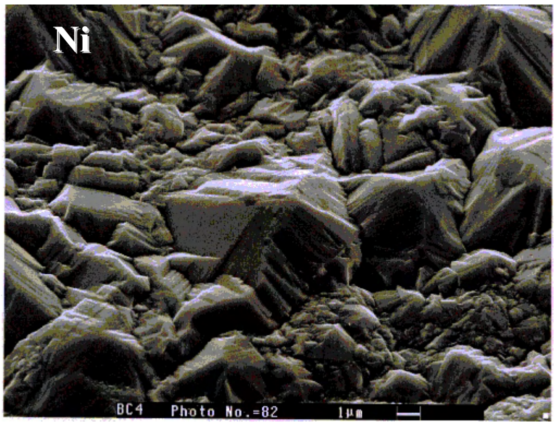

Fig. 2*. SEM surface morphology of pure Ni coatings.*

The surface analysis was performed on composite surface with X-ray disperse energy system (EDS) on the same surface area of the samples. From the general EDS analysis, the total amount of nano SiC particles inside the deposit was calculated at 8.99% as weight percent or 25% as volume percent. The volume percent of nano –SiC is higher because of lower density of particles (3.2 gdm^{-3}) compared to nickel matrix (8.9 gdm^{-3}).

3.2. AFM-EFM study of biofilm formation

Epifluorescence microscopy (EFM) images of a DAPI – stained biofilm sample of SRB on the surface of nickel and SiC/Ni nano composite coatings obtained at different parameters for electrodeposition are presented in Figs. 3-4.

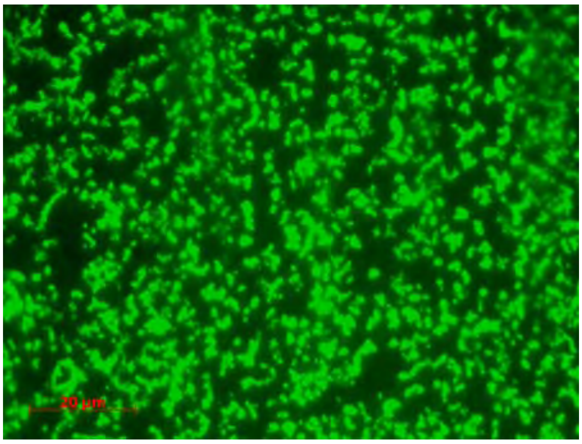

Fig. 3*. Fluorescence microscopy image of SRB on pure nickel surface obtained at current density 4A/dm^2, 60min.*

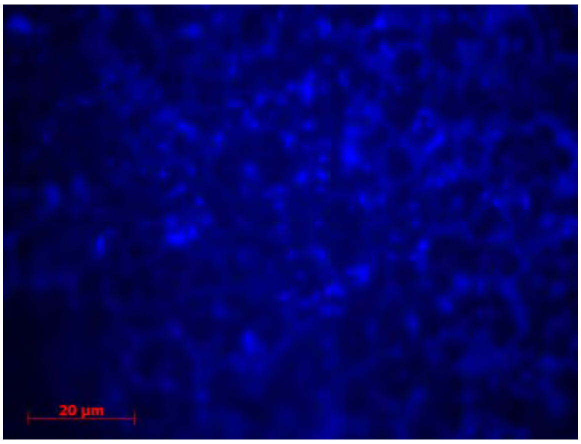

***Fig. 4**. Fluorescence microscopy image of SRB on SiC/Ni nano composite coatings surface obtained at current density 4A/dm^2, 60 min.*

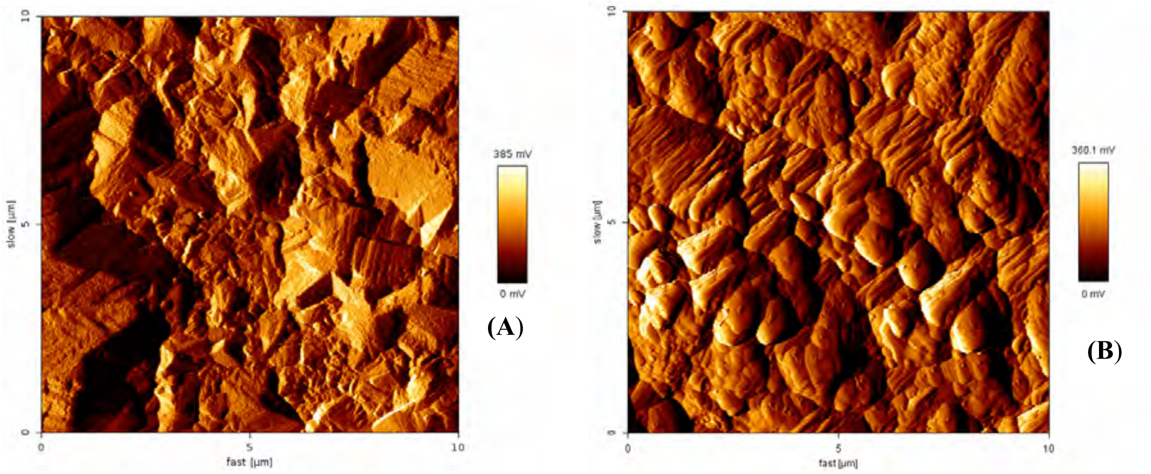

***Fig. 5**. AFM of nickel surface (i = 4 A/dm^2 for 1h): A- untreated surface; (B) with SRB, 2D – Vertical deflection.*

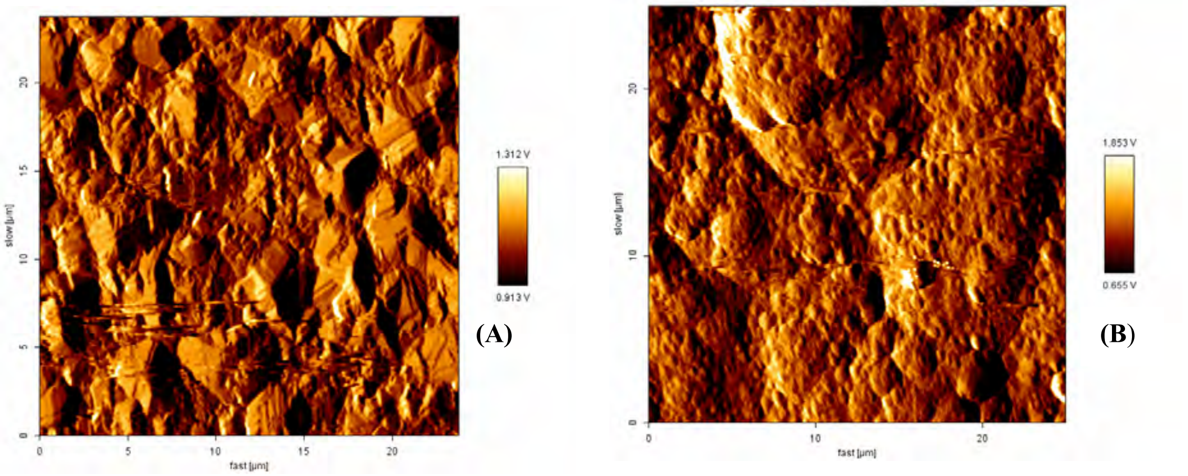

***Fig. 6.** AFM of SiC/Ni nano composite coating surface 2D – Vertical deflection (i = 4 A/dm2 for 1h): (A) – untreated; (B) – with SRB bacteria.*

Figs 5-6 show the vertical deflection images of the AFM scan acquired by contact mode in air on pure nickel coating and SiC/Ni nano composite surfaces untreated and after SRB attachment and biofilm formation. The differences between untreated surfaces and treated with SRB are visible, representing the attached cells of Sulfate Reducing Bacteria on the surfaces.

The differences of SRB biofilm formation on two types of surfaces could be observed also by AFM images presented in 3D high mode, see Figs. 7-8.

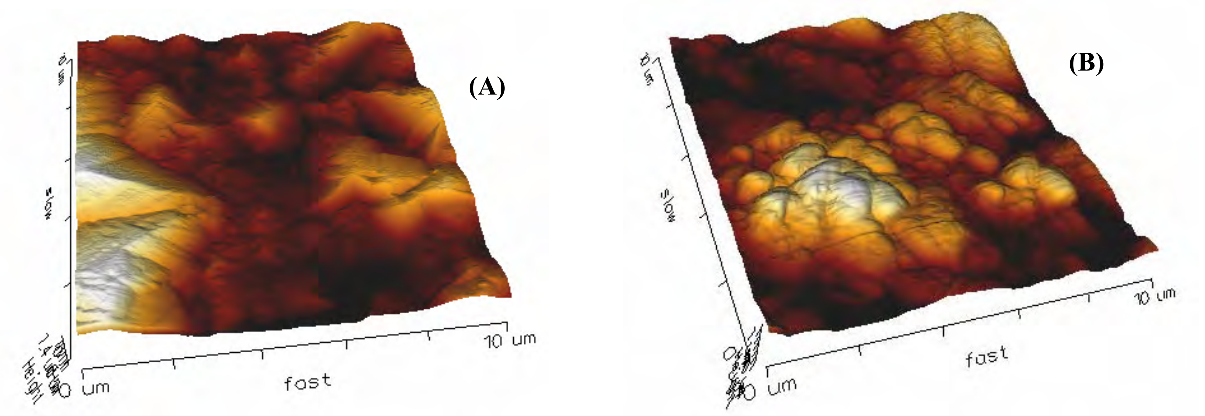

***Fig. 7.** AFM of pure nickel surface 3D – Heigh (i = 4 A/dm^2 for 1h): (A) - untreated; (B)- with SRB bacteria*

From the EFM and AFM microscopy images we could observe that the attachment of SRB bacteria on nano composite coatings is less than that on pure nickel coatings. Those facts indicated that the SiC/Ni nano composite coatings are more resistant to the attack of microorganisms like SRB. These AFM-EFM images indicate an adherence process of the microorganisms on the studied surfaces. The use of microscopy to count adhered cells on surfaces is a viable technique, since, on a microscopic scale, surfaces can be found to have cracks and crevices, quite unlike the macroscopic appearance.

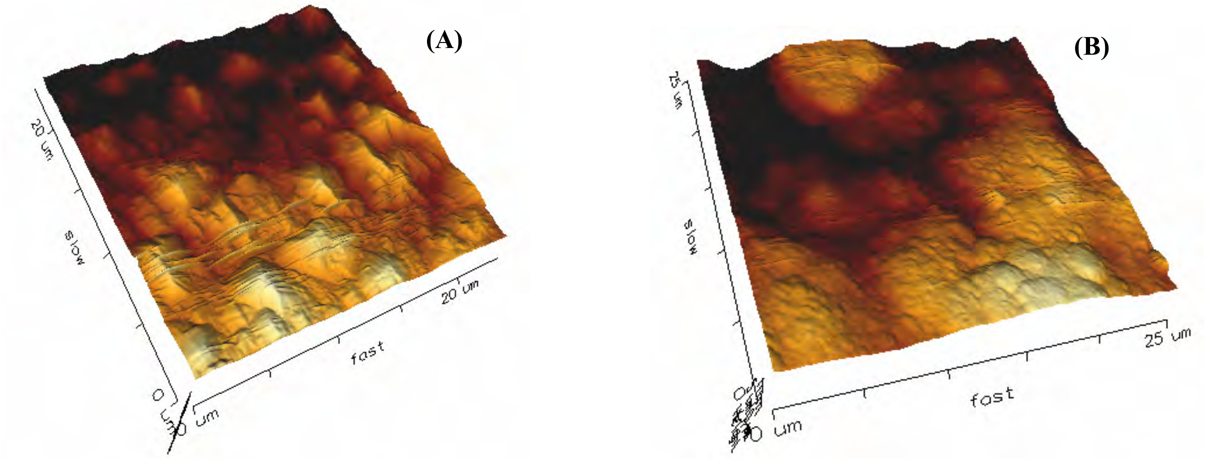

***Fig. 8.** AFM of SiC/Ni nano composite coating surface 3D - Heigh (i = 4 A/dm^2 for 1h): (A) – untreated; (B) - with SRB.*

These surface imperfections protect the microorganisms against removal by swab or rinse, for example. Microscopes coupled with image analysis systems can help the count process of adhered cells on surfaces by EP.

For all systems tested we could observe that the surface roughness decreases after the attachments of bacteria, that indicate the uniformity of biofilm and extra-cellular polymer formation [10].

Decreases of the surface roughness was also reported for two types of stainless steel austenitic AISI type 304 and the superduplex UMS S32750 after immersed in seawater containing Desulfovibrio vulgaris ssp vulgaris DP4 [11].

SiC/Ni nanocomposite coatings seem to have better resistance to SRB attachment and biocorrosion followed by biofilm formation.

4. Conclusions

The Sulfate Reducing Bacteria (concentration about 10^{9}cells/mL) are attached on the pure nickel and less on the SiC/Ni nano composite coatings after an incubation of 24h.

From the epifluorescence microscopy and atomic force microscopy images we could observe that the SiC/Ni nano composite coatings are more resistant to the attack of the Sulfate Reducing Bacteria compared to pure nickel coatings.

The surface roughness decreases after the attachments of bacteria and biofilm formation.

The new system for combining imaging of AFM and EFM on nickel and SiC/Ni nano composite coatings is feasible for the application to study the biofilm formation by Sulfate Reducing Bacteria on these surfaces.

Acknowledgments

The authors gratefully acknowledge the European Project **COST D33 - Electrochemical and biotribocorrosion studies of interfaces between materials (composites, metallic, polymeric, ceramic) and microorganisms**.

References

[1]. Flemming HC and Wingender J., Water Sci. Technol. 43, (2001) 1-8.

[2]. Flemming HC and Wingender J., Water Sci. Technol. 43, (1999) 9-16.

[3]. Damien Feron, Chantal Compère, Isabelle Dupont, Michel Magot, "*Biodétération des matériaux métalliques ou biocorrosion*", in Corrosion des métaux et alliages: Mécanismmes et phénomènes, Edited by G. Béranger and Henri Mazille, Lavoisier 2002, ISBN 2-7462-0466-5

[4]. B. J. Little, R. I. Ray, P. A. Wagner, J. Jones-Mehan, C. C. Lee and F. Mansfeld; Biofouling, Vol.13 , 4 (1999), 301-321.

[5]. Stephen L. Hodson, Christipher M. Burke, Andrew P. Bissett; Aquaculture 184, (2000) 227-290.

[6]. Mohamed O. Saeed, A.T. Jamaluddin, I. A. Tisan, D. A. Lawrence, M.M. Al-Amri, Kamran Chida; Desalination 128, (2000) 177-190.

[7]. Lidia Benea, Pier Luigi Bonora, Alberto Borello, Stefano Martelli, Wear 249 (2002).

[8]. Lidia Benea, Pier Luigi Bonora, Alberto Borello, Stefano Martelli, Francois Wenger, Pierre Ponthiaux, Jacques Galland, Solid State Ionics 151 (2002) 89.

[9]. L. Benea, M. Mardare, B. Tribollet, *Dispersed nano-sized SiC in nickel to improve the corrosion properties of composite coatings*; CD Proceeding Eurocorr 2009, 5^{th}-10^{th} September Nice-France.

[10]. L. Benea, A. Ciubotariu, B. Tribollet, W. Sand, *Surface modifications to influence biofilm formation on material surfaces*; CD Proceeding Eurocorr 2009, 5^{th}-10^{th} September Nice-France.

[11]. Bernardez L A, de Andrade Lima LRP, Almeida PF., 2007. *Corrosion of stainless steels exposed to seawater containing sulfate reducing bacteria*. Brazilian Journal of Petroleum and Gas. 1:51 – 58.

THE ANNALS OF “DUNAREA DE JOS” UNIVERSITY OF GALATI.
FASCICLE IX. METALLURGY AND MATERIALS SCIENCE
N^0. 3 – 2010, ISSN 1453 – 083X

AIR POLLUTION CONTROL

Dumitru POPA, Aurel CIUREA, Marian BORDEI
“Dunărea de Jos” University of Galati
email: popadtru@yahoo.com

ABSTRACT

Air pollution is an important issue nowadays, and combustion plants have a significant contribution in this regard. In this paper we are going to present some of the techniques that can be used to avoid creating pollutants or cleaning effluents before they are released into the atmosphere. All these will lead to withholding of pollutants and maintaining the harmony between human activity and nature.

KEYWORDS: air pollution, emission control, cleaning effluents, electrostatic filter

1. Particles removal

Physical particles removal, by attracting them into a trap made of porous cotton clothing, glass or as best fibers cellular allows air to pass through it, but it retains the solid particles. The efficient collection is relatively intensive depending on: the type of fuel, fly ash composition, particle size and electrical properties. Filters are, generally, designed as giant vessels from 10 to 15 m high and 2 or 3 m wide.

The gas which flows is left at the bottom of the container and then it exits through holes (Fig. 1). After a few days or weeks the containers are cleaned of dust.

These filters are normally much cheaper to install than electrostatic filters.

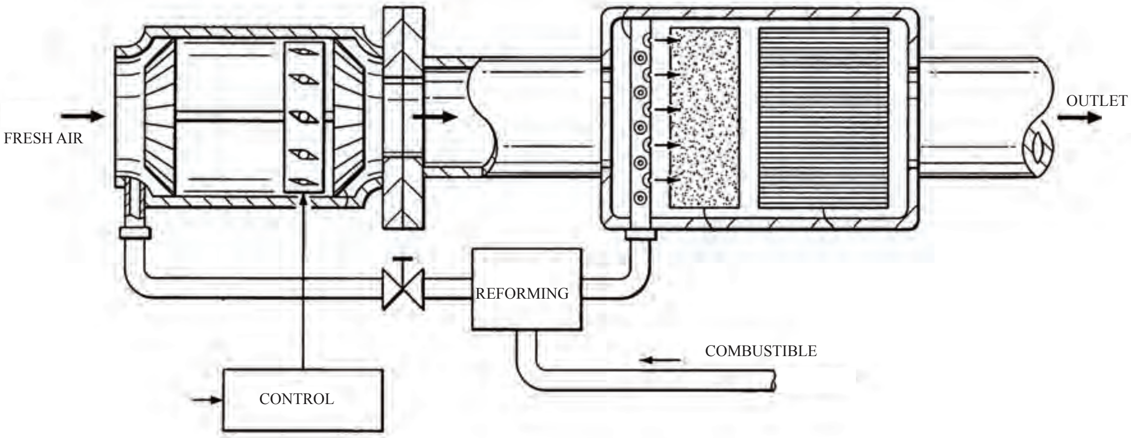

***Fig.1**. Typical devices of emissions control.*

Electrostatic filters are the most common methods of control in power plants.

Fly ash particles raise an electrostatic charged surface, while they pass through the electrodes on leakage current.

This causes particle migration and accumulation in the collector plate. These filters consume a large amount of electricity, but their maintenance is relatively simple and efficient, the collection is up to 99%. The performance depends on particle size, chemistry, electric field strength and acceleration of gas flow.

The ash collected by these techniques is a solid waste (often dangerous because of heavy metals and other components traces of coal ash or other sources) that must be buried in solid waste disposal sites.

2. Removing sulfurs

The sulfur oxide is one of the most dangerous air pollutants in terms of human and ecosystem health. It is important to reduce the sulfur loading. This can be done either by using low sulfur fuel or by removing the sulphide emissions.

3. Fuel changing and cleaning

A method may be a shift from a coal with high sulfur coal with low sulfur content, thus can significantly reduce the sulfur emission. The change of fuel, such as natural gas or nuclear energy can eliminate sulfur emissions, particles and heavy metals. Natural gas is more expensive and difficult to transport and store than coal; however, many people prefer the risk of pollution caused by coal plants than nuclear threats.

Alternative energy sources such as solar power could also be a solution. In the interim period, coal can be crushed and washed to remove sulfur and metals prior to combustion; this improves heat content and combustion properties, but does not replace air pollution and solid waste and does not solve water pollution problem. Coal gasification can also reduce sulfur emissions.

4. Limestone injection and combustion flow fluidization

Sulfur emissions can be reduced by up to 90% by mixing crushed limestone with coal, before being introduced into the combustion plant. Calcium from limestone reacts with sulfur and produces calcium sulfate $CaSO_3$, calcium sulfate $CaSO_4$ or gypsum $CaSO_4 * 2H_2O$. In ordinary ovens, this procedure creates slag which reduces the combustion efficiency.

A relatively new technique for burning is called the combustion flow fluidization; this provides several advantages in pollution control. In this procedure a mixture of crushed coal and limestone particles with a depth of approx. 1 m is scattered into a perforated distribution net in the combustion chamber (Fig. 2).

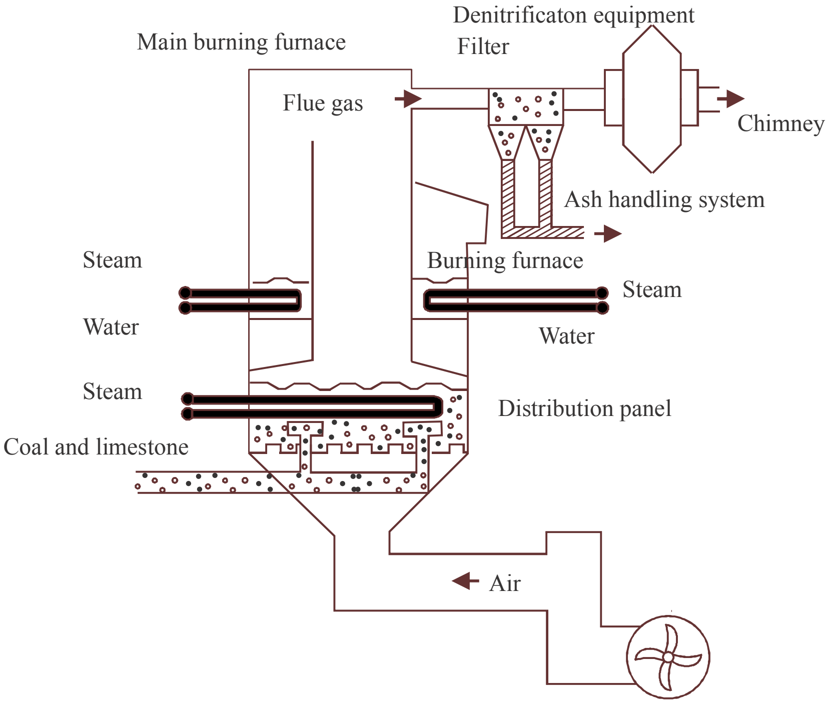

Fig. 2. *Combustion flow fluidization: the fuel is raised by powerful jets of air from the bottom of the shell. The efficiency is good for a wide variety of fuels, and SO_2, NO_x and CO emissions are much lower than conventional combustion.*

When the air with great power is forced to enter the room, the fuel surface rises up to a meter and results a hot fluid with particles jumping up and down. The oil is sprayed in suspended mass in order to start burning. During the operation, the fresh coal and the limestone are continuously fed at the flow surface, while the ash and slag are drawn to the bottom. The fresh air supply and the constant movement in the burning room, lead to efficient burning and prevent the construction of slag deposits.

Steam generating pipes are integrated directly into the fluid flow and heat exchange is more effective than in the walls with water of a conventional boiler. More than 90% of SO_2 is captured by the limestone particles, and NO_x formation is reduced by maintaining a temperature of 800^0C instead of dual-temperature in other boilers. These low temperatures exclude also the slag formation. The efficient combustion in the case of this process makes possible the use of the cheaper fuel such as lignite or dirty coal, instead of high-priced coal.

5. Flue gas desulphurization

The crushed limestone, calcium oxide or alkaline (sodium carbonate or bicarbonate) may be injected into a chimney in order to remove sulfide after combustion. This process is called scrubbing of gas combustion. The spraying of alkaline wet solution or of limestone oxide is relatively cheap, but its maintenance can be difficult. The hard rock plaster and ash layers from coal existing in spray chamber must be maintained regularly. The corrosive solutions from sulfates, chlorides and fluorides erode metals surface. Electrostatic filters do not work well because of the electrodes increase and decrease after wet washing. A hybrid procedure, called dry spraying was successfully tested in a pilot experiment in a factory. In this process, a limestone oxide which was sprayed is atomized into a gas flow. The spray rate and droplet size are carefully controlled, the sprayed water evaporates and thus, a dry granular filter is produced. A large power plant produces one million tones of waste per year.

6. The sulfur recovery process

In case of the waste manufacture, sulfur can be removed from flue gases by processes that delay the use of the product, such as elementary sulfide, sulfuric acid. The catalytic converter is used in these recovery processes to oxidize or reduce sulfur and to create chemical compounds that can be collected and sold. The contamination with fly ash must be reduced as much as possible.

7. Control of nitrogen oxide

The best way to prevent nitrogen oxide pollution is to avoid creating it. A substantial quantity of these emissions is associated with mining, and energy production should be eliminated through conservation. The combustion, where the air and fuel flow are carefully controlled can reduce nitrogen oxide formation up to 50%. This is true for both internal combustion engines and industrial boilers. The fuel is first burned at a high temperature in a poor oxygen medium, where NO_x can not be formed. Waste gases then pass through a column in which more air is added and the final combustion takes place in a medium with much air, less fuel and low temperature, fact that reduces also the formation of NO_x. Stratified charged engines and new engines of cars use this principle in order to meet emissions standards without catalytic converters. The approach adopted by the U S A in terms of car manufacturers to reduce NO_x was the use of selective catalysts to change pollutants into harmless substances. The three-way catalytic converter uses platinum catalyst - palladium and radium in order to remove a large amount of NO_x, hydrocarbons, carbon monoxide at the same time (Fig. 3). Unfortunately, this approach is not used for diesel engines, power plants, foundries or other sources of pollution because of problems caused by pressure, the lifetime of the catalyst, corrosion and the occurrence of unwanted side products such as ammonium sulphate (NH_4SO_4), which cheat the system. RapreNox (rapid removal of nitrogen oxide) is a new technique for removing nitrogen oxide which has been developed by the Department of Energy Laboratory in Livermore, USA, California. The emitted gases are passed through a container of acid, non-toxic cyanide. When heated to 350^0C, hydrogen cyanide gas releases an isocyanic acid, which reacts with NO_x to produce CO, CO_2, H_2O and N_2. In a small-scale test, this includes diesel engines; this system has eliminated 99% of NO_x. It is to be seen whether this application will work on a large scale, particularly in the waste gas contaminated with fly ash.

8. Hydrocarbons control

Hydrocarbons and volatile organic compounds are produced by incomplete combustion of fuels or evaporation of solvents from chemical plants, paints, plastics and other industrial processes that use a variety of volatile organic chemicals. Closed systems that prevent the escape of gases can reduce many of these emissions. In automobiles, for example, crankcase engine ventilation (PCV), the system which collects the oil escaping from the piston and from unburned fuel and directs it to the engine for combustion. The change of the carburetor and fuel system prevents fuel evaporation (Fig. 3).

After-combustion is often the best way for the destruction of volatile chemicals from industrial exhaust chimneys. The high rate of air-fuel from automobile engines and other combustions minimizes hydrocarbons and carbon dioxide emissions, but also causes the production of nitric oxide in excess. Careful monitoring of the air-fuel of the inlet and exhaust gas oxygen level can minimize all these pollutants.

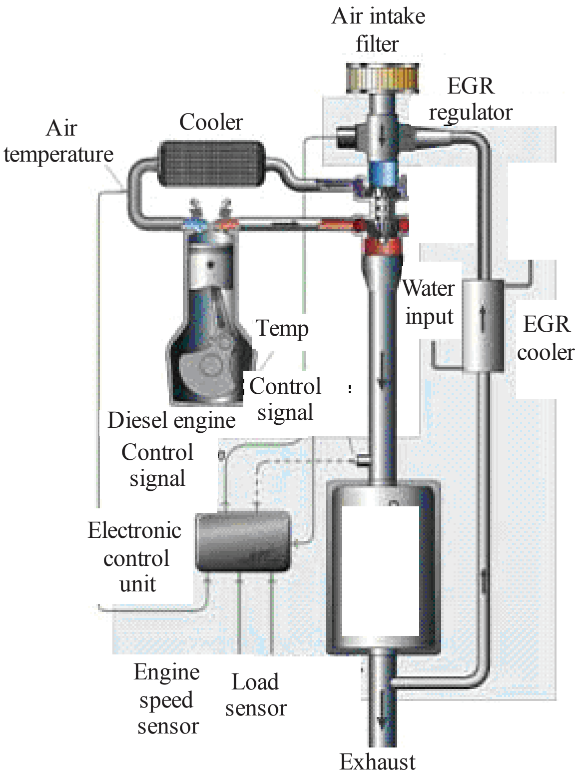

Fig.3. *Emission control system elements of a modern car. A closed loop, an electronically controlled carburetor or fuel injector which carefully measures the fuel / air rate for combustion optimization. Exhaust air sensor measures the combustion fuel level.*

9. Conclusions

The best way to reduce pollution is prevention. Because we cannot be sure that pollution does not produce, it is necessary to eliminate the possible emissions and, not lastly, to examine the causes and prevent it to increase.

References

[1]. Bălan G., *Principles for elaboration of the technical system with sonic injectors,* Doctor Habilitation Thesis, U.T.M, Chisinau, 2001;

[2]. Bălan G., *Aero-gas-dynamic*, Technical -INFO Ed., Chisinau, 2003;

[3]. Bălan G., *Applied gas-dynamic. Calculus methods,* Technical -INFO Ed., Chisinau, 2000;

[4]. Constantinescu G., *The theory of sonic technology*, Romanian Acad. Ed., ed. 2, vol. 2, 1985.

[5]. Avvaru B., Patil M.N., Gogate P.R., Pandit A.B., *Ultrasonic atomization: Effect of liquid phase properties*, Ultrasonic 44 (2006), pp. 146–158

[6]. Baukal C.E., *Industrial burners handbook,* CRC Press LLC, USA, 2004.

[7]. Bălan G., Ciurea A., Bălan V., Bordei M., *The Sonic Technologies*, Quatrieme edition du Colloque Francophone en Energie, Environnement, Economie et Thermodynamique *COFRET'08, 11 – 13 June 2008, Nantes - France*, pp. 20-29.

[8]. Gong J.S., Fu Wei-Biao, *The experimental study on the flow characteristics for a swirling gas–liquid spray atomizer*, Applied Thermal Engineering 27 (2007), pp. 2886–2892.

[9]. Kermes V., Belohradsky P., Oral J., Stehlk P., *Testing of gas and liquid fuel burners for power and process industries*, Energy 33 (2008), pp. 1551–1561.

[10]. Lang R.J., *Ultrasonic atomization of liquids*, Journal of the Acoustical Society of America, Vol. 34, 1962, pp. 6-8.

[11]. Rajan R., Pandit, A.B., *Correlations to predict droplet size in ultrasonic atomization*, Ultrasonic, Vol. 39, 2001, pp. 235–255.

[12]. *** SR EN ISO 3744:1997 "*Acustică - Determinarea nivelurilor de putere acustică ale surselor de zgomot utilizând presiunea acustică - metoda tehnică aproximativă, în condiții asemănătoare de câmp liber, deasupra unui plan reflectant*".

THE ANNALS OF "DUNAREA DE JOS" UNIVERSITY OF GALATI.
FASCICLE IX. METALLURGY AND MATERIALS SCIENCE
N^0. 3 – 2010, ISSN 1453 – 083X

AUTOMATED APPARATUS-PROGRAM SYSTEM FOR EVALUATING THE STRENGTH OF A REDUCER SHAFT

Daniela ZHELEZAROVA[1], Silviu MACUTA[2], Ivan BALASHEV[1]
[1]Technical University of Gabrovo, Bulgaria
[2]"Dunarea de Jos" University of Galati
email: Silviu.Macuta@ugal.ro

ABSTRACT

The paper deals with a design of automated system for studying the strength of a reducer shaft according to the probabilistic evaluation method concerning the examination of machine elements. The apparatus-program system is Windows-based with an opportunity for connection with program packages about a numerical study of objects and details according to the finite element method. The data about the studied objects are obtained by means of two ways, namely: directly from an integrated system for measuring parameters of details, which is worked in the mode of real time, or from files containing data about studied objects, that are received as a result of other examinations. The automated apparatus-program system is open for development in the following directions: addition of methods for evaluating various machine elements; expansion of control-measurable system with regard to different methods and systems for measuring the studied quantities.

KEYWORDS: reducer shaft, probabilistic evaluation method, automated control-measurable systems, analysis according to the finite element method

1. Introduction

In the process of operation many machine elements experience the action of alternating stresses in the time. Furthermore, the known methods for calculating the operational strength of machine elements allow to account for only the force loading with a constant character without accounting for its probabilistic variation. The stressed-and-strained state of shaft and of assembly is determined by physical-mechanical characteristics of their material by the values of external forces and moments, by the contact conditions of separate elements, by the distribution character of loading, etc.

All these indices have a probabilistic character and therefore the stresses provoked by them will also possess a probabilistic character.

In connection with the statements mentioned above, it is imposed the necessity for determining the fracture probability of shaft in the process of assembly operation to be specified as a criterion for assessment of the stress in the critical section of shaft.

2. Model and Design of Automated System

The construction of real input shaft from the reducer about rope electric hoist is shown in Fig.1.

Fig. 1. *Construction of real input shaft from the reducer about rope electric hoist.*

The paper deals with the reducer shaft tested by means of laboratory stand according to the joint project between Central Mechanical Engineering Institute-Sofia and BRV-TESMA-Gabrovo as the loading of tested shaft is given in Fig.2 [1].

On the basis of obtained data from the testing a numerical parametric model of this shaft has been developed by means of the finite element method, which allows the simulation of process and the transmission of torque. The model is made in the medium of COSMOSWorks – specialized application towards SolidWorks [2, 3], destined for solving tasks from mechanics of solid deformable body according to the finite element method as the solved task is from linear statics (Fig.3).

On the units of external cylindrical surfaces of splines, which are in contact with the left radial-axial bearing support (immovable), the following kinematical constraints are imposed: radial and axial zero displacements. On the surface of splines, which are in contact with the splines of central gear, zero angular displacements are imposed. On the surface of contact with the right radial bearing support, zero radial displacement is imposed.

On the external cylindrical surfaces of splines towards the clutch, zero radial displacement is imposed as this corresponds to the radial bearing support. On this surfaces of shaft splines, which are in contact with the splines of clutch, the torque M_{yc}=85 Nm is set.

The external cylindrical surfaces of splines (upper ones – according to the scheme), which are in contact with the central gear, are six in number and are loaded by the force P_1=1800 N that is parallel to the Y-axis. The surface of eventual contact of the shaft with the planet carrier is loaded by the force P_2=4200 N that is also parallel to the Y-axis.

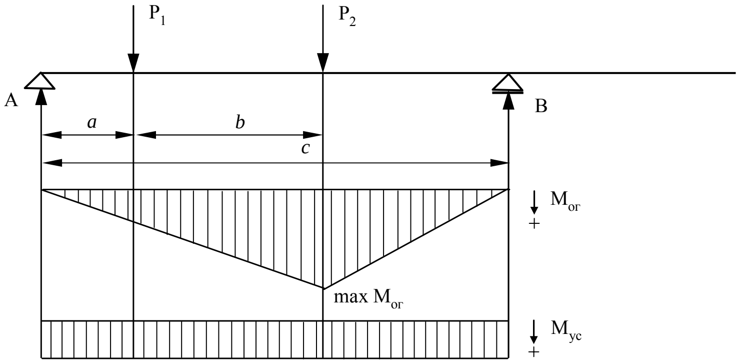

Fig. 2. *Loading of reducer shaft tested on laboratory stand.*

The developed finite-element model of reducer shaft affords an opportunity to determine the following stresses: the equivalent stresses as well the tangential stresses τ_{yc}, the bending stresses σ_{or}, the shearing stresses τ_{xz} and τ_{xy}, respectively [6].

The data obtained by the testing of shaft enter an automated system for studying the strength of reducer shaft according to the probabilistic evaluation method concerning the examination of machine elements [4].

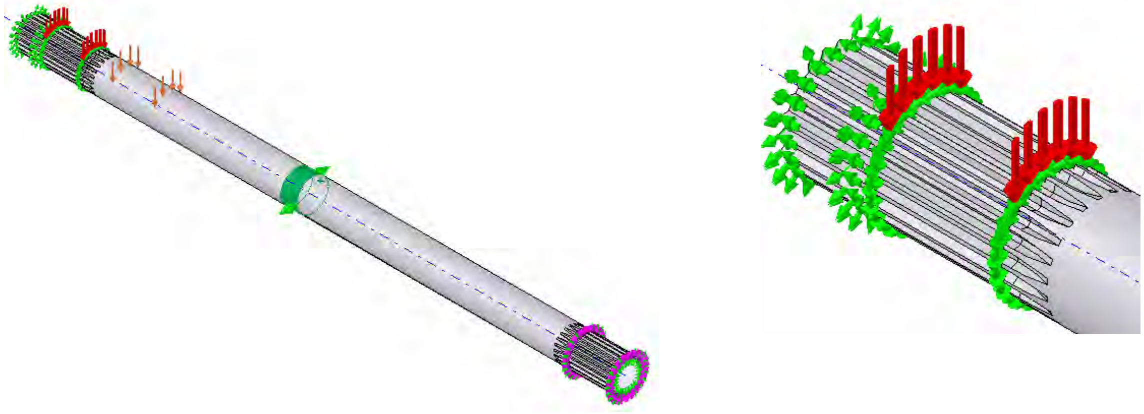

a) b)

Fig. 3. *Model of the reducer shaft: a) loading and constraints of shaft; b) spline part of shaft that is in contact with the central gear.*

The apparatus-program system is Windows-based with an opportunity for connection with program packages about a numerical study of objects and details according to the finite element method (Fig.4). The data about the studied objects are obtained by means of two ways (Fig.5), namely: directly from an integrated system for measuring parameters of details, which is worked in the mode of real time, or from files containing data about studied objects, that are received as a result of other examinations.

For evaluating the mutual influence between acting forces as well the originated internal stresses, a program module about statistic and variance analysis is used.

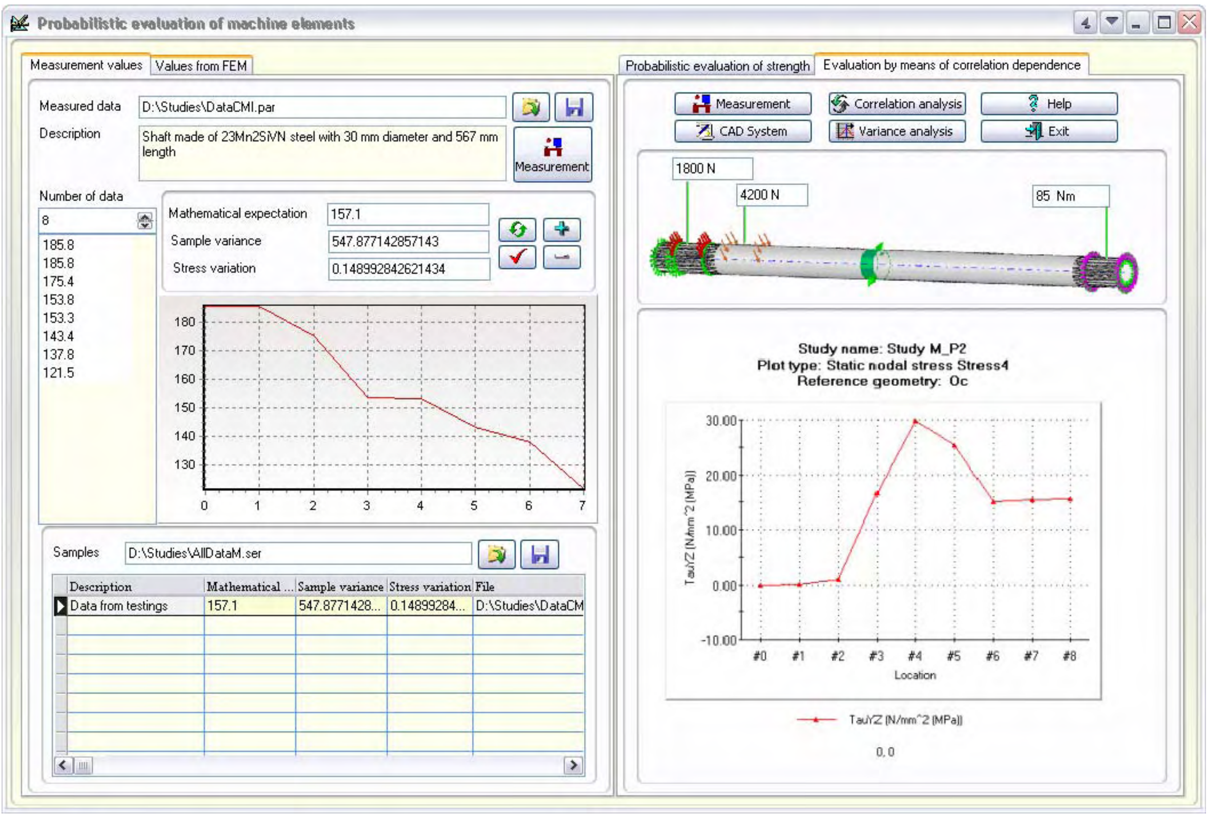

Measured data: D:\Studies\DataCMI.par

Description: Shaft made of 23Mn2SiVN steel with 30 mm diameter and 567 mm length

Number of data: 8

185.8
185.8
175.4
153.8
153.3
143.4
137.8
121.5

Mathematical expectation: 157.1
Sample variance: 547.877142857143
Stress variation: 0.148992842621434

Samples: D:\Studies\AllDataM.ser

Description	Mathematical ...	Sample variance	Stress variation	File
Data from testings	157.1	547.8771428...	0.14899284...	D:\Studies\DataCM

Fig. 4. System for probabilistic evaluation of forces, moments and stresses originated in machine elements.

In the developed software product, two methodologies destined for evaluating the fracture probability of detail have been used.

By an application of the first methodology it is aimed to evaluate the machine element according to the following indices: coefficient of reserve over strength and probability of failure by means of the preliminarily accepted criterion for assessment, i.e. a stress in the critical section [7].

Since a series of loadings acts on the shaft, then the mathematical expectation of a stress in the critical section $M(\tilde{\sigma}_p)$ will be equal to the sum of mathematical expectations of stresses from each loading as follows:

$$M(\tilde{\sigma}_p) = \frac{\sum_{i=1}^{n} M(\tilde{\sigma}_{pi})}{n} \qquad (1)$$

where: i is a set serial number of the acting force loadings on the element; n is a quantity (number) of these loadings; $M(\tilde{\sigma}_{pi})$ is mathematical expectation of the i-th sample.

Analogically it can be written:

$$M(\tilde{\sigma}_m) = \frac{\sum_{j=1}^{m} M(\tilde{\sigma}_{mj})}{m} \qquad (2)$$

where: $\tilde{\sigma}_m$ and $\tilde{\sigma}_p$ are strength experimental and calculated characteristics of the machine element (the reducer shaft), respectively.

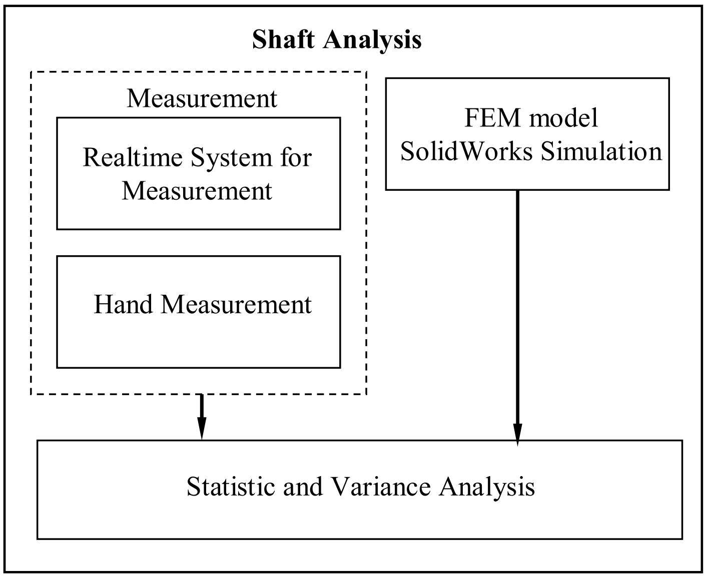

Fig. 5. *Organization of the system for shaft analysis.*

The variance of resultant stress is determined according to the following dependence:

$$D(\sigma_m) = \frac{\sum_{j=1}^{m} \left(\tilde{\sigma}_{mj} - M(\sigma_m)\right)^2}{m} \tag{3}$$

where: $\tilde{\sigma}_{mj}$ is the magnitude of j-th loading; m is a number of loadings; j is a set serial number of loading.

Analogically it can be written:

$$D(\sigma_p) = \frac{\sum_{i=1}^{n} \left(\tilde{\sigma}_{pi} - M(\sigma_p)\right)^2}{n} \tag{4}$$

Knowing the variance and the mathematical expectation, the variation coefficient of stresses can be determined as their relative characteristic in the following type:

$$\nu(\sigma_m) = \frac{\sqrt{D(\sigma_m)}}{M(\sigma_m)} \tag{5}$$

Analogically it can be written:

$$\nu(\sigma_p) = \frac{\sqrt{D(\sigma_p)}}{M(\sigma_p)} \tag{6}$$

The condition for non-fracture of element is worked on the following dependence [7]:

$$\tilde{u} = \tilde{\sigma}_m - \tilde{\sigma}_p > 0 \tag{7}$$

where: $\tilde{u}$ is a function of strength; $\tilde{\sigma}_m$, $\tilde{\sigma}_p$ are strength experimental and calculated characteristics of the element.

From where it follows, that: $M(\tilde{\sigma}_m) > M(\tilde{\sigma}_p)$.

Therefore the coefficient of reserve over strength ξ can be determined by the following ratio and it has to possess a value, which is larger than unity:

$$\xi = \frac{M(\tilde{\sigma}_m)}{M(\tilde{\sigma}_p)} \tag{8}$$

Since the values of stresses obtained by experiment and calculations in the critical section have probabilistic character with normal law of distribution, then the fracture probability can be presented in the following type:

$$P(\tilde{u}) = \frac{1}{\sqrt{2\pi\left[D(\sigma_p) + D(\sigma_m)\right]}} \cdot \int_0^\infty exp\left[-\frac{1}{2}\left[\frac{\left(u - M(\sigma_p) + M(\sigma_m)\right)}{D(\sigma_p) + D(\sigma_m)}\right]\right] du \tag{9}$$

In the developed programme (Fig.6) the data obtained during measurements from the testing of reducer shaft according to Fig. 2 have been introduced (Fig. 6.a) as well the data obtained by the finite-element model according to Fig. 3 (Fig. 6.b).

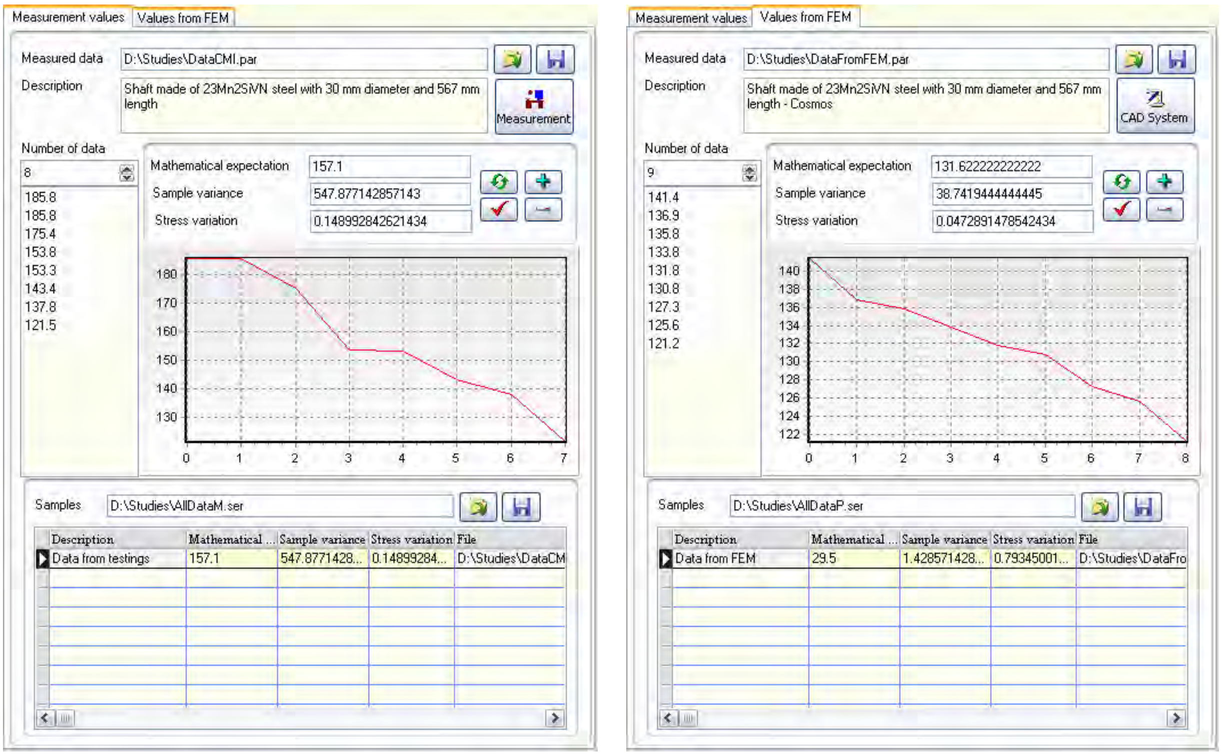

Measured data: D:\Studies\DataCMI.par
Description: Shaft made of 23Mn2SiVN steel with 30 mm diameter and 567 mm length
Number of data: 8
185.8
185.8
175.4
153.8
153.3
143.4
137.8
121.5
Mathematical expectation: 157.1
Sample variance: 547.877142857143
Stress variation: 0.148992842621434
Samples: D:\Studies\AllDataM.ser

Description	Mathematical ...	Sample variance	Stress variation	File
Data from testings	157.1	547.8771428...	0.14899284...	D:\Studies\DataCM

Measured data: D:\Studies\DataFromFEM.par
Description: Shaft made of 23Mn2SiVN steel with 30 mm diameter and 567 mm length - Cosmos
Number of data: 9
141.4
136.9
135.8
133.8
131.8
130.8
127.3
125.6
121.2
Mathematical expectation: 131.622222222222
Sample variance: 38.7419444444445
Stress variation: 0.0472891478542434
Samples: D:\Studies\AllDataP.ser

Description	Mathematical ...	Sample variance	Stress variation	File
Data from FEM	29.5	1.428571428...	0.79345001...	D:\Studies\DataFro

a) b)

Fig. 6. *Data obtained during measurements from testing of reducer shaft (a) and data obtained by the finite-element model (b).*

After performing the calculations, the probabilistic evaluation of the machine element strength, i.e. the reducer shaft has been obtained (Fig.7), which yields a conclusion about the strength of detail in the corresponding studied ranges.

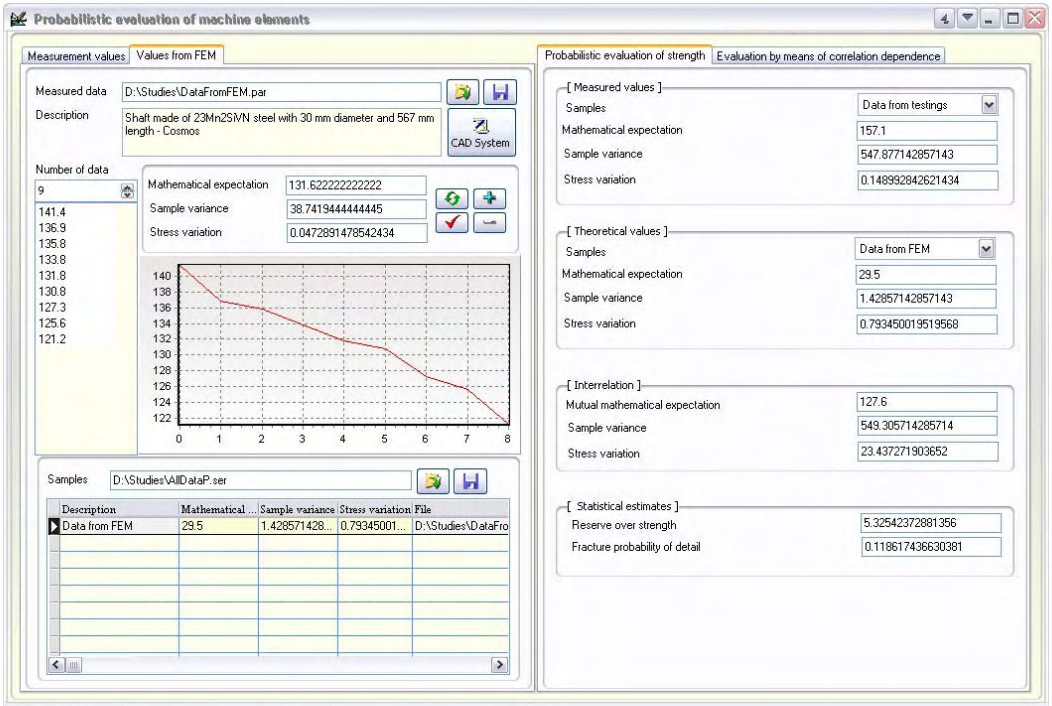

Measured data: D:\Studies\DataFromFEM.par
Description: Shaft made of 23Mn2SiVN steel with 30 mm diameter and 567 mm length - Cosmos
Number of data: 9
141.4
136.9
135.8
133.8
131.8
130.8
127.3
125.6
121.2
Mathematical expectation: 131.622222222222
Sample variance: 38.7419444444445
Stress variation: 0.0472891478542434
Samples: D:\Studies\AllDataP.ser

Description	Mathematical ...	Sample variance	Stress variation	File
Data from FEM	29.5	1.428571428...	0.79345001...	D:\Studies\DataFro

[Measured values]
Samples: Data from testings
Mathematical expectation: 157.1
Sample variance: 547.877142857143
Stress variation: 0.148992842621434

[Theoretical values]
Samples: Data from FEM
Mathematical expectation: 29.5
Sample variance: 1.42857142857143
Stress variation: 0.793450019519568

[Interrelation]
Mutual mathematical expectation: 127.6
Sample variance: 549.305714285714
Stress variation: 23.437271903652

[Statistical estimates]
Reserve over strength: 5.32542372881356
Fracture probability of detail: 0.118617436630381

Fig. 7. *Probabilistic evaluation of the strength of reducer shaft.*

The second methodology is based on synthesized mutual correlation dependence between the stresses and their originating forces as some constraints are accounted for.

The correlation function is generated by virtue of some type models whose parameters are adjusted depending on the properties of studied detail. The coefficients of correlation function are adjusted automatically by means of specialized software about adjustment of models, which works on the basis of heuristic algorithm for global optimization with accelerated convergence [5].

3. Conclusions

The developed apparatus-program system affords an opportunity for studying the strength of reducer shaft according to the probabilistic evaluation method concerning the examination of machine elements. The automated apparatus-program system is open for development in the following directions: addition of methods for evaluating various machine elements, expansion of control-measurable system with regard to different methods and systems for measuring the studied quantities.

References

[1]. Theme B-1808. Studying the Durability of Details made by 23Mn2SiVN Steel from Reducer about Rope Electric Hoist 50 kN, Central Mechanical Engineering Institute-Sofia. BRV-TESMA-Gabrovo, 1980 (in Bulgarian).

[2]. Alyamovskii, A. A. et all. *SolidWorks. Computer Modelling in Engineering Practice*, Sankt-Peterburg, BHV-Peterburg, 2005 (in Russian).

[3]. Nedelcheva, P. M. *Modelling the Characteristics of Collet Chucks with Cross-Feathers of Intermediate Colle*t, 7th International Conference RaDMI 2007, 16-20 September 2007, Belgrade, Serbia, 2007, pp.224-229.

[4]. Paskaleva, K. *Automated Analysis and Synthesis during Design of Epicyclic Gear Mechanisms*, Thesis, Sliven, 2001 (in Bulgarian).

[5]. Yordanov, S. *Application of Heuristic Algorithm for Global Optimization with Accelerated Convergence at Tuning the Governor Parameters for Controlling of Water Turbine from Banki Type*”, Journal “IMK-14 Istrazivanje i razvoj”, Institute IMK “14.octobar”, Broj (28-29) 1-2/2008, Krusevac, Srbija, pp. 43-55.

[6]. Zhelezarova, D., I. Balashev. *Stressed State of Input Shaft from the Reducer about Rope Electric Hoist*, Journal of scientific papers “Technology and Technique of Typography”, National Technical University of Ukraine “Polytechnic Institute of Kiev”, v.3-4 (21-22), Kiev, 2008, Ukraine, pp.27-33.

[7]. Zhelezarova, D., I. Angelov. *Forming the Methodology and Algorithm for Reliability Estimate of Machine Elements in virtue of the Indices: Coefficient of Reserve over Strength and Probability of Failure*, Scientific conference Smolyan 2004, 26-27 June 2004, Technical College of Smolyan, pp. 248-254 (in Bulgarian).

MANUSCRISELE, CĂRŢILE ŞI REVISTELE PENTRU SCHIMB, PRECUM ŞI ORICE CORESPONDENŢE SE VOR TRIMITE PE ADRESA:

MANUSCRIPTS, REVIEWS AND BOOKS FOR EXCHANGE COOPERATION, AS WELL AS ANY CORRESPONDANCE WILL BE MAILED TO:

LES MANUSCRIPTS, LES REVUES ET LES LIVRES POUR L'ECHANGE, TOUT AUSSI QUE LA CORRESPONDANCE SERONT ENVOYES A L'ADRESSE:

MANUSCKRIPTEN, ZIETSCHRITFTEN UND BUCHER FUR AUSTAUCH SOWIE DIE KORRESPONDENZ SID AN FOLGENDE ANSCHRIFT ZU SEDEN:

UNIVERSITATEA "DUNĂREA DE JOS" DIN GALAŢI
REDACŢIA ANALELOR
Str. Domnească nr. 47 – 800036 Galaţi,
ROMÂNIA
email: mbordei@ugal.ro

After the latest evaluation of the journals achieved by National Center for the Science and Scientometry Politics (**CENAPOSS**), as recognition of its quality and impact at national level, the journal is included in B category, 215 code (http://www.cncsis.ro/2006_evaluare_rev.php).

The journal is indexed in Cambridge Scientific Abstract (http://www.csa.com/ids70/serials_source_list.php?db=materials-set-c).

The papers published in this journal can be visualized on the "Dunarea de Jos" University of Galati site, the Faculty of Metallurgy, Material Science and Environment, page: www.fmsm.ugal.ro.

AFFILIATED WITH:

- *ROMANIAN SOCIETY FOR METALLURGY*
- *ROMANIAN SOCIETY FOR CHEMISTRY*
- *ROMANIAN SOCIETY FOR BIOMATERIALS*
- *ROMANIAN TECHNICAL FOUNDRY SOCIETY*
- *THE MATERIALS INFORMATION SOCIETY (ASM INTERNATIONAL)*

Annual subscription (4 issues per year)

Edited under the care of
Faculty of
METALLURGY, MATERIALS SCIENCE AND ENVIRONMENT
and Research Center
QUALITY OF MATERIALS AND ENVIRONMENT

Edited date: 30.09.2010
Issues number: 200
Printed by
Galati University Press
accredited CNCSIS
47 Domneasca Street, 800036 Galati,
Romania